2018

GEOCHEMICAL DIFFERENCES IN CALCIC HORIZONS DUE TO PARENT MATERIAL AND ANTHROPOGENIC WATER INPUT IN SOUTHEASTERN ARIZONA

Alicia Fischer

GEOCHEMICAL DIFFERENCES IN CALCIC HORIZONS DUE TO PARENT MATERIAL AND ANTHROPOGENIC WATER INPUT IN SOUTHEASTERN ARIZONA

Alicia Fischer

A thesis submitted to the Faculty of the Geology
Department of Colby College in fulfillment of the
requirements for Honors in Geology

Waterville, Maine

May, 2018

GEOCHEMICAL DIFFERENCES IN CALCIC HORIZONS DUE TO PARENT MATERIAL AND ANTHROPOGENIC WATER INPUT IN SOUTHEASTERN ARIZONA

Except where reference is made to the work of others, the work described in this thesis is my own or was completed in collaboration with my advisory committee

Alicia Fischer

Certificate of Approval

Dr. Robert Gastaldo
Whipple-Coddington Professor of Geology
Colby College

Dr. Craig Rasmussen
Professor of Environmental Pedology
The University of Arizona

Dr. Tasha Dunn
Clare Boothe Luce Assistant Professor of Geology
Colby College

Dr. Bruce Rueger
Visiting Assistant Professor of Geology
Colby College

ABSTRACT

Calcic soil horizons are significant carbon sinks. Yet, despite their abundance in semiarid environments, calcic soils are enigmatic for two reasons: (1) some authors hypothesize that dust input does not, independently, control the geochemical properties of these soils; and (2) few studies have examined how these calcic soils change geochemically with respect to irrigation. A 2017 pilot study used portable x-ray fluorescence (pXRF) on calcic soils in Southeastern Arizona (SEAZ) to address these questions. However, this technology has not been widely employed to evaluate soils. The current study addresses whether pXRF and XRF data obtained from the same soil samples are comparable. As such, calcic soils sourced from basalt, rhyolite/andesite, limestone, and mixed alluvium were collected from SEAZ and analyzed using pXRF and XRF. Analysis revealed that pXRF obtained significantly lower elemental values compared to XRF, indicating that one must exert caution when using pXRF analyses on soils. The XRF data show that there are clear geochemical differences between the calcic horizons originating on different parent materials, which suggests that dust input does not, solely, control the calcium input into these soils. And, the geochemical composition of sprinkler-irrigated mineral A-horizons of soil does differ from non-irrigated soil, which indicates that high-volume water input (>240 gallons/hour) is needed to alter the soil composition. Yet, irrigation over 100 years has not completely changed the calcic soil composition. Thus, a longer time of irrigation (greater than 100 years) is needed to potentially initiate the release of carbon sequestered in these calcic soils.

Acknowledgements

First, to Dr. Gastaldo, I want to thank you for mentoring me and guiding me throughout the Honors Thesis project as well as the preparations for graduate school. I honestly would have no idea where I would be if you hadn't prodded me to participate in an REU program. Thanks to the program, I discovered the area of research I would like to continue into as a graduate student at Auburn. Moreover, you spent so many hours reading not only mine, but Kaci Kus' Honors Thesis drafts, week after week, while you were teaching and completing your own research. I don't know how you do it, but in whatever field I end up after Colby, I want to have your diligence, firmness, and passion. I sincerely thank you for everything.

Next, to Dr. Rasmussen, I want to thank you for allowing me to participate in your REU project last summer, as I learned a plethora about pedology. Although I ultimately did not decide to pursue a soils-based graduate school program, the laboratory-and-field techniques, as well as the mental grit, I learned during the project will serve me invaluably in graduate school and beyond. I also want to take you for assisting in my collection of calcic soils in January 2018. Thank you for taking time out of your schedule to help me complete my Honors Thesis.

I also want to thank all of the Geology professors I have met during my undergraduate years at Colby. I want to thank Bruce Rueger for saying, "hey, you're pretty good at this Geology stuff. You should think about continuing if you like the material." This comment alone is what led me to take more Geology classes after my first semester at Colby and to eventually declare a major in Geology. Also, I want to thank Dr. Tasha Dunn, Dr. Bob Nelson, Dr. Bill Sullivan, and Dr. Bess Koffman, in addition to Dr. Gastaldo and Bruce, for the challenging classes and your high expectations, which continually pushed me to put in the best effort that I possibly could. Moreover, I thank all of you for making the material taught interesting and fun so that I would enjoy classes every day.

Of course, I have to acknowledge the funding that has made my Honors Thesis research possible. Thanks to the NSF EAR grant #1659546 "REU Site: Earth Systems Research for Environmental Solutions," I had the chance to participate in REU research at the University of Arizona and Biosphere 2. Moreover, the Davis Connects Funding Committee and the Linda K. Cotter Internship Fund through Colby College enabled me to travel back to Arizona during January 2018 and collect additional soil samples that were necessary for my Honors Thesis.

Lastly, I have to thank my family and friends. To my new-found friends from the REU program this past summer, Cori, David, Elizabeth, Ericka, Eunice, Evelin, Harrison, Jasmine, Joe, John, Maggie, and Mychal, thank you for your different opinions about everything from research to life and for your fun and unique spirits. Thank you to all my friends in the Geology department, Don, Emma, Erica, Kaci, Nam, Sam, and Zena, for making the classes and my life at Colby more enjoyable. And, to my parents, Shawn and Andrea, and my sister, Victoria "Toria," thank you for the constant support in all my endeavors. Thank you for giving me the freedom to do what I wanted and the encouragement to get me through my struggles and hardships. Finally, my pets, Autumn, Black Jack, Kiwi, Pandora, and Sadie, deserve all the love in the world, as they have kept me smiling throughout these four years, due to their stupidity and endearing personalities.

Table of Contents

Introduction....1

Background....4

Goals....10

Methodology....11
- Locality....11
- Field Sampling and Analyses....12
- Laboratory Analyses....13

Results....16
- Parental Material....16
- Irrigated Soils....18
- Parent and Soil pXRF and XRF Data....18
  - Basaltic Soil (Sentinel Peak)....19
    - pXRF....19
    - XRF....19
  - Limestone Soil (Santa Rita and Whetstone)....19
    - pXRF....19
    - XRF....20
  - Rhyolitic Soil (Tucson Mountains)....20
    - pXRF....20
    - XRF....20
  - Alluvial Soil (Saddlebrooke)....21
    - pXRF....21
    - XRF....21
- Non-Irrigated Soil Profile Trends....22
- Irrigated Soil Trends....22

Parent Material vs. Originating Soil Geochemistry 23

Discussion 25
pXRF vs. XRF Analyses 26
Bedrock vs. Soil Geochemistry 30
The Effects of Irrigation 37

Conclusions 44

References 49

Figures and Tables 55

Attached Excel Appendices ..... N/A
Appendix A: pXRF Elemental Data 1
Appendix B: ANOVA Tests 2
Appendix C: Soil Munsell Color 3
Appendix D: XRF Elemental Data 4
Appendix E: XRF Variation 5

INTRODUCTION

Arid and semiarid areas in the Western United States, such as Southeastern Arizona (SEAZ), have remained relatively unpopulated until the last century. Settlement in the dry climate of SEAZ required significant amounts of water to be redirected towards these communities. Since the 1970s, population density rose drastically as a result of increased migration to the Sun Belt, with these new and expanding communities excavating roads and developing large cities (e.g., Tucson). Soils that characterize this region tend to be calcium-rich. Because of increased anthropogenic input of water into the system, as well as changes in the landscape from expanding cities, the soil chemistry of these areas could be altered significantly. As Lybrand et al. (2011) note, changes in water availability and distribution will likely alter the dynamics of soil-and-regolith environments. Thus, we need to know how calcic soils respond to, and change from, these anthropogenic forces. This is especially true as these soils sequester significant amounts of carbon, which can act as a global warming agent if released and paired with oxygen.

The increased calcium in SEAZ soils has traditionally been correlated with dust input. Past studies, such as Batchily et al. (2003), have identified only calcium-rich dust as a factor for the development of calcic horizons in the region. Yet, to date, the hypothesis that an increasing concentration of calcium-rich dust is the main contributor to calcic horizonation has not been tested. A preliminary pilot project compared the geochemical properties of calcic (and petrocalcic) horizons originating on different parent materials (Fischer et al., 2017). That project discovered that parent material influenced geochemical differences between the calcic horizons, as there were notable differences in the chemical properties of these soils. Fischer et al. (2017) also found that many horizons possessed a notable-to-significant dust fraction across the four

soils studied, each of which originated on a different parent regolith. They reasoned that dust is a significant factor in forming calcic horizons. However, other factors, such as parent material, can partially explain the formation of these calcic (and petrocalcic) horizons in the region.

Soils are the largest reservoir of carbon in the terrestrial realm, as they not only contain organic carbon and inorganic carbon, but also likely sequester atmospheric carbon (Kraimer and Monger, 2009; Zamanian et al., 2016). In fact, soils are the third largest pool of carbon on Earth (2,470 Pg C), after oceans (38,725 Pg C) and fossil fuels (4,000 Pg C) (Kraimer and Monger, 2009; Zamanian et al., 2016). These calcium carbonate-rich soils are also widespread, covering approximately 13% of Earth's surface, which helps explain why they collectively sequester a large quantity of carbon (Alonso-Zarza and Wright, 2010). Moreover, it has been noted that calcic soils in desert-and-arid regions hold more carbon than terrestrial vegetation (Kraimer and Monger, 2009).

Soils serve as the important connector between soil inorganic carbon (SIC), and its long-term geological carbon cycling with atmospheric CO_2 (thousands to millions of years), to its short-term biotic carbon cycling (hours to hundreds of years) (Zamanian et al., 2016). In semiarid and arid regions like SEAZ, SIC plays an even larger function because it is the largest reservoir of soil carbon (Zamanian et al., 2016). Specifically, areas that receive less than 250 mm of precipitation a year, such as the Sahara and the Western United States, have approximately 320 to 1,280 Mg C ha^{-1} (Zamanian et al., 2016). Yet, Zamanian et al. (2016) note that human-induced changes to the environment and soils, such as N fertilization and irrigation, could release large quantities of SIC and, thus, increase the emissions of CO_2 into our atmosphere. These concerns are founded upon environmental changes during the Holocene and Pleistocene, at a

time during which 400 to 500 Pg C were released from SIC-induced climate warming (Zamanian et al., 2016).

The focus in this study concerns a specific carbonate that usually forms in arid and semiarid regions: pedogenic carbonate, otherwise known as pedogenic calcrete or caliche (Alonso-Zarza and Wright, 2010). Pedogenic carbonates originate from the SIC reservoir and from the dissolution and redistribution of carbonates in soils (Zamanian et al., 2016). Pedogenic carbonate also forms by two different processes: per ascensum and per descensum mechanisms (Candy and Black, 2009). Ascensum methods involve the rise of Ca^{+} up through the soil as a function of evaporation (Candy and Black, 2009). In contrast, per descensum calcrete forms from soil waters dissolving carbonate in the top mineral A-horizon and, then, percolating down and reprecipitating the carbonate in the lower B-horizons, typically in the Bt horizon (Candy and Black, 2009). Per descensum calcrete horizons and profiles are more relevant to SEAZ soils because they are the most common carbonates and are heavily affected by and, thus, respond to the prevailing climate (Candy and Black, 2009). As these carbonates originate from rainfall and evaporation, they can be used as strong recorders of climate and environmental change (Candy and Black, 2009). However, calcic soils in desert regions do not solely contain pedogenic carbonate. Many SEAZ soils that originated on alluvial fans are likely a mixture of pedogenic and groundwater calcretes, considering that alluvial fans were closed drainage systems where the water table could rise from lake expansion or processes operating in other bodies of water (Alonso-Zarza and Wright, 2010). Yet, regardless of the formation mechanism of these calcic soils, calcrete is shown to be sensitive to environmental and climatic changes, specifically from changes in precipitation and water availability (Alonso-Zarza and Wright, 2010).

BACKGROUND

Due to the interconnectivity between biotic and abiotic systems, and a strong control of surface albedo, Kraimer and Monger (2009) and Singhvi et al. (2010) claim that deserts and arid regions are ideal places to observe the connection between geology and climate. This is because of the vast expanse of soils enriched with calcium carbonate in these dry regions. Calcium carbonate leaches down the soil profile from the surface to some depth, which results in the precipitation of the well-known calcic horizons of desert soils (Bachman and Machette, 1977; Machette, 1985). Calcic soils and pedogenic carbonates in semiarid and arid regions vary in age and can represent the product of thousands to millions of years of formation (Adamson et al., 2015; Machette, 1985; Pfeiffer et al., 2012). Calcic soils possess different amounts of calcium carbonate based on their age, distribution, and concentration of Ca^{2+} in rainfall, and the concentration of $CaCO_3$ in dust and sand (Bachman and Machette, 1977; Machette, 1985). In addition, $CaCO_3$ precipitates in deserts when the seasonal drought decreases the soil-pore pCO_2 and increases ^{18}O values in the soil water as a consequence of evaporation (Schlesinger, 1985). Furthermore, the key difference between carbonate-enriched calcic and petrocalcic soil horizons is that petrocalcic soils possess extremely well-cemented calcic horizons (Soil Survey staff, 2006). As such, calcic soils are good proxies for climate and environmental change throughout the Pleistocene and Holocene epochs (Adamson et al., 2015; Machette, 1985).

Quaternary deposits vary in their accumulation, history, physical and chemical characteristics, and outcrop exposure throughout Arizona. Yet, soils in SEAZ are generally consistent in composition and classification (Fig. 1; Hendricks, 1985; Morrison, 1985). Moreover, studies have placed the diverse alluvium deposits in SEAZ into four major groups: (1) deformed continental sediments deposited in a subtropical climate and fan conglomerates eroded

from the surrounding mountains during a semiarid climate; (2) lake-bed deposits from natural damming of drainage during a more seasonal period of time; (3) coarse fan deposits from heavy erosion during glaciation; and (4) young, fine-grained cienegas (desert wetlands) in climatic conditions similar to today (Melton, 1965). In the time during which these soil groups formed, a change from humid to semiarid climate occurred beginning in the early to middle Miocene (19.9 ± 1.6 million), as orogenic activity likely disrupted the movement of humid air through the area (Melton, 1965). Moreover, rhyolitic ash beds and andesite flows occurred during this time, and slow water movement in valleys resulted in lake-bed deposits of saline, lacustrine mudstone interlayered with freshwater limestone (Melton, 1965). Coarse fan deposits can be found across the base of most mountain ranges in southern Arizona, and are usually found at elevations between 1,500 and 4,000 feet (Melton, 1965). Some soils on alluvial fans, especially those in the Sonoran Desert, are identified as calcium-rich and basaltic due to the presence of basalt boulders (Melton, 1965; Morrison, 1985). In fact, soils that have developed on these alluvial fans contain large petrocalcic horizons (Naiman et al., 2000). Lastly, cienegas are the least stable landforms in southern Arizona and are easily destroyed; yet, they can have carbonate-rich zones attaining 1-3 feet in thickness (Melton, 1965). This diversity in soil regime explains the difficulty in classifying the mixed alluvium soil deposits in the area.

Once the origin and chemical composition of the calcic soils in question are determined, one can investigate how these soils respond to climate change. Studying past climate change through the lens of soils can aid in determining how today's climate has affected soil composition (Pavich and Chadwick, 2004). Pavich and Chadwick (2004) pose a relevant question: once soils are formed, are they insensitive to climate change? Soils integrate the conditions of the past climate into their horizons, as they are the boundary between Earth's

atmosphere and its lithosphere (Pavich and Chadwick, 2004). They note that soil characteristics and compositions can drastically change on a timescale between 1,000 and 10,000 years, with marked physical and chemical changes decreasing after 10,000 years. Although carbonate-cemented horizons form in less than 10,000 years, these soils are thought to develop over longer periods of time (>10,000 years) when they are significantly impacted by dust input (Pavich and Chadwick, 2004). In fact, studies have shown that dust recovered from soils, which are calcium and titanium rich, can determine pollution and land-use levels, and be indicative of rapid climate change (Pavich and Chadwick, 2004). Yet, the question remains: how do increased amounts of water in dry environments affect a soil's composition?

Water, or the lack thereof, is the one factor that characterizes arid regions. All arid regions have specific mean annual precipitation constraints, which suggest that CO_2 sequestration and emissions are tied to them. By observing positive oxygen-and-carbon isotopic values in calcareous soils, one can determine that evaporation and aridity are the key environmental factors for controlling carbonate production (Adamson et al., 2015; Pfeiffer et al., 2012). Moreover, Amit et al. (2010) researched the effects on rare rainstorms in two "hyperarid" deserts in Africa (<50 mm yr^{-1} of precipitation): the Negev and Namib deserts. Although these areas currently receive less rainfall, when compared to the Southwestern deserts of the United States (Tucson receives 45–95 cm yr^{-1} for comparison), they noted that calcic horizons in the Namib desert are analogous to the Mojave Desert in Nevada, especially with respect to comparable $\delta^{13}C$ values (Amit et al., 2010; Lybrand and Rasmussen, 2015). One of the most important aspects of $\delta^{13}C$ measurements is that these values can indicate the strength of carbon-dioxide sink in the terrestrial realm (Raymo and Ruddiman, 1992). An increase in, or more positive, $\delta^{13}C$ values likely indicate that an increased amount of ^{12}C, and carbon dioxide, is

sequestered in plants and other terrestrial materials (Raymo and Ruddiman, 1992). As the Namib soil carbonates possess a more positive $\delta^{13}C$ value (+2.8‰), Amit et al. (2010) reasoned that these carbonates sequestered a significant amount of atmospheric and soil-respired CO_2 during their formation. In fact, the calcretes that formed on siliceous rocks sequester CO_2 during the weathering processes of these rocks, which illustrates that carbonates are key sinks for CO_2 (Huerta et al., 2015). However, Huerta et al. (2015) stress that the CO_2 in these soil carbonates mostly originate in the soil rather than a result from weathering. Amit et al. (2010) also noted that the rainfall duration in desert environments is important for forming particular soil horizons. As such, a range of low rainfall is needed to promote the formation of calcic horizons. In contrast, an overabundance of water will prohibit their genesis. This balance indicates that increased water input into the soil systems from anthropogenic sources will likely impede the production of carbonates and, thus, the drawdown and sequestration of CO_2.

It is important to determine the timescales over which a decrease in CO_2 drawdown occurs in response to an increase in water input. This is especially true as Stiles et al. (2003) indicate that soils forming in dry, semiarid and arid climates take longer to reach geological equilibrium when subjected to any environmental change. Moreover, semiarid regions that experience a short-term increase in precipitation/water input showcase a change in their soil profiles' chemical composition. Under increased episodes of precipitation, these soils accumulate organic carbon in the upper horizons (Bescansa et al., 2006; Monger, 2010). In addition, Assouline et al. (2016) examined the reciprocal relationship between Ca and Na in soil as a consequence of increased rainfall/water availability. They found that an increase in freshwater or wastewater input from irrigation in a semiarid area of Israel resulted in a decrease of Ca content

and a subsequent increase in the Na-adsorption ratio. This suggests that changes in a soil's chemical composition from increased water input occurs over relatively short timescales.

Other researchers, though, argue that these changes in soil chemistry occur over longer timescales. McDonald et al. (1996) examined the effects of increased and decreased precipitation on soils formed on alluvial-fan deposits in the Mojave Desert, California, using a Simultaneous Heat-and-Water model. They found that short-term intervals of increased precipitation (100 years or less) had little impact on the carbonate distribution in a soil profile. In contrast, they discovered that longer intervals of increased precipitation (400 years or greater) had a significant impact on carbonate distribution. This is because the increased amount of water percolated to the lower 75-150 cm of the soil profile, allowing the carbonate to form in these deeper horizons. Other studies, including Monger (2010), also confirm this trend of a downward-shift in calcic horizons with increased precipitation. They examined semiarid environments that experienced an interval of wetter climate and found the downward carbonate shift in the soil profile. Intriguingly, McDonald et al. (1996) also report that an increase in soil CO_2 correlates with increased precipitation. Yet, Monger (2010) determined that an increase in erosion in semiarid regions does not correlate to an increase in CO_2 emissions from calcic horizons. Thus, Monger (2010) surmised that calcic horizons are CO_2 reservoirs.

Field techniques have been developed to rapidly assess the chemical composition of soils *in situ*. The advent of portable x-ray fluorescence (pXRF) devices has allowed researchers to bring laboratory analyses to the field. The advantages of pXRF instrumentation are its small size and quick analyses. Most pXRF instruments can easily fit into a suitcase and are light-weight, allowing researchers to carry the equipment around while collecting and examining field samples. Moreover, the pXRF instrument can be plugged into a laptop computer's USB outlet to

easily run and store any pXRF analyses on field samples. Furthermore, with a quick data collection time of approximately four minutes, pXRF allows one to efficiently collect measurements regarding the composition of any desired specimen by simply holding the pXRF device up against the material for that duration. Given the pXRF's handheld size, ease of use, and quick analyses, there is little wonder as to why pXRF has gained rapid appeal in the scientific community as an up-and-coming technology.

Yet, the question remains as to the accuracy of pXRF data and its use. Although most geochemical analyses of soils are performed using laboratory-based XRF, Chakraborty et al. (2017) advocated that the pXRF analysis of soils yields accurate data at a low-cost and through a nondestructive method when compared to other traditional approaches. They reported that Zhu and Weindorf (2009) found an R^2 value of 0.986 when comparing pXRF-determined Ca levels with laboratory-determined Ca values. Similarly, these workers reported that Weindorf et al. (2013) used pXRF as a proxy for gypsum, and obtained a R^2 value of 0.912 when relating these values to laboratory-quantified gypsum concentrations. To demonstrate the accuracy of pXRF analysis, they analyzed the pXRF data to prove that it depicted the elemental differences in the six stages of carbonate soil development. The question remains, though, as to the accuracy and utility of hand held, portable XRF when compared with standard XRF methodologies. The comparison between pXRF and XRF analyses has been made with rock samples. For example, Craig et al. (2007) found consistent trends between their obsidian artifact's pXRF and XRF data, but discovered that the two instruments showed significant differences between the analyses, which they found could be solved with cross calibration. Moreover, archeological bricks have been compared using pXRF and XRF analyses, which produced good results with a few critical

differences between the two datasets (Bonizzoni et al., 2013). However, to date, there has been little to no comparison between the two instruments with respect to soil analyses.

GOALS

There are three overarching goals associated with the current project. The first is to compare and contrast pXRF spectra from Fischer et al. (2017) with XRF instrumental spectra. The intent is to determine if the pXRF soil data compares favorably with x-ray fluorescence (XRF) analyses of the same soil samples. These analyses will determine whether Chakraborty et al.'s (2017) claims are valid by testing the accuracy of pXRF data. If there are significant and irreconcilable differences between the pXRF and the XRF datasets, then one must be cautious when using pXRF for determining the soil chemistry.

A second goal is to determine whether parent material influences the formation of the overlying soils. Although the pilot project compared the geochemical properties of calcic soils originating on different parent materials, the study only utilized pXRF to reach its conclusions and did not analyze samples of the parent bedrock for comparison. As such, the current study intends to identify bedrock exposures of the four different types of parent material on which these originated (colluvial basalt, rhyolite/andesite, limestone, and mixed alluvium) and characterize the geochemical nature of these parent materials in comparison with the soils' compositions. These geochemical analyses include determining the mineralogy of bedrock clasts in soils and their elemental composition using XRF. It is important to determine the degree to which the bedrock affects the soils' geochemistry, and how to adequately measure a soil's compositional changes with respect to it.

The third, and final, goal is to determine whether human-induced irrigation affects the calcic soils' composition. McDonald et al. (1996) found that increased water supply likely

leaches the Ca and carbonate from calcic soils. This removal of calcium carbonate could be a serious concern for communities in arid and semiarid regions, as irrigation could hinder the calcic soil's ability to sequester carbon and could force the soil to release its carbon into the atmosphere (Monger, 2010; Zamanian et al., 2016). Thus, it is important to determine if a significant change in the chemical composition of irrigated calcic soils has occurred, especially with respect to Ca concentrations, as any geochemical alteration could indicate that irrigation is indeed removing the calcium carbonate. Furthermore, it will be interesting to see whether McDonald et al.'s (1996) model holds true when analyzing soils originating on different parent materials, and if increased water supply will increase CO_2 emissions from calcic horizons.

METHODOLOGY

Locality

Five soil profiles were collected at Sentinel Peak, the Tucson Mountains, the Santa Rita Mountains, Whetstone, and Saddlebrooke. These SEAZ soils are all aridisols in the Thermic Soil Zone, which vary from other soils in the state of Arizona due to the mean temperature differences under which they formed (Fig. 1; Hendricks, 1985). These sites were chosen based on their differing parent or bedrock materials. Sentinel Peak's parent material is mostly basalt, the Tucson Mountains are largely comprised of Mesozoic felsic volcanic rocks, the Santa Rita Mountains and Whetstone have expansive exposures of carbonate rocks and bedrock, and Saddlebrooke is an old alluvial fan with thick petrocalcic horizons (Naiman et al., 2000). Thus, the parent materials for each site are determined to be colluvial basalt (obtained from Sentinel Peak), rhyolite/andesite (obtained from the Tucson Mountains), limestone (obtained from the Santa Rita Mountains and Whetstone), and mixed alluvium (obtained from Saddlebrooke) (Soil Profiles 1-5; Fig. 2). It is important to note that mixed alluvium is a very loose term used to

identify samples that originated from an ancient alluvial fan; there is little consensus on their parent material composition.

Field Sampling and Analyses

Soil profiles with calcic and petrocalcic horizons from different SEAZ sites were collected in June and July 2017 (Fig. 2; Table 1). The color of each was characterized with a Minolta CR-200 handheld digital chromameter, which determines Munsell soil color. The soils from Sentinel Peak, the Tucson Mountains, the Santa Rita Mountains, Whetstone, and Saddlebrooke were recollected in January 2018 to examine the parent materials' geochemical composition (Table 1). The irrigated soils also were collected in January 2018 on the University of Arizona campus to determine whether any geochemical changes are induced by increased water input. As the University of Arizona lies on mixed alluvium, the irrigated soils are compositionally mixed alluvium. To better compare the effect of increased water on desert soils, two different kinds of irrigated soil were collected: drip-irrigated and sprinkler-irrigated soils.

Funding through Colby College's DavisConnects program allowed for more samples to be collected in Arizona. As such, additional soil samples from the five summer sites were revisited and recollected in January 2018. Dr. Craig Rasmussen was available to visit these sites and identify the parent material. It is important to note that for many sites, especially the Saddlebrooke site that has mixed alluvium as parent material, it was nearly impossible to acquire representative samples of parent material. However, with Dr. Rasmussen's assistance, the best representatives for parent material were collected. For the second half of the excursion, irrigated soils were obtained from the University of Arizona campus. Two kinds of irrigated soils were acquired for the analysis and comparison: drip-irrigated and sprinkler-irrigated soils. Compared to sprinklers, drip irrigation uses a network of tubes to deliver water to plants and roots slowly to

reduce water loss through evaporation (Rasmussen, pers. comm. 2018). Both types of irrigation systems on the University of Arizona campus draw from retreated water (Rasmussen, pers. comm. 2018). In total, nine irrigated soil samples were collected, five from drip-irrigated sites and four from sprinkler-irrigated sites.

Laboratory Analyses

The elemental composition of each sample initially was analyzed in the laboratory with a portable x-ray fluorescence (pXRF) instrument (Thermo Scientific Niton™ XL3t GOLDD+ XRF Analyzer) at the University of Arizona (Appendix A). These analyses were necessary to determine whether the soil profiles differed based on their parent material's composition. In addition, electrical conductivity (EC) and pH were determined using Mettler Toledo's SevenCompact™ Duo S213 pH/Conductivity Meters, and loss on ignition (LOI) for each sample (Table 1; Fig. 3). Water, KCl, and $CaCl_2$ washes were used to acquire the pH and EC values of each soil horizon (Table 1). These three compounds were used for the washes, as they are standards for soil pH and EC comparisons (Rasmussen, pers. comm. 2017). However, for the purposes of the current study, the pH and EC values obtained from the water wash are used for comparison because water is a more common and, thus, relatable compound for understanding the pH and EC comparisons (Fig. 3). These tests also helped determine if the parent material controls other chemical properties of the soil profile, such as the Ca, Fe and Si concentrations (Fig. 4). However, there had to be an accurate method to determine the degree to which the soil profiles were influenced by parent material versus atmospheric dust, which is the most favored mechanism for the formation of calcic soils in SEAZ. Thus, dust input was calculated by comparing Ti:Zr ratios from the pXRF data for dust-and-parent material (Fig. 5; Appendix A). Dust input was also recalculated using the larger Ti:Zr ratios from the XRF data.

Ti and Zr are immobile index elements, and any increase in these elements is considered to be the result of dust deposition (Rasmussen, pers. comm. 2017; Stiles et al., 2017). The Ti-Zr ratios against which geochemical comparisons are made are based on Lybrand's unpublished data on the spectral reflectance of the Santa Rita Experimental Range soils (Rasmussen, pers. comm. 2017). Moreover, only percent change and molecular weight values were used to calculate the Ti:Zr ratios. This protocol was used because Lybrand's unpublished data employed these methods to determine the dust input in soils, and, as such, the same method was followed in this study (Rasmussen, pers. comm. 2017).

A principal component analysis (PCA) was undertaken to determine which variables (including elemental composition, pH, EC, etc.) were linearly uncorrelated and, thus, were distinct for each of the four parent material classifications (Fig. 6; Table 1). The program R was used to perform the PCA and run a regression of the variables. This allowed the parent materials to be easily separated and compared to each other based on the variables employed. PCA results allowed geochemical differences to be identified between the calcic horizons based on parent material.

These pilot-project data were all obtained from the pXRF analyses during June and July 2017, and they lacked confirmation from laboratory instrumental analysis. Thus, the soil profiles were also analyzed using Colby College's M4 TORNADO XRF instrument, which has been proven as a reliable analyzer of the elemental composition of soils, rocks, and other materials (Bonizzoni et al., 2013; Craig et al., 2007). To analyze the loose-soil samples, one-sided sticky tape was used to pick up the fine (sieved to <2 mm) components of the soils, while thin pieces of tape were used to adhere the back side and edges of the tape of soil to the M4 TORNADO's retractable platform. In addition, the number of sampling points at which elemental values were

the most reliable (i.e., the least variation in a sample) was determined by running experiments at 50, 100, 150, 200, 250, and 300 gridded sampling points. The gridded rectangles analyzed by the XRF were between 25,000 and 50,000 microns^2 in area to maintain the comparability between each sample. However, at the lower-end of sample points (50, 100, and 150 points), elements including Fe did not vary in the data set, while others, including Ca, varied by two or more standard deviations. It is important to note that the spacing of the gridded sampling points varied within the area that was maintained at constant dimensions. This could account for some variability in the results, but, as demonstrated, the variation is relatively non-existent in immobile elements such as Fe and should be minor for the mobile elements.

Thus, the decision was made to examine four representative soil samples of each of the parent material using 200 points under two conditions: (1) using the sieved soil as it was sent from Dr. Rasmussen, and (2) using a sediment sample splitter and a mortar-and-pestle to homogenize the sample. The reasoning for the method was that the unhomogenized soils likely had grains of significantly different compositions which greatly affected and varied the signal. Yet, although there was some variation between the unhomogenized and homogenized soils' compositions, these differences were not significant. As such, it was determined that a high sample-point number, higher than 150 points, was necessary for the XRF analysis. Moreover, several Colby faculty raised questions about whether 100 or even 200 points was truly capable of capturing soil composition, so each sample was analyzed using no less than 300 points. Thus, all of the XRF analyses were run using 300 points and completed during January 2018, after the January trip to collect additional soil and parent material samples.

When comparing the standard deviations between the non-irrigated soils and their parent material, and between the irrigated soils and the non-irrigated soils, 1σ was usually sufficient to

indicate that the difference was significant. However, for cases where standard deviations of 2σ were preferred for increased accuracy, single-factor ANOVA tests were utilized (Appendix B). These tests were chosen because Excel, the program that the current study used to determine the standard deviations at 1σ, cannot easily calculate standard deviations at 2σ. Yet, single-factor ANOVA through Excel easily determined the significance of the standard deviations with its calculations of p values.

RESULTS

Parental Material

The four soil profiles examined for this study differ in their thickness and physical parameters which, in part, are the consequence of the parental bedrock. Each soil exhibits both an organic-rich and an enriched calcium-carbonate cemented horizon, although the exact depth in each soil profile differs for the latter feature. The upper horizons (mineral A-horizons) range in color from dark brown to reddish (10YR 5/3 to 5YR 4/6) (Appendix C). The lower horizons (enriched calcium-carbonate B-horizons) are white to light gray (7.5YR 8/1 to 10YR 7/1) (Appendix C). The location of the five soils are Saddlebrooke, Sentinel Peak, Santa Rita Mountains, Tucson Mountains, and Whetstone Mountains (Tables 1-5). A brief description of each soil profile follows.

The Sentinel Peak soil overlies a colluvial basalt parent and is approximately 2.77 m in thickness (Fig. 7A; Table 2). The top soil horizons are thin, gray (7.5YR 6/1) and light gray (10YR 7/1) mineral A-horizons wherein humus is mixed with rock clasts. Two calcium-carbonate enriched horizons, herein termed the B-horizon are separated by a well cemented B petrocalcic horizon restricting water and root penetration. The entire thickness of the B-horizon is 1.89 m, with the hardpan attaining a thickness of 93 cm. The petrocalcic horizon interval

occurs between a depth of 153 and 246 cm. The B-horizon is light gray (10YR 7/1), as is the Bx horizon. The underlying C-horizon is composed of unconsolidated basalt material, with clasts ranging from 0.5 to 2.0 cm in diameter.

The Santa Rita Mountain soil formed on limestone bedrock (Fig. 7B, Table 3). The maximum thickness at the sample locality is 190 cm. The top soil horizons are thin, dark grayish brown (10YR 4/2) and thick grayish brown (10YR 5/2) mineral A-horizons wherein humus is mixed with rock clasts. Non-woody roots with a diameter of 1 mm penetrate this interval. The calcium-carbonate enriched horizon, herein termed the B-horizon, is 92 cm thick. The B-horizon is white (7.5YR 8/1) and the underlying C-horizon is composed of unconsolidated limestone.

The Whetstone Mountain soil also formed on limestone bedrock (Fig. 7C, Table 4). The maximum thickness of the locality where sampled is 200 cm. The top soil horizons are grayish brown (10YR 5/2) and thicker light gray (10YR 7/2) mineral A-horizons wherein humus is mixed with rock clasts. Non-woody roots with a diameter of 1 mm penetrate this interval. The calcium-carbonate enriched horizon, herein termed the B-horizon, is 92 cm. The B-horizon is very pale brown to light gray (10YR 8/2 and 10YR 7/2). The underlying C-horizon is composed of unconsolidated limestone, with clasts ranging from 0.5 to 3 cm in diameter.

The Tucson Mountain soil formed on rhyolite/andesite bedrock (Fig. 7D, Table 5). The maximum soil thickness of the locality where sampled is 304 cm. The top soil horizons are thin, dark brown (10YR 5/3) and thicker light brown (7.5YR 6/3) mineral A-horizons wherein humus is mixed with rock clasts. Creosote bushes and non-woody roots with a diameter of 1 mm penetrate this interval. The calcium-carbonate enriched horizon, herein termed the B-horizon, is 170 cm and is light gray (10YR 7/2). The underlying C-horizon is composed of unconsolidated rhyolite/andesite material, with clasts ranging from 0.5 to 2 cm in diameter.

The Saddlebrooke soil formed on mixed alluvium (Fig. 7E, Table 6). The maximum thickness at the locality where it was sampled is 400 cm. The top soil horizons are thin very dusky red (2.5YR 2.5/2) and yellowish red (5YR 4/6) mineral A-horizons wherein humus is mixed with rock clasts. Roots penetrate these horizons and creosote bushes colonize the side of the outcrop. The calcium-carbonate enriched horizon, herein termed the B-horizon, is 245 cm and is white (7.5YR 8/1). The underlying C-horizon is composed of unconsolidated mixed alluvium material, with clasts ranging from 1 to 7 cm in diameter.

Irrigated Soils

Soils sampled from both irrigated and non-irrigated sites are 15-20 cm in thickness due to the constraints of obtaining profiles on the University of Arizona campus. The nine soils all represent the mineral A-horizon, and their coloring ranges from brown (10YR 5/3) to very dark grayish brown (10YR 3/2) (Fig. 8; Appendix C). Small pebbles were abundant in the drip-irrigated soils, while roots and aerial debris of grasses were present in the sprinkler-irrigated soils. Furthermore, many of the drip-irrigated soils had pockets of calcium-carbonate glaebules.

Parent and Soil pXRF and XRF Data

The compiled soil data are the result of pXRF analyses during June and July 2017, and XRF analyses of January 2018. Instrumental data include Mg, Al, Si, P, S, K, Ca, Ti, Cr, Mn, Fe, Zn, Rb, Sr, and Zr with a sampling grid strategy of 300 points using the M4 TORNADO. Major elements comprising a significant portion of the soil, 20% to >50%, are described in the following text. Trends were examined between the parent material types, as well as the pXRF and XRF data, through scatterplots and bar charts.

Basaltic Soil (Sentinel Peak)

pXRF

The hand-held instrument was used on site during summer 2017 to analyze elemental concentrations of the soil formed on basaltic parent material. These soils have mean values of 0.35% Mg, 0.43% Al, 3.90% Si, 17% Ca, 0.22% Ti, 1.80% Fe, and 0.01% Zr (Appendix A). A comparable data set is not available for the Sentinel Peak basaltic bedrock (parent material). The pXRF instrument was unavailable in January 2018 when the site was resampled. Hence, only instrumental XRF data are presented below.

XRF

Soils originating from the basalt-parent material exhibit the same dominant fractions throughout the profile, with mean values of 24% Si, 5.40% Al, and 1.50% Fe (Appendix D). The soils also contain mean values of 3.60% Mg, 19% Ca, 0.40% Ti, and 0.01% Zr (Appendix D). Geochemistry of the basalt-parent material is dominated by Si, Al, and Fe, with mean XRF values of 27% Si, 10% Al, and 6.00% Fe (Appendix D). The parent material also is characterized by mean values of 1.10% Mg, 5.50% Ca, 0.89% Ti, and 0.06% Zr (Appendix D). Only the Ca values varied by a factor of 2.4 between the parent material and the overlying soils.

Limestone Soil (Santa Rita and Whetstone)

pXRF

Soils originating on the limestone-parent material have mean elemental values of 0.35% Mg, 0.43% Al, 3.9% Si, 16.5% Ca, 0.18% Ti, 1.76% Fe, and 0.01% Zr (Appendix A). Geochemistry of the limestone-parent material is characterized by mean elemental values of 0.26% Mg, 0.31% Al, 4.20% Si, 7.70% Ca, 0.27% Ti, 2.50% Fe, and 0.02% Zr (Appendix A). The limestone-parent material's composition compares well with the soils' composition.

However, the soils' Ca concentrations vary compared to the parent material's Ca value by a factor of 2.1.

XRF

Soils originating above the bedrock have similar compositions throughout their profiles, with mean values of 20% Si and 26% Ca (Appendix D). These soils also contain mean values of 2.00% Mg, 5.50% Al, 0.38% Ti, 1.80% Fe, and 0.01% Zr (Appendix D). Geochemistry of the limestone-parent material is dominated by Ca and Si, with mean values of 29% and 8.10%, respectively (Appendix D). The parent material also contains mean values of 2.50% Mg, 7.90% Al, 0.46% Ti, 2.10% Fe, and 0.07% Zr (Appendix D). Ca values compared between the parent material and the overlying soils are the only values that greatly differ, as they deviate by a factor of 2.4.

Rhyolitic Soil (Tucson Mountains)

pXRF

The hand-held instrument was used on site during summer 2017 to analyze elemental concentrations of the soil formed on rhyolite parent material. These soils have mean values of 0.35% Mg, 0.34% Al, 4.30% Si, 14% Ca, 0.18% Ti, 1.80% Fe, and 0.02% Zr (Appendix A). A comparable data set is not available for the Tucson Mountains rhyolitic bedrock (parent material). The pXRF instrument was unavailable in January 2018 when the site was resampled. Hence, only instrumental XRF data are presented below for the bedrock samples.

XRF

Soils originating from the rhyolitic parent material have the same composition throughout their soil profiles, with mean values of 1.90% Mg, 6.40% Al, 22% Si, 22% Ca, 0.37% Ti, 2.00% Fe, and 0.02% Zr (Appendix D). Geochemistry of the rhyolite-parent material is dominated by

Si, Al, and Fe with mean values of 33% Si, 7.70% Al, and 3.10% Fe (Appendix D). The parent material also is characterized by mean values of 1.70% Mg, 0.90% Ca, 0.50% Ti, and 0.03% Zr (Appendix D). Many of the elemental trends in the parent material appear consistent with the soils (Appendix D). However, Ca concentrations in the soil are much higher, by a factor of 25, compared to the parent material's low Ca value.

Alluvial Soil (Saddlebrooke)

pXRF

The hand-held instrument was used on site during summer 2017 to analyze elemental concentrations of the soil formed on rhyolite parent material. These soils have mean values of 0.38% Mg, 0.27% Al, 1.50% Si, 21% Ca, 0.18% Ti, 1.90% Fe, and 0.01% Zr (Appendix A). A comparable data set is not available for the Saddlebrooke mixed alluvium (parent material). The pXRF instrument was unavailable in January 2018 when the site was resampled. Hence, only instrumental XRF data for the parent material are presented below.

XRF

Soils originating on the mixed alluvium do not show the same dominant elemental distribution, as considerable variability exists within the soil profile (Appendix D). Thus, standard deviations have been added to the following mean elemental values to highlight this variance. The Si, Al, and Ca mean values in the soil are 12% Si ± 10 (1σ), 5.00% Al ± 5.00 (1σ), and 40% Ca ± 25 (1σ), respectively (Appendix D). In addition, mean values of 1.40% Mg ± 0.35 (1σ), 0.29% Ti ± 0.25 (1σ), 2.20% Fe ± 0.24 (1σ), and 0.02% Zr ± 0.003 (1σ) are found in these soils (Appendix D). Geochemistry of the mixed-alluvium parent is dominated by Si and Al, with mean values of 31% and 9.20%, respectively (Appendix D). The parent material also contains a

low Ca value of 4.0% and is characterized by mean values of 2.40% Mg, 2.20% Ti, 2.20% Fe, and 0.01% Zr (Appendix D).

Non-Irrigated Soil Profile Trends

Down-profile trends in the four different SEAZ soils show similar features in both pXRF and XRF data (Figs. 9-16, 17-23). However, the difference between pXRF and XRF values are notable. For example, the XRF data have consistently higher Al, Si, and Ca values, whereas the pXRF data show slightly higher proportions of Zr. Moreover, the difference for K in the XRF data represent a 1.1 fold increase, Ca values show a 1.4 fold increase, Mg values show a 5.3 fold increase, Si values show a 4.5 fold increase, and Al values show a 15 fold increase (Table 7). In the case of more immobile elements, values for Ti show a 1.84 fold increase, values for Fe show a 0.18 fold increase, and values for Zr show a 0.08 fold decrease in the XRF data (Table 7). For a few samples, the Ca values varied significantly based on the 300-point analysis; these ranged from a 0.1 to a 1 fold increase (Appendix E). The Ti and Zr ratios, based on the XRF data, are much higher, by a factor of 1.1, than the summer pXRF pilot-project data (Figs. 5, 16). A full comparison between the mean values obtained using both pXRF and XRF instrumentation for major elements can be found in Table 7 and in Appendix E.

Irrigated Soil Trends

Analyses of drip-irrigated and sprinkler-irrigated soils exhibit the same elemental trends down the profile of the mineral A-horizon (Figs. 17-23). For example, the values for Si and Fe in both drip-irrigated and sprinkler-irrigated soils are non-significant, because the standard deviation for each encompasses the mean value for the other system (Figs. 18, 20). Yet, intriguingly, Fe values for drip-irrigated soils vary considerably when compared to sprinkler-irrigated soils (Fig. 21). The drip-irrigated soils' Fe values range from 1.93% to 5.94% ± 1.68

(1σ), while the values of sprinkler-irrigated soils' Fe are more constrained, from 2.40% to 2.87% ± 0.21 (1σ; Fig. 21). However, a few elements are significantly different when the drip-irrigated soils and the sprinkler-irrigated soils are compared. For Ca, the drip-irrigated horizons have an average value of 4.29% Ca ± 1.75 (1σ), while the sprinkler-irrigated have an average value of 6.07% Ca ± 1.65 (1σ; Fig. 19). Also, the Al value in the drip-irrigated soils average 9.07% Al ± 0.41 (1σ), while the average sprinkler-irrigated soils is 8.28% Al ± 0.33 (1σ; Fig. 17). Ti values are low and comparable between the drip- and sprinkler irrigated soils (0.0446% Ti versus 0.0462% Ti) and both have standard deviations greater than 1 (Fig. 20). Moreover, the drip-irrigated soils have an average value of 0.014% Zr ± 0.001 (1σ), while the sprinkler-irrigated soils had a narrower range of Zr values, with an average value of 0.0096% ± 0.002 (1σ; Fig. 22). Furthermore, the Ti:Zr ratio between the drip- and sprinkler-irrigated soils is quite disparate. The drip-irrigated soils' mean Ti:Zr ratio is 32.0 ± 18.7 (1σ), while the sprinkler-irrigated soils' mean Ti:Zr ratio is 48.3 ± 18.0 (1σ; Fig. 23). Although the mean ratios of both soils fall within the other group's standard deviation, the overlap of standard deviation is minimal.

Parent Material vs. Originating Soil Geochemistry

Scatterplots were used to assess the comparability of the soil-profile data between samples as well as their parent material. The rhyolite-derived soils (from the Tucson Mountains) overlap the plots of soils of basaltic origin (Sentinel Peak) and limestone origin (the Santa Rita Mountains and the Whetstone Mountains) (Figs. 24-27). All three soil types differ from the alluvial soil data set (Figs. 24-27).

The limestone soils overlap the plots of the igneous soils of basalt-and-rhyolite origin with respect to their Fe and Ca values (Fig. 24). However, the limestone soils overlap with the rhyolite soils with respect to Al and Ca, while the basalt soils separated from this group based on

their Al values (Fig. 25). Similarly, the limestone-derived soils plot separately from the basalt-derived soils based on Ti concentrations, whereas rhyolite-derived soils plot between these two soil types (Fig. 26). The limestone and igneous-derived soils are comparable with respect to Si concentrations (Fig. 27). Moreover, although the soil elemental values of Fe, Al, Ca, Si, and Ti did separate from the parent material, the parent material, in some instances, plotted near the soil data fields (Figs. 24-27).

The basaltic soils are depleted in Fe and enriched in Ca when compared with the basalt parent material (Fig. 24). In contrast, limestone soils are generally similar in Fe values but are enriched in Ca when compared with the limestone parental rock (Fig. 24). Rhyolite soils are slightly depleted in Fe and enriched in Ca when compared with the rhyolite parental bedrock (Fig. 24). There are two different clusters of elemental data for the mixed alluvium soils (Fig. 24). One cluster exhibits an enrichment in Fe, only, whereas a second data set is slightly depleted in Fe and enriched in Ca (Fig. 24).

Comparing the Al versus Ca concentrations, the basalt-derived soils soils are depleted in Al and enriched in Ca when compared to these elements in the basalt parent material (Fig. 25). Al values of limestone-derived soils are depleted in some cases, whereas all samples show an enrichment in Ca (Fig. 25). A similar trend is found for soils formed on rhyolitic parent material (Fig. 25). And, similar to the plots of Fe:Ca (Fig. 24), there are two distinct groups of mixed alluvial soil data (Fig. 25). One group shows a slight enrichment in Al but no enrichment in Ca (Fig. 25). In contrast, the second group shows depletion in Al along with enrichment in Ca (Fig. 25).

Regarding Ti and Ca concentrations, the basaltic soils are depleted in Ti and enriched in Ca relative to the basalt parent material (Fig. 26). In contrast, limestone soils are generally

similar in Ti values but are enriched in Ca when compared with the limestone parental rock (Fig. 26). Rhyolite-derived soils are slightly depleted in Ti and enriched in Ca when compared with the rhyolite parental bedrock (Fig. 26). Similar to the Fe:Ca and Al:Ca plots (Figs. 24-25), there are two different clusters of elemental data for the mixed alluvium soils (Fig. 26). One cluster exhibits a slight Ti enrichment and depletion in Ca compared with the alluvial parent material, whereas the second data set is depleted in Ti and enriched in Ca (Fig. 26).

The Si versus Ca bivariate plot depicts that the basaltic soils are slightly depleted in Si and enriched in Ca when compared to these elements in the basalt parent material (Fig. 27). Si values of limestone-derived soils are depleted, and their Ca values are enriched relative to the limestone parent material (Fig. 27). A similar trend is found for soils formed on rhyolitic parent material (Fig. 27). Again, there are two distinct groups of mixed alluvial soil data (Fig. 27). One group shows a slight depletion in Si but no enrichment in Ca compared with the alluvial parent material (Fig. 27). In contrast, the second group shows depletion in Si along with enrichment in Ca relative to the alluvial parent material (Fig. 27).

DISCUSSION

Three pressing questions arise from the data. (1) How well do pXRF soil analyses align with XRF soil analyses, and why do these trends occur? (2) Do the data support Fischer et al.'s (2017) conclusion that the geochemical composition of calcic soils is influenced by their parent material, in addition to dust input? And, (3) do the data clearly indicate that irrigation has significantly altered the geochemical composition of calcic soils? Thus, the discussion section will fully address these concerns by fully examining the data and incorporating the findings of other relevant studies.

pXRF vs. XRF Analyses

Since the advent of portable x-ray fluorescence, researchers have desired to utilize this efficient and low-cost instrumentation and determine whether it could become a reasonable counterpart to the expensive and slow, but more detailed, XRF analyses conducted in the laboratory. Thus, several researchers in the last two decades have compared the accuracy between the two instruments to determine if pXRF could serve as a reliable tool in the field (Potts et al., 1995; Clark et al., 1999; Moioli and Seccaroni, 2000; Kilbride et al., 2006). Craig et al. (2007) and Bonizzoni et al. (2013) found consistent trends between elemental data obtained from obsidian and brick artifacts, respectively, although they noted that results from the two instruments give significantly different elemental values. In contrast, Chakraborty et al. (2017), citing Zhu and Weindorf (2009) and Weindorf et al. (2013), found a high degree of comparability between the pXRF and XRF-derived values of Ca and gypsum in soils. Yet, although there seems to be general agreement that pXRF and XRF instrumental analyses for rocks and other archeological relics are comparable, soils have remained excluded. A few studies, including Clark et al. (1999) and Kilbride et al. (2006), have attempted to use pXRF data to determine the concentration of metal contaminants in soils.

Although studies have found comparable results exist between the pXRF and XRF instruments in detecting the metal contaminants, they did not focus on whether pXRF instruments can accurately measure the bulk geochemical composition of soils. Thus, Chakraborty et al. (2017) used pXRF analyses to see whether the instrument could distinguish the subtle elemental differences between the six stages of carbonate-soil development in the Southwestern U.S. Their study focused specifically on arid and semiarid regions of New Mexico, Texas, Kansas, and Colorado. From their analyses, Chakraborty et al. (2017) found that the

pXRF could not distinguish the difference between primary and secondary Ca in soil. In addition, they reported that pXRF data sometimes exhibited a wide variation in the Ca content. Despite these limitations, they found that 83.3% of stage I samples, 83.3% of stage II samples, 91.03% of stage III samples, 91.66% of stage IV samples, 60% of stage V samples, and 33.33% of stage VI samples were correctly identified as stage I, II, III, IV, V and VI, respectively. Thus, Chakraborty et al. (2017) concluded that pXRF gave "satisfactory" results and determined that pXRF can accurately measure the increase in Ca concentration with the increase in calcium-carbonate development stage.

These studies confirmed that pXRF and XRF analyses were comparable and suggested that similar correlative results would be seen in the current study on SEAZ soils. However, the data from the current study challenge this notion. Although pXRF data of each major element traced through the soil profiles follow the same, or similar, trends as those determined using XRF, individual elemental values are not the same (Figs. 9-16). Data from the current study reveal that pXRF largely underrepresents the values of major elements (Table 6). While differences in the values of the more immobile elements (Ca, Fe, and Ti) are only less than two times lower (or higher in the case of Zr), the mobile elements (Mg, Al, Si, and K) show the lowest values, which are 2.2 times lower for K to 15 times lower for Al values when compare to the laboratory XRF (Table 6). Figures 9-16 emphasize this disparity. The pXRF values for the major elements, which do generally follow the trends of the XRF data, plot as lower values when compared with the XRF values on all scatterplots (Figs. 9-16). As a consequence, trends of the pXRF data are diminished when compared with the trends using the XRF values. This is evident in the Al, Si, and Ca scatterplots, which reveal very erratic trends between the pXRF and XRF

data (Figs. 10-12). Despite these apparent differences, the immobile elements parallel and overlap the XRF data to a greater degree than the mobile elements (Figs. 13-16).

Why might there be such a notable difference between the values derived using either method, especially with respect to the mobile elements? The duration of the analyses, the size of the analytical window, and the energy of the instrument (in electron-volts) may best explain these differences. Soils used in both analyses were the same; both samples were sieved to remove large pebbles or material >2 mm which could interfere with the results. However, the handheld Thermo-Scientific pXRF instrument takes a four-minute snapshot of the elemental composition of the soil across a 3-mm diameter window, while the M4 TORNADO runs a 3-hour test of the elemental composition of the soil across 300 separate points at a 25-micron diameter scale. Moreover, there are notable differences in energy between the instruments. pXRF has a *maximum* energy output of 185 eV, whereas XRF has a *minimum* energy output of 145 eV. In fact, XRF usually has an energy output several factors greater than pXRF. With respect to both of these factors, it is possible that the larger soil particles may be overrepresented, skewing the data to diminish the major elements present in the soil. In contrast, the XRF analyses can fully distinguish between small and larger grains and average these differences together. Thus, it is largely because of the averaging of the XRF's 300 point analyses, of which the pXRF lacks, that ensures the higher accuracy of the acquired data.

This explanation is further confirmed based on XRF data obtained when the analytical grid was less than 300 points. The current study examined the variations in elemental values between 50, 100, 150, 200, and 250 point analyses before data were collected using the 300-point strategy. The 50-point data set showed the most variability between the major elements, while the 250-point data set showed the least amount of variability (Appendix E). For instance,

soil #2358 (Tucson Mountains, rhyolite-derived soil from the B-horizon) was evaluated using counts of 50, 100, 150, 200, 250, and 300 points. Ca values of the sample were 23.73% ± 5.69% (1σ), 24.68% ± 4.23% (1σ), 24.1% ± 4.91% (1σ), 24.16% ± 3.67% (1σ), 24.00% ± 2.79% (1σ), and 24.14% ± 3.83% (1σ), respectively (Appendix E). Although one might conclude from these data that a 200 point-count total is as good as the 300-point strategy utilized in this study, only Ca concentrations at 200 point-counts compared well with the 300 point-count. 300 point-counts were needed to reduce the amount of variability in the soil's other elemental values. From these data, one can observe how the Ca concentration focuses around the higher number of points chosen for the analysis, with the largest deviations of approximately ± 4.00-6.00% occurring under the conditions of the least number of points analyzed (50, 100, and 150 points). Yet, these differences are minimal when compared to the value of 14.16% ± 0.128% (1σ) Ca for soil #2358 obtained using the pXRF, which is a value that is approximately 70% less (Appendices A and E). These data highlight the fact that the more points that are analyzed over a longer period of time, results in a more accurate data set. Thus, although pXRF analyses can be useful for determining the initial elemental trends in a soil profile, pXRF cannot replace XRF elemental analyses for distinguishing and determining the true chemical differences in, and the compositions of, the soils.

Chakraborty et al. (2017) concluded that pXRF and XRF data were comparable for calcium-enriched soils when they evaluated the six stages of calcium-carbonate development in soils (Machette, 1985). As such, they were interested primarily in the increasing Ca content trends associated with increasing calcification. These authors were not interested in a detailed analysis of the elemental spectra of the soils, unlike this study. In addition, they used vector-machine analyses on the soil and the soil aggregates (e.g., soil particles that bind together) to

support their observations of the calcium-carbonate development stages in the soils. Support vector machine (SVM) analyses utilize models that include learning algorithms (Chakraborty et al., 2017). This allows the models to classify the data into groups and run regressions to analyze the data (Chakraborty et al., 2017). Chakraborty et al. (2017) used the SVM analyses for quadratic programming on a subset of the samples. The result is a SVM classification plot that can compare the soil and the soil aggregates to Machette's (1985) six stages of calcic soil development (Chakraborty et al., 2017). With this plot, Chakraborty et al. (2017) confirmed the classification of each sample's developmental stage and compared these classifications with the pXRF data classifications. Thus, the question addressed by Chakraborty et al. (2017) did not require highly precise measurements of the Ca content in these soils to determine the increasing Ca trends. The soil trends could be explained satisfactorily using results from their pXRF analyses.

Soil studies that require an accurate assessment of a soil's elemental composition cannot rely solely on pXRF analyses. Values obtained in the field using a handheld portable device must be crosschecked with other instruments including both XRF and XRD. Thus, future studies designed to rely on pXRF analyses to measure the elemental compositions of soils should be done with caution. The current study demonstrates that pXRF data can depict the general elemental trends of a soil profile. However, these data are not obtained at high resolution because they report lower values for the major elements when compared with laboratory XRF analyses.

Bedrock vs. Soil Geochemistry

Based on the pilot project of Fischer et al. (2017), there were clear indicators that the bedrock (parent material) affected the composition of the overlying soils (Appendix A). PCA results show a clear separation between soil horizons derived from limestone-parent material and

soil horizons derived from volcanic parent material (Fig. 6). Moreover, the Ti:Zr scatterplots proved that dust was not the only factor in controlling the geochemical properties of soils in arid and semiarid regions (Fig. 5; Table 1). This conclusion is contrary to that which was previously believed. While several soil horizons did plot close to the calculated dust-indicator line, others deviated away from the line, indicating that additional factors, including parent material, affect the formation and composition of these soils. These conclusions about the geochemical differences between the soil profiles were drawn exclusively from pXRF data, with a limited number of samples and parent material equivalents. The current study demonstrates that relying solely on pXRF analyses is questionable, requiring these samples to be reanalyzed to determine whether conclusions drawn from the pilot project data are accurate. Thus, to effectively measure geochemical differences between the soils, samples were grouped based on their data. Moreover, pH and EC measurements, calculated Ti:Zr ratios, and bivariate plots of elemental composition were utilized to determine if the geochemical properties of the soils were directly connected to, and likely derived from, their parental bedrock.

The pilot project acquired pH and EC values of the soil horizons in the hopes of revealing any indication of a significant geochemical contribution from the parent (Fig. 6; Table 1). However, the pH and EC values show that the soil horizons originating on the four parent materials (basalt, rhyolite, limestone, and mixed alluvium) are not significantly different, given the data's large standard deviations (Fig. 6; Table 1). The soils from these parent materials have similar basic pH values, and their EC standard deviations overlap (Fig. 6; Table 1). The only point of potential interest is that the volcanic-derived soils (basalt and rhyolite) have noticeably lower EC values compared to the limestone and alluvial soils (Fig. 6). Otherwise, the parent material does not largely influence the overlying soils' pH and EC properties.

It can be seen that the Ti:Zr ratio of the four soil types differs dramatically not only between the parent rock and the overlying soils, but also down each soil profile (Fig. 16). The Ti:Zr ratio is used to infer whether calcium was introduced in SEAZ soils via eolian dust (Lybrand, unpublished data). Using Lybrand's unpublished data, the study determined that Ti:Zr ratios greater than 61 are indicative of calcium enrichment as a function of dust input, whereas ratios below this "dust line" are interpreted to have other factors that contribute more strongly to their formation (Fig. 16). The only soils where a significant dust enrichment is identified occurs in the volcanic-derived soils (Sentinel Peak basalt and Tucson Mountain rhyolite), where enrichment is seen in both the upper and lower sections of their soil profiles, as these horizons plot close to, or even extend beyond, the dust line (Fig. 16). This indicates that dust strongly influences their geochemical composition. In fact, if the horizon plots close to the line, then dust likely influenced the majority of its geochemical signature, and if the horizon extends past the dust line, then dust input likely controlled nearly all of the horizon's geochemical composition (Rasmussen, pers. comm. 2018). Conversely, the volcanic-derived soils' middle horizons were not largely influenced by dust input, as these ratios plot farther from the dust line (Fig. 16). In addition, neither the limestone nor mixed alluvium soils appear to have a large dust signature anywhere in their profiles (Fig. 16). Thus, by examining bivariate plots of both elemental soil composition and the Ti:Zr dust fractions, it can be seen that the XRF data confirm that the soil geochemistry is influenced, partially, by the parent materials' composition (Figs. 16, 24-27).

When soil data are plotted based on their parent materials, it can be seen that most soils lie in relatively discrete fields (Figs. 24-27). Soils derived from one parent material generally or exclusively plot close together (Figs. 24-27). The basalt, limestone, and rhyolite data fields consistently plot at the center of these figures, whereas the outliers at the high and low ends

represent the two data fields of mixed alluvium (Figs. 24-27). Soils from the Santa Rita and Whetstone Mountains, formed on limestone, plot in a single data field and separate from the parent (Figs. 24-27). Elemental values of soils derived from rhyolite-precursor rock plot with, and overlap, limestone soils (Figs. 24-27). And, soils formed from basalt, in general, plot in a field that overlaps the lower values of both the limestone and rhyolite data. The one soil type that does not conform to a single data field is the mixed alluvium. Here, two discrete data fields are identified on all bivariate plots, and neither field overlaps the geochemistry of the parent. However, there are a couple of exceptions to these data field groupings. One exception is sample #2353 from the mineral A-horizon of the Tucson Mountains (Appendix D). Intriguingly, sample #2353 plots separately from the rhyolite data field and consistently near the rhyolite parent (Figs. 24-27). Yet, this sample also has a large amount of dust input (Fig. 16). These two findings seemingly contradict each other, but the best explanation is that, perhaps, the soil sample coincidentally has a similar composition to the parent, as most of its composition is derived from dust influence. The other exception is sample #2398 from the B-horizon of Saddlebrooke (Appendix D). Although sample #2398 plots near the mixed alluvium soil horizons that are enriched in Ca, it consistently lies outside of this data field because of its lower Ca concentration and higher values in the other major elements (Figs. 24-27). Thus, sample #2398 was not included in either of the two mixed alluvium data fields because of its distinct geochemical differences (Figs. 24-27). In all cases, elemental values of soils derived from these parent materials do not overlap those of their parent rock.

The volcanic-derived basalt-and-rhyolite soils have clear geochemical similarities when compared to the limestone-derived soils. In many of the bivariate plots, rhyolite-derived soil data lie amongst the fields of the basalt and limestone soils (Figs. 24-27). In addition, the rhyolite

soils compare closer to the limestone-derived soils in their Mg (Fig. 9) and Al (Fig. 10) values than to the basalt-derived soils (Fig. 25). Al in the soils is so low as to plot close to all of these soil types based on pXRF data (Fig. 10). When the XRF data are compared, the basalt values plot closer to the limestone than the rhyolite (Fig. 25). Yet, the basalt and rhyolite soils have similar pH and EC values that deviate from the limestone (Fig. 6). An explanation to these findings is that perhaps the soils are influenced by other factors besides parent-material composition and dust input. The pilot work by Fischer et al. (2017) opened the door to the possibility of other factors influencing the geochemical composition of desert soils in addition to the hypothesis of solely dust input (Batchily et al., 2003). Thus, the current study could reveal that while volcanic-derived soils do show similar geochemical variation, the rhyolite-derived soils overlap with the limestone soils because of other variables affecting their composition.

The rhyolite-, basalt-, and limestone-derived soils do show geochemical variations from their parent material's composition. Although the rhyolite-parent material plots somewhat near the rhyolite-derived soils and their data field, the soils have enriched Ca concentrations and depleted Al and Si concentrations compared to their rhyolite parent (Figs. 24-27). These enriched Ca values can be explained by Ca leaching from the soil and solidifying as a thin layer on the underside of the soil grains (Rasmussen, pers. comm.). Moreover, the rhyolite parent only truly plots extremely close to soil #2353 from the Tucson Mountain's mineral A-horizon (Figs. 24-27). The limestone parent material also plots near the limestone-derived soils and their data field; yet, the limestone-derived soils have enriched Ca concentrations, slightly depleted Al values, and depleted Si concentrations compared to their limestone parent (Figs. 24-27). The basalt parent bedrock was the only parent that did not consistently plot near the basalt-derived soils and their

data field (Figs. 24-27). Compared to the basalt parent, the basaltic soils were enriched in Ca and depleted in Fe, Al, and Ti (Figs. 24-27).

Considering these apparent geochemical similarities and differences, one could reason that the soils were not largely influenced by the underlying parent material during their formation. Yet, the rhyolite- and limestone-derived soils did not show any significant enrichment or depletion in their Fe and Ti concentrations compared to the parent (Figs. 24, 26). The basalt-derived soils also had similar Si values compared to the basalt bedrock (Fig. 27). Moreover, the basalt-derived soils' compositional differences could be attributed to the soils' large dust input. In the Ti:Zr ratio scatterplot from the pilot project, many of the colluvial basalt soil horizons plot very close to the dust line, compared to the other soil profiles originating on different parent materials (Fig. 5). The basalt-derived soils' close proximity to the dust line indicates that many of the horizons received significant eolian dust input during their formation, which could alter their basaltic geochemical compositions over time and result in the soils to having compositional differences from the basalt parent (Fig. 5).

The current study's XRF data and its Ti:Zr ratios for the soil horizons also support that the basalt-derived soils received a significant amount of dust contribution (Fig. 16). Many of the lower basalt-derived soil horizons plot close or past dust line, indicating that dust input contributed the most to these horizons' formation (Fig. 16). And, because the upper horizons did not receive a significant amount of dust input, this reveals that the basalt parent material or other factors likely influenced these horizons and their formation (Fig. 16). The rhyolitic and limestone-derived soils were moderately influenced by dust input during their formation, although dust significantly influenced the upper horizons of the rhyolite-derived soils (Fig. 16), and their elemental compositions vary somewhat from their parent regarding their Ca, Al, and Si

concentrations (Figs. 25, 27). Yet, the rhyolite- and limestone-derived soils did not vary in their Fe and Ti concentrations from their parent (Figs. 24, 26). Considering the moderate influence from dust and geochemical similarities, parent material does still control the composition of these soils to some degree. The only difference is that perhaps the pilot project's pXRF data overemphasized the impact the parent material has on the originating calcic soil. Thus, the XRF data from the current study demonstrate that the soils' geochemical properties are partially influenced by their parent materials' compositions.

As expected, the mixed alluvium soils showed the most variability, plotting separately from the rhyolite-, basalt-, and limestone-derived soils (Figs. 24-27). The mixed alluvium soil has high concentrations of Ca in greater than 50% of the soil samples, higher than even the limestone-derived soils (Figs. 24-27). One mixed alluvium data field has depleted Al and Si concentrations and slightly depleted Fe and Ti concentrations compared to other soil types (Figs. 24-27). However, the other data field has enriched Fe and Al values and depleted Ca values compared to the other soil types (Figs. 24-25). Moreover, these soils showed considerable variability within the profile, as the upper horizons had high concentrations of Fe, Al, Ti, and Si compared to the lower horizons, and as they had low values of Ca compared to lower horizons (Figs. 9-14, 24-27). However, the mixed alluvium parent plots closer to the upper mixed alluvium soil horizons that lie in the data field that is depleted in Ca (Figs. 24-27). This geochemical similarity confirms that the parent influences the formation of these alluvial soil horizons (Figs. 24-27). Although the parent material plots separately from the other alluvial soil data field, which represents the lower horizons of the soil profile, the parental bedrock does bridge the gap by plotting somewhat between the two mixed alluvium fields and the nonconforming sample #2398 (Figs. 24-27). Moreover, the mixed alluvium soil profile did not

receive a significant amount of dust contribution during its formation because the horizons' Ti:Zr ratios do not plot close to the dust line (Fig. 16). As such, these data indicate that the composition of the mixed alluvium soils are moderately controlled by their parent material, in addition to calcium-rich dust contribution that is dictated by atmospheric circulation patterns. Thus, the XRF data from the current study, when compared with the pXRF data from the pilot study, show that the calcic soils derived from basalt, rhyolite, limestone, and mixed alluvium and their geochemical properties are partially influenced by their parent material compositions.

The Effects of Irrigation

Numerous studies have focused on the effects of increased water input on soils, particularly on calcic soils, and these have found a change in the soil's geochemical composition from a consistent, long-term input of water (Adamson et al., 2015; Amit et al., 2010; McDonald et al., 1996; Monger, 2010; Pavich and Chadwick, 2004; Pfeiffer et al., 2012). These calcium-carbonate enriched soils in the arid to semiarid region of SEAZ, which are a function of a restricted water supply, should be prohibited from developing in irrigated settings (Adamson et al., 2015; Amit et al., 2010; Pfeiffer et al., 2012). Thus, one could reason that such calcic soils would degrade over time, losing calcium carbonate from the increased water supply penetrating these horizons and leaching the $CaCO_3$ from the soil, resulting in a change in their geochemical composition (Amit et al., 2010; McDonald et al., 1996; Monger, 2010). Thus, the current study attempts to examine how calcic soils geochemically respond to increased water input from human irrigation systems. By comparing the geochemical composition of mineral A-horizons between irrigated soils and non-irrigated calcic soils from the same general area (in-and-around Tucson, AZ), one can assess the degree to which water has affected their composition.

Additionally, it is important to understand if different irrigation methods significantly affect the geochemical composition of calcic soils.

The geochemical data acquired from the mineral A-horizons of the calcic soils irrigated by sprinklers or drip techniques do not deviate from each other with respect to geochemical composition (Figs. 17-22). Although elemental values from the sprinkler-irrigated soils have small standard deviations for Fe and Zr compared to the drip-irrigated soils (Figs. 21-22), these overlap with those of the drip-irrigated soils' standard deviations. This relationship also is true for elemental concentrations of Si, Ca, and Ti (Figs. 18-20). However, these soils differ in Al concentrations, as these data do not overlap (Fig. 17). It should be noted that the calculated standard deviations are only at 1σ. If recalculated for 2σ, the values may result in no significant Al variation between these two irrigated soil types. A single factor ANOVA test of Al variation resulted in p values less than 0.05 ($p = 0.02$) (Appendix B). This test indicates that the drip- and sprinkler-irrigated Al values are significantly different. However, in the context of the drip- and sprinkler-irrigated soils' overall similarity, the type of irrigation does not appear to significantly impact the geochemical composition of irrigated calcic soils over a timescale of decades.

This finding is quite intriguing because sprinkler-irrigation systems introduce more water per volume to soils when compared to drip-irrigation systems. In fact, sprinkler systems can easily introduce 300 gallons of water each hour, whereas drip irrigation usually only provides 1-4 gallons of water in one hour (Clark and Smajstrla, 1996; Ley, 1992). Considering this large difference in the volume of water that these irrigation systems discharge, one might expect there to be apparent geochemical differences in the calcic soils if water supply alters the soil composition. Yet, no significant geochemical differences are found in the mineral A-horizon between sprinkler- and drip-irrigated soils, and, perhaps, may indicate that water does not play a

large role in the geochemical composition of the upper horizon of these soils. However, to assess this hypothesis, one must compare the geochemical composition of these irrigated calcic soils to the composition of non-irrigated soils.

Both irrigated soils originated on mixed alluvium, and one should be able to compare the mixed alluvium soil from Saddlebrooke to the University of Arizona campus soils to determine if there is any clear indicator of irrigation influencing their geochemical composition. Figures 28-31 combine data of the drip- and sprinkler-irrigated soils (Figs. 17-19, 21) with the data from the mineral A-horizons from the four parent materials to yield a better comparison between the irrigated and non-irrigated soils. The large variability that exists within the mixed alluvium's geochemical composition is revealed when comparing its elemental values to the irrigated soils' values. Thus, the mean Al, Si, Ca, and Fe values of the mixed alluvial soils, which do differ from those of the irrigated soils, especially those of the sprinkler-irrigated soils, do not show a complete picture about the mixed alluvium versus the irrigated soils (Figs. 28-31). Instead, the mixed alluvium's mineral A-horizon shows large standard deviations for Al, Si, Ca, and Fe, which overlap with those of the drip-irrigated soils. In contrast, the standard deviation for Si and Fe of the mixed alluvial soils overlap with the standard deviation of the sprinkler-irrigated soils (Figs. 28-31). Yet, there is a significant difference between the drip-irrigated soils' and the mixed alluvium's Al value, as determined by an ANOVA single factor test ($p < 0.05$; $p = 0.02$; Appendix B). Except for the Al concentrations, the drip-irrigated soils are geochemically indistinguishable from the non-irrigated mixed alluvium soils, which indicates that a moderate increase in water volume since anthropogenic development does not significantly change the composition of these calcic soils.

There are notable differences in elemental values between the mixed alluvium and the sprinkler-irrigated soils, despite the mixed alluvium's high degree of variability. The standard deviations calculated for Al and Ca for sprinkler-irrigated soils do not overlap with the mixed alluvium's Al and Ca values (Figs. 28, 30). This is corroborated by an ANOVA single factor test for Al ($p < 0.05$; $p = 0.02$) and for Ca ($p = 0.05$) (Appendix B). Thus, although the sprinkler-irrigated soils share a similar geochemical composition to the non-irrigated and drip-irrigated mixed alluvium soils, they are not completely comparable to these soils. This indicates that the volume of water introduced into this soil type does affect the geochemical signature of these calcic soils to some degree. The data suggest that an increased volume of water over a short period of time is needed to begin to alter the non-irrigated soils' geochemical composition.

The chemical composition of the irrigated mixed-alluvium soils does not differ significantly from other SEAZ soils derived from volcanic rocks (Figs. 28-31). The drip-irrigated soils' mean Al, Si, Ca, and Fe concentrations and standard deviations all overlap with those elements in the basalt- and rhyolite-derived soils, whereas the sprinkler-irrigated soils' concentrations also overlap with the basalt and rhyolite data (Figs. 28-31). The only volcanic element that was significantly different when compared to the sprinkler-irrigated soils was the rhyolite's Ca concentration (Fig. 30). Yet, if we take into account the slight difference of the sprinkler-irrigated soils' Ca and the rhyolitic soils' Ca, along with the high comparability between their Al, Si, and Fe concentrations, then it is reasonable to conclude that the sprinkler-irrigated and drip-irrigated soils are not significantly different from the volcanic soil (Figs. 28-31).

In contrast, some variation exists between the irrigated and the limestone-derived soils' geochemistry. The drip- and sprinkler-irrigated soils' Al, Si, and Ca concentrations differ from

the limestone-derived soils' Al, Si, and Ca concentrations (Figs. 28-30). The standard deviation for Al and Si lies above those of the limestone soils, whereas Ca lies below that of the limestone's Ca (Figs. 28-30). The only comparable elemental value recorded for irrigated soils when compared to the limestone is Fe (Fig. 31). This indicates that the irrigated soils are not significantly different from the volcanic-derived top soils, while they are significantly different from the limestone-derived soils. However, considering that the irrigated soils originated on mixed alluvium, it is reasonable for these trends to exist. This is because the upper horizons of the non-irrigated mixed alluvium soils are not significantly different from the volcanic-derived top soils with respect to Al, Si, Ca, and Fe values, while they are significantly different compared to the limestone-derived soils with respect to their Al and Ca values (Figs. 28-31). Yet, the fact that the mineral A-horizons of the irrigated mixed-alluvium soil vary more than the limestone-derived soils compared to the non-irrigated mixed alluvium suggests that the geochemical differences between these may stem from the volume of water introduced into their soil systems.

One aspect of the current study that these bar charts highlight is that the mixed alluvium is derived from mountain ranges that vary in their bedrock composition. Thus, without any studies confirming the source(s) of the mixed alluvium at Saddlebrooke or soils in Tucson, it is hard to say whether the relationships between the irrigated soils and the basalt-, rhyolite-, and limestone-derived non-irrigated soils are reasonable. Are these irrigated soils derived from these parent materials, which would explain the similarity between their geochemical compositions? Or should one focus solely on the comparison between the mixed alluvium and the irrigated soils? If the former is true, then perhaps irrigation did not significantly impact the composition of the University of Arizona's mixed alluvium soils. However, if the latter is true, then irrigation plays a role in transforming the "typical" mixed alluvium characteristics of the Saddlebrooke

soil. Without this clear distinction, the effects of irrigation on desert soils will remain somewhat inconclusive. Yet, as the irrigated soil originated from mixed alluvium, there should be some degree of comparability with the non-irrigated mixed alluvium samples. Moreover, as the current study is comparing mineral A-horizons between the irrigated and non-irrigated mixed alluvium soils, any slight difference in the two locations' parent material should not greatly affect the data comparisons and conclusions.

Considering the major elemental trends and variances between the irrigated and non-irrigated mixed alluvium soils, and between the irrigated soils and the non-irrigated volcanic- and limestone-derived soils, some explanation must exist for why these trends occur. Assouline et al. (2016) found that increased water supply to calcic soils in Israel did cause a subsequent decrease in the Ca concentration. This compares somewhat well with the findings of the current study where Ca concentrations in irrigated soils are low when compared to the Ca-enriched limestone-derived soils (Fig. 30). However, the sprinkler-irrigated soils have higher Ca concentrations compared to the non-irrigated mixed alluvium, differing from Assouline et al.'s (2016) data (Fig. 30). One should expect that the water-rich, sprinkler-irrigated, mixed alluvium soils to have lower Ca concentrations compared to their non-irrigated counterpart; yet, this is not observed. However, the best explanation for these discrepancies is that although the University was founded in 1885, irrigation on the main campus grounds of the University of Arizona has only occurred over roughly 100 years or less (Rasmussen, pers. comm. 2018). Hence, the water source to these campus calcic soils is short-term. McDonald et al. (1996) found that increased water input into calcic soils over short-term timescales, which they determined were less than 100 years, had little impact on the carbonate distribution. Thus, McDonald et al.'s (1996) work indicates that short-term increases in water input is not enough to leach the carbonate from these

calcic horizons. However, they also discovered that long-term increases in water input, greater than 400 years, removed the calcium carbonate from the upper horizons. This indicates that these calcic soils have likely not been irrigated for a long enough time to see any drastic changes in their geochemical composition.

Given the fact that the irrigated soils have not received a long-term source of water input, might there be any effect on the CO_2 sequestered and/or released by these soils? Considering that calcic soils are significant carbon sinks, one could reason that an increase in water input, which would inhibit the production of $CaCO_3$, would impede the calcic soils' ability to sequester carbon (Amit et al., 2010; Monger, 2010; Zamanian et al., 2016). In the worst-case scenario, the carbon trapped in these calcic soils could be removed by percolating water to eventually mix with the atmosphere and exacerbate the CO_2 crisis of our warming planet (Zamanian et al., 2016). Thus, comparing the Ca concentrations of the irrigated soils with the non-irrigated soils would help to determine if there is any notable shift and/or decrease in the content due to increased water input. There is a clear decrease of Ca in the drip- and sprinkler-irrigated soils compared to the limestone-derived soils, which would be expected to store the most amount of Ca due to originating on calcium-carbonate enriched limestone (Fig. 30). However, there is no significant difference ($p < 0.05$) between the drip-irrigated and mixed alluvium soils regarding their Ca values (which have a p value of 0.2) (Appendix B). Yet, there is a slight significance difference between the sprinkler-irrigated and mixed alluvium soils regarding their Ca concentrations ($p = 0.05$) (Appendix B).

What is intriguing is that the Ca content increased in the irrigated soils relative to the non-irrigated mixed alluvium, which does not support the previous claims by Amit et al. (2010) and Assouline et al. (2016) regarding increased water content and decreased Ca and $CaCO_3$

content. This again brings up the concern of whether the mixed alluvium from Saddlebrooke originated from the mountain ranges and parent material(s) as the mixed alluvium in the center of Tucson. Although the two locations are in close proximity to each other (30 miles away), it is hard to know for certain without conducting a full geological analysis of these profiles. Yet, there should be some degree of similarity in their origin given their proximity. Thus, water does impact that geochemical composition of calcic soils. However, the rate of compositional alteration is slow, and, as this study indicates, greater than 100 years. Because the alteration is so slow, this could explain the discrepancy between the increased Ca content in the irrigated soils (McDonald et al., 1996). And, because the soils were collected in the beginning or middle of their alteration, the water has not enough time to alter and reduce their $CaCO_3$ concentrations.

The concentration of Ca in the irrigated soils that is similar to the mixed alluvium parent material indicates that any decrease in calcic soil carbon sequestration and increase in released CO_2 has not occurred within the last 100 years due to increased irrigation. As such, a longer amount of time (likely greater than 400 years) of consistent high-volume water input is needed to fully change the geochemical composition of these soils (McDonald et al., 1996). However, if humans continue to dwell in these unsustainable desert regions and introduce large amounts of water to the calcic soil system, we could expect a decrease in the CO_2 sequestered and a subsequent increase in the CO_2 released by these soils, which would further exacerbate climate warming.

CONCLUSIONS

Arid and semiarid areas, like Southeastern Arizona, have witnessed drastic increases in population since the 1900s. To sustain these booming communities, increased volumes of water have been redirected to provide needed drinking water and irrigation. However, soils in these dry

regions are calcium-carbonate enriched and are significant carbon sinks. Hence, there is reasonable concern that the addition of water to the soil system will alter their geochemical properties. This will likely prevent calcic soils from serving as carbon sinks and, potentially, allow the soils to release CO_2 into the atmosphere.

The formation and geochemical composition of SEAZ soils have been explained, in large part, by dust input. Yet, when Fischer et al. (2017) compared the geochemistry of calcic soils originating on different parent materials, they found that parent material influenced the geochemical compositions between soil types. However, these data were obtained using a hand-held pXRF, which has not been widely used for soil analyses. Thus, to determine whether their conclusions could be replicated, the calcic soils collected from four types of parent material (basalt, limestone, rhyolite/andesite, and mixed alluvium) were reanalyzed with the M4 TORNADO XRF.

Results from the current study indicate that the pXRF data follow the same or similar trends of the XRF data for each soil type. But, the recorded values from the pXRF are significantly lower for all major elements. Considering that the pXRF's data-collection time is quicker than the XRF's data-collection process (4 minutes versus 3 hours), its output energy is lower than the XRF's (pXRF's maximum 185 eV compared to XRF's minimum 145 eV), and its data analytical window is 100 times larger than the XRF's (3 mm versus 25 μm), the pXRF data will disproportionally measure the composition of the larger particles. This will inevitably skew the results to the composition of these large particles. This is of special concern when the material is heterogenous, as is the case with soil. Thus, one must exert caution when using pXRF analyses for soils and crosscheck these data values with other instrumentation. For future research, it would be ideal to assess the comparability between pXRF and XRF when using the

same analytical window or area of analysis, compared to the current study's use of a larger analytical window for XRF (25-50 mm) and a smaller area for pXRF (3 mm).

However, both pXRF and XRF data sets demonstrate that the parent rock influences the composition of calcic soils. Soils originating on the four different parent materials plot in similar data fields. Basalt-derived soils consistently plot separate from the limestone-derived soils. Although the rhyolite-derived data usually overlap with both the basalt and limestone data fields, the rhyolite-derived soil shows distinct geochemical differences. The basalt, rhyolite, and limestone parent material plots somewhat near their respective soils' data fields. The limestone- and rhyolite-derived soils have comparable Fe and Ti concentrations to their parent, and the basalt-derived soils do compare well with the basalt parent regarding their Si values. Given these geochemical similarities, the parent material does influence the geochemical composition of the calcic soils. Mixed alluvium was the only soil type to show a high degree of geochemical variability in the soil profile, resulting in data clustering in two distinct fields. The single sample of mixed alluvium parent material plots between the two data fields, which also indicates that the geochemical composition of the mixed alluvium soil horizons is controlled by the parent rock's composition.

There are noticeable differences between the parent material and the overlying soils. The limestone- and rhyolite-derived soils are enriched in Ca and depleted in Al and Si relative to their parent bedrock. The basaltic soils also do not compare well with their basalt parent regarding any of their major elemental concentrations, as the soils are enriched in Ca and depleted in Fe, Al, and Ti relative to the basalt parent. These notable differences may be explained by dust input and other factors influencing the composition of calcic soils. Significant dust input to the lower basaltic soil horizons and the upper rhyolitic soil horizons were confirmed using Ti:Zr ratios.

Moreover, all of the soil horizons did indicate dust affecting their geochemical properties from the Ti:Zr ratios, but the limestone and alluvial soils received noticeably less dust input compared to the volcanic soils. Thus, parent material *partially* influences the geochemical composition of the SEAZ calcic soils. The current study confirms the conclusion of the pilot project by Fischer et al. (2017) but has determined that parent material controls the calcic soils' composition to a lesser degree compared to the pilot project's findings.

The geochemistry of the mineral A-horizons from irrigated soils of mixed alluvium origin were compared to their non-irrigated soil counterparts to determine whether increased water supply had altered their properties. Drip- and sprinkler-irrigated soils did not vary significantly when Mg, Al, Si, Ti, Fe, and Zr concentrations were compared using XRF data. Thus, it appeared that a significant increase in water had little effect on the geochemical composition of these calcic soil horizons. However, when they were compared with non-irrigated mixed alluvium soils, distinct differences were found. The drip- and sprinkler-irrigated soils had significantly depleted Al values, and the sprinkler-irrigated soils had significantly enriched Ca values when compared to the mixed alluvium counterpart. Yet, Si and Fe data from both irrigated soils did overlap in bivariate plots. Due to sampling constraints, it is unknown whether the non-irrigated and the irrigated mixed-alluvium soils share the exact parent material(s). As such, the geochemistry of the irrigated soils was compared to the mineral A-horizons of soils originating on basalt, rhyolite, and limestone. The irrigated soils showed chemical similarities to the volcanic-derived soils, but were dissimilar to the limestone-derived soils, especially with respect to lower Ca values.

Given these limitations and unknowns, the geochemical data do demonstrate that the sprinkler-irrigated soils' compositional differences originate from the increased amount of water

introduced into their system. However, the soil has not been irrigated for a long enough time to observe distinct and complete geochemical alterations from the increased amount of water. Considering that these soils have only been irrigated less than 100 years, anthropogenic water input via irrigation has not had enough time to geochemically alter the calcic soils. There is no indication that the calcic soils have been hindered in storing carbon and that their carbon has been released into the atmosphere as carbon dioxide. Yet, if humans continue to reside in and irrigate these arid regions, then one could expect that the geochemical alteration of these calcic soils will be clearly evident in, perhaps, less than 400 years. Thus, in the near future, these calcic soils will likely lose their $CaCO_3$ content from long-term water input, which will likely decrease their total amount of carbon stored and increase the amount of soil CO_2 that is released.

REFERENCES

Adamson, K., Candy, I., Whitfield, L., 2015. Coupled micromorphological and stable isotope analysis of Quaternary calcrete development. Quaternary Research 84(2), 272-286.

Alonso-Zarza, A.M., Wright, V.P., 2010. Chapter 5: Calcretes, in: Alonso-Zarza, A.M., Tanner, L.H. (Eds.), Developments in Sedimentology: Carbonates in Continental Settings: Facies, Environments, and Processes. Elsevier 61, pp. 225-266.

Amit, R., Enzel, Y., Grodek, T., Crouvi, O., Porat, N., Ayalon, A., 2010. The role of rare rainstorms in the formation of calcic soil horizons on alluvial surfaces in extreme deserts. Quaternary Research 74(2), 177-187.

Assouline, S., Narkis, K., Gherabli, R., Sposito, G., 2016. Combined effect of sodicity and organic matter on soil properties under long-term irrigation with treated wastewater. Vadose Zone Journal 15(4), 1-10.

Bachman, G.O., Machette, M.N., 1977. Calcic soils and calcretes in the southwestern United States (No. 77-794). US Geological Survey.

Batchily, A.K., Post, D.F., Bryant, R.B., Breckenfeld, D.J., 2003. Spectral reflectance and soil morphology characteristics of Santa Rita Experimental Range soils, in: Santa Rita Experimental Range: 100 years (1903 to 2003) of accomplishments and contributions, conference proceedings, 2003, October 30-November 1, Tucson, AZ. Proc. RMRS-P-30. Ogden, UT: U.S. Department of Agriculture, Forest Service, Rocky Mountain Research Station, pp. 175-182.

Bescansa, P., Imaz, M.J., Virto, I., Enrique, A., Hoogmoed, W.B., 2006. Soil water retention as affected by tillage and residue management in semiarid Spain. Soil and Tillage Research 87(1), 19-27.

Bonizzoni, L., Galli, A., Gondola, M., Martini, M., 2013. Comparison between XRF, TXRF, and PXRF analyses for provenance classification of archaeological bricks. X-Ray Spectrometry 42(4), 262-267.

Candy, I., Black, S., 2009. The timing of Quaternary calcrete development in semi-arid southeast Spain: investigating the role of climate on calcrete genesis. Sedimentary Geology 218(1-4), 6-15.

Chakraborty, S., Weindorf, D.C., Weindorf, C.A., Das, B.S., Li, B., Duda, B., Pennington, S., Ortiz, R., 2017. Semi-Quantitative Evaluation of Secondary Carbonates via Portable X-ray Fluorescence Spectrometry. Soil Science Society of America Journal 81(4), 844-852.

Clark, G.A., Smajstrla, A.G., 1996. Design considerations for vegetable crop drip irrigation systems. HortTechnology 6(3), 155-159.

Clark, S., Menrath, W., Chen, M., Roda, S., Succop, P., 1999. Use of a field portable X-ray fluorescence analyzer to determine the concentration of lead and other metals in soil samples. Annals of Agricultural and Environmental Medicine 6(1), 27-32.

Craig, N., Speakman, R.J., Popelka-Filcoff, R.S., Glascock, M.D., Robertson, J.D., Shackley, M.S., Aldenderfer, M.S., 2007. Comparison of XRF and PXRF for analysis of archaeological obsidian from southern Peru. Journal of Archaeological Science 34(12), 2012-2024.

Fischer, A.B., Rasmussen, C., Shepard, C., 2017. Geochemical differences in petrocalcic and calcic horizons due to soil parent material in Southeastern Arizona. The University of Arizona and Biosphere 2's Earth and Environmental Systems REU program. Geological Society of America poster presentation. https://gsa.confex.com/gsa/2017AM/meetingapp.cgi/Paper/303806 (accessed 08 April 2018).

Hendricks, D.M., 1985. Arizona Soils. The Arizona Board of Regents, College of Agriculture, University of Arizona.

Huerta, P., Rodríguez-Berriguete, Á., Martín-García, R., Martín-Pérez, A., Fernández, Á.L.I., Alonso-Zarza, A.M., 2015. The role of climate and aeolian dust input in calcrete formation in volcanic islands (Lanzarote and Fuerteventura, Spain). Palaeogeography, Palaeoclimatology, Palaeoecology 417, 66-79.

Kilbride, C., Poole, J., Hutchings, T.R., 2006. A comparison of Cu, Pb, As, Cd, Zn, Fe, Ni and Mn determined by acid extraction/ICP–OES and ex situ field portable X-ray fluorescence analyses. Environmental Pollution 143(1), 16-23.

Kraimer, R.A., Monger, H.C., 2009. Carbon isotopic subsets of soil carbonate—a particle size comparison of limestone and igneous parent materials. Geoderma 150(1-2), 1-9.

Ley, T.W., 1992. Sprinkler irrigation – Application rates and depths. Washington State University Cooperative Extension and the U.S. Department of Agriculture, 1-2.

Lybrand, R. A., Rasmussen, C., 2015. Quantifying Climate and Landscape Position Controls on Soil Development in Semiarid Ecosystems. Soil Sci. Soc. Am. J. 79, 104-116.

Lybrand, R., Rasmussen, C., Jardine, A., Troch, P., Chorover, J., 2011. The effects of climate and landscape position on chemical denudation and mineral transformation in the Santa Catalina mountain critical zone observatory. Applied geochemistry 26, S80-S84.

Machette, M.N., 1985. Calcic soils of the southwestern United States. Geological Society of America Special Papers 203, 1-22.

McDonald, E.V., Pierson, F.B., Flerchinger, G.N., McFadden, L.D., 1996. Application of a soil-water balance model to evaluate the influence of Holocene climate change on calcic soils, Mojave Desert, California, USA. Geoderma 74(3-4), 167-192.

Melton, M.A., 1965. The geomorphic and paleoclimatic significance of alluvial deposits in southern Arizona. The Journal of Geology 73(1), 1-38.

Moioli, P., Seccaroni, C., 2000. Analysis of art objects using a portable x-ray fluorescence spectrometer. X-Ray Spectrometry 29(1), 48-52.

Monger, H.C., 2010. Soil morphology adaptations to global warming in arid and semiarid ecosystems, in: 19th World Congress of Soil Science, Brisbane, Australia, pp. 1-6.

Morrison, R.B., 1985. Pliocene/Quaternary geology, geomorphology, and tectonics of Arizona. Geological Society of America Special Papers, 203, 123-146.

Naiman, Z., Quade, J., Patchett, P.J., 2000. Isotopic evidence for eolian recycling of pedogenic carbonate and variations in carbonate dust sources throughout the southwest United States. Geochimica et Cosmochimica Acta 64(18), 3099-3109.

Pavich, M.J., Chadwick, O.A., 2004. Soils and the Quaternary climate system. Developments in Quaternary Sciences 1, 311-330.

Pfeiffer, M., Aburto, F., Le Roux, J.P., Kemnitz, H., Sedov, S., Solleiro-Rebolledo, E., Seguel, O., 2012. Development of a Pleistocene calcrete over a sequence of marine terraces at Tongoy (north-central Chile) and its paleoenvironmental implications. Catena, 97, 104-118.

Potts, P.J., Webb, P.C., Williams-Thorpe, O., Kilworth, R., 1995. Analysis of silicate rocks using field-portable X-ray fluorescence instrumentation incorporating a mercury (II) iodide detector: A preliminary assessment of analytical performance. Analyst 120(5), 1273-1278.

Potts, P.J., Williams-Thorpe, O., Webb, P.C., 1997. The bulk analysis of silicate rocks by portable X-ray fluorescence: effect of sample mineralogy in relation to the size of the excited volume. Geostandards and Geoanalytical Research 21(1), 29-41.

Raymo, M.E., Ruddiman, W.F., 1992. Tectonic forcing of late Cenozoic climate. Nature 359(6391), 117-122.

Schlesinger, W.H., 1985. The formation of caliche in soils of the Mojave Desert, California. Geochimica et Cosmochimica Acta 49(1), 57-66.

Singhvi, A.K., Williams, M.A.J., Rajaguru, S.N., Misra, V.N., Chawla, S., Stokes, S., Chauhan, N., Francis, T., Ganjoo, R.K., Humphreys, G.S., 2010. A ~200 ka record of climatic change and dune activity in the Thar Desert, India. Quaternary Science Reviews 29(23-24), 3095-3105.

Soil Survey staff, 2006. Keys to Soil Taxonomy, tenth ed. USDA-NRCS, Washington, DC.

Stiles, C.A., Mora, C.I., Driese, S.G., Robinson, A.C., 2003. Distinguishing climate and time in the soil record: Mass-balance trends in Vertisols from the Texas coastal prairie. Geology 31(4), 331-334.

Weindorf, D.C., Herrero, J., Castañeda, C., Bakr, N., Swanhart, S., 2013. Direct soil gypsum quantification via portable x-ray fluorescence spectrometry. Soil Sci. Soc. Am. J. 77(6), 2071-2077.

Zamanian, K., Pustovoytov, K., Kuzyakov, Y., 2016. Pedogenic carbonates: Forms and formation processes. Earth-Science Reviews 157, 1-17.

Zhu, Y., Weindorf, D.C., 2009. Determination of soil calcium using field portable x-ray fluorescence. Soil Sci. 174(3), 151-155.

FIGURES AND TABLES

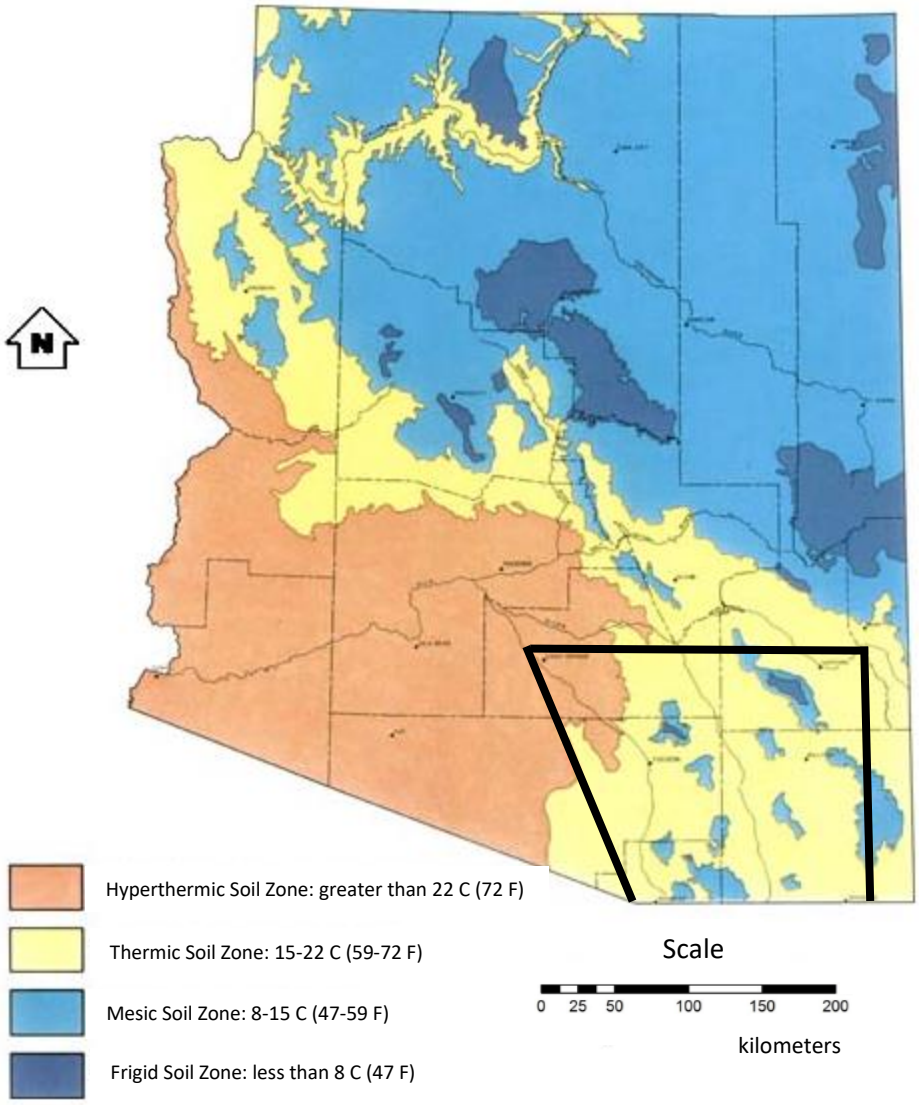

Figure 1. Soil classification scheme of Arizona (from Hendricks, 1985). Hyperthermic soils (orange) are those characterized by prevailing warm environments, in areas greater than 22 °C temperatures. Thermic soils (yellow) form at temperatures ranging between 15 and 22 °C and contrast with mesic soils (blue), which exist in temperature that ranges from 8 to 15 °C. Frigid soils (dark blue) only exist in areas with a mean annual temperature of less than 8 °C throughout the year. The study area is indicated by the black polygon. Scale in kilometers.

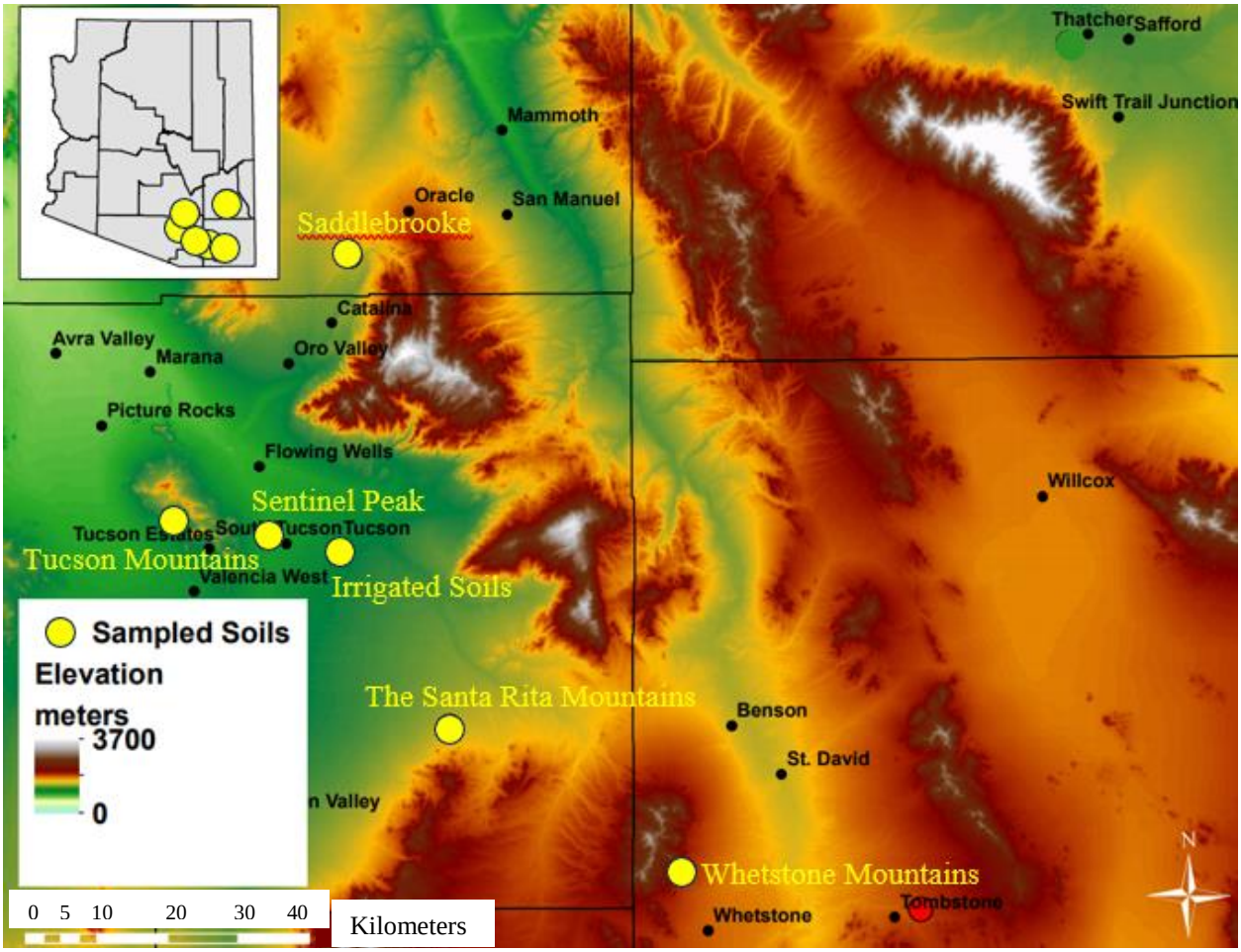

Figure 2. Map of the five sites that were sampled in SEAZ. These include Saddlebrooke, the Santa Rita Mountains, Sentinel Peak, the Tucson Mountains, and Whetstone. See Table 1 for the GPS coordinate locations and parent material composition of each site. Scale in kilometers.

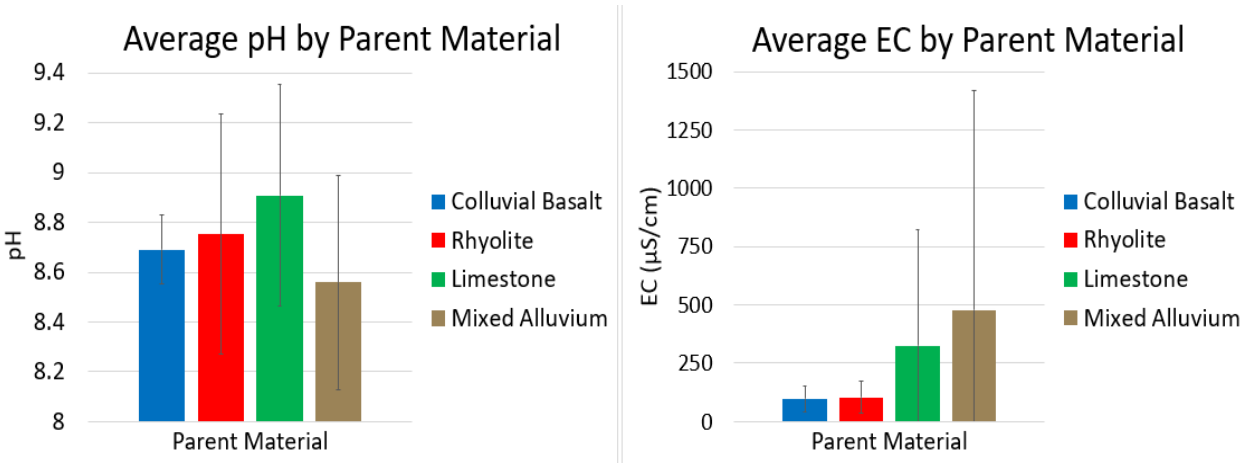

Figure 3. Average pH (based on H_2O) and EC values of the soil horizons, which are grouped by parent material. Values are taken from Table 1 (from Fischer et al., 2017).

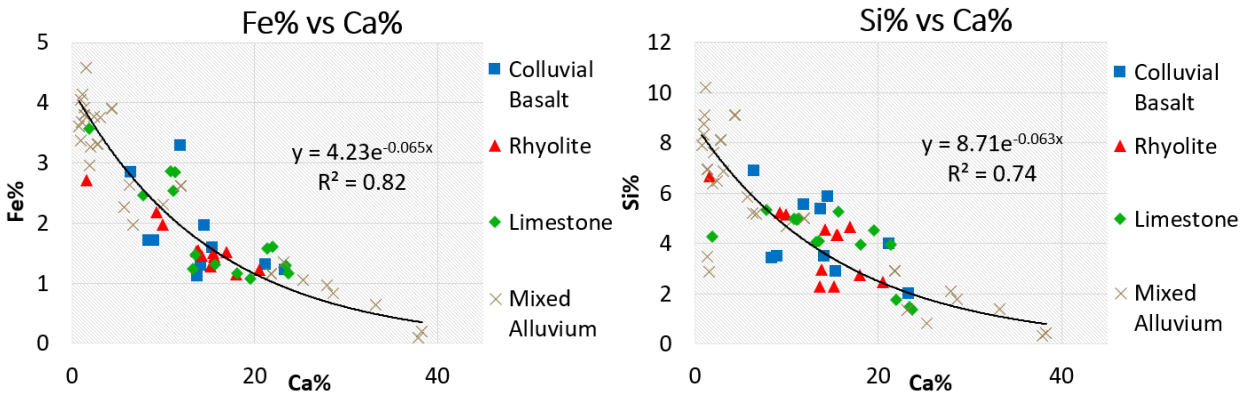

Figure 4. Correlations between Ca and Fe and Si data obtained from pXRF and produced by grouping the soils based on their parent material locations.
Ca-Fe R^2 = 0.82 and Ca-Si R^2 = 0.74 (from Fischer et al., 2017).

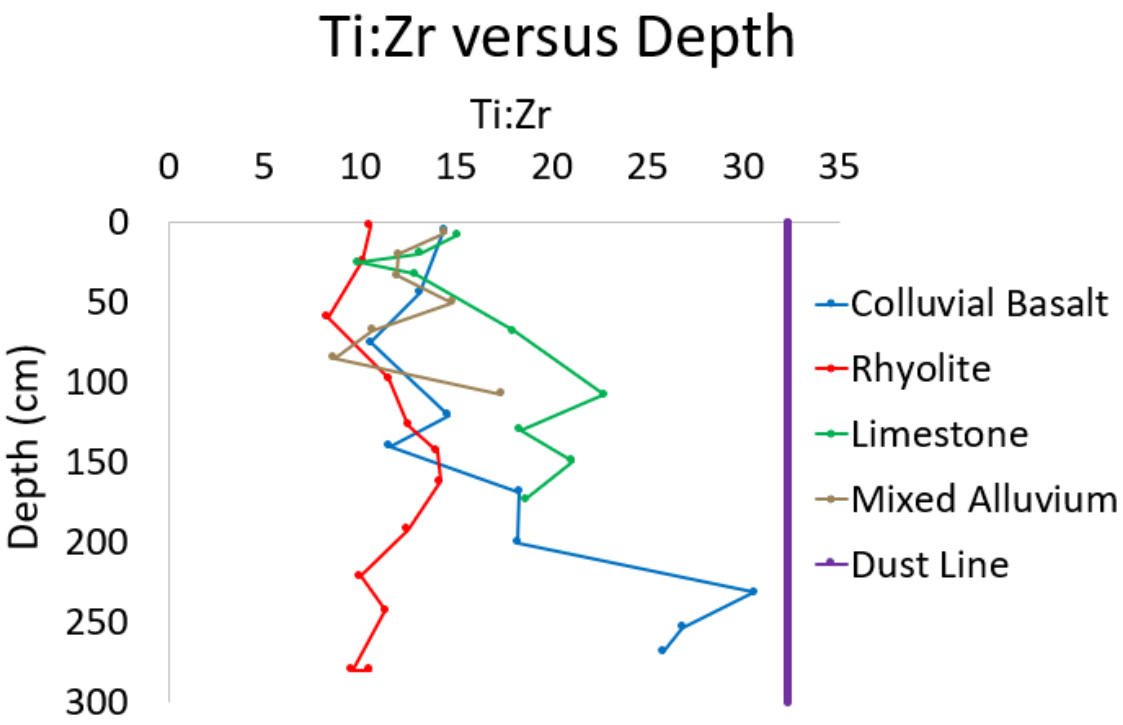

Figure 5. Depth plots of Ti:Zr for sample basalt, rhyolite, limestone, and mixed alluvium soils using the pXRF data from the pilot project. The proportion of these two elements that reflects input by dust has been calculated using the method of Lybrand (unpublished data), which is used in the current study (Rasmussen, pers. comm. 2017). As such, the increases in Ti:Zr ratios are likely indicative of dust input (from Fischer et al., 2017).

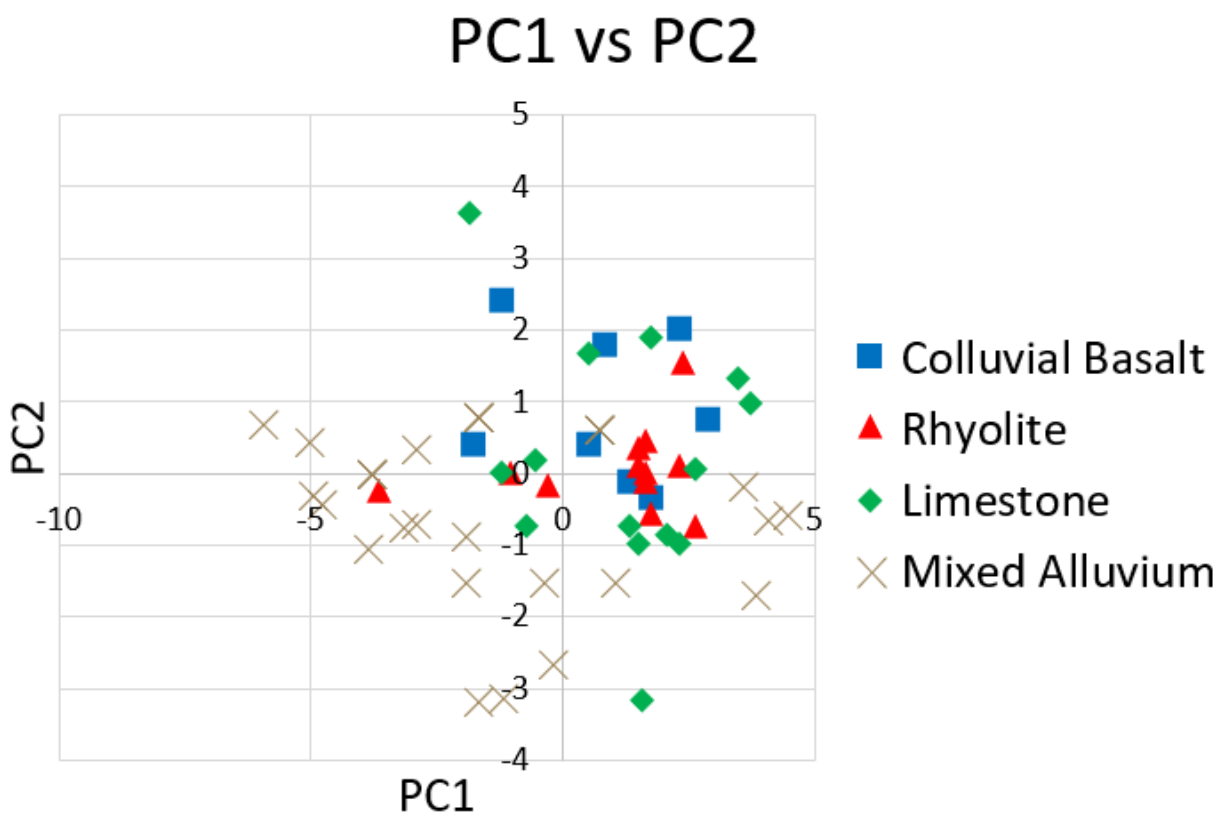

Figure 6. Principal component analysis, which shows scores for PC1 vs. PC2. PC1 represents degree of replacement by Ca and increased pH, and PC2 represents concentration of Ba and Sr present (from Fischer et al., 2017).

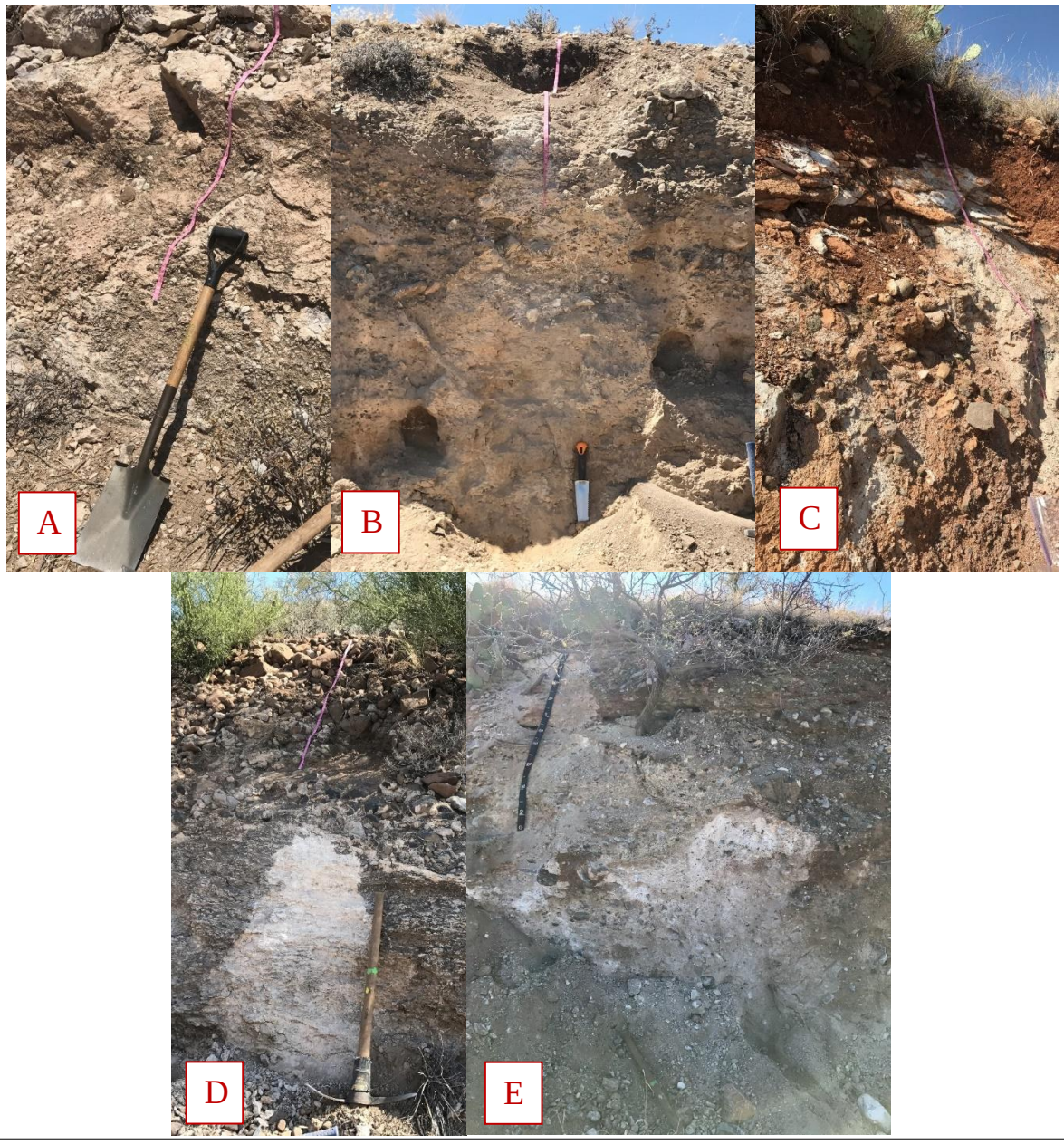

Figure 7. The five sampled soil profiles are from Sentinel Peak, Santa Rita Mountains, Tucson Mountains, Whetstone Mountains, and Saddlebrooke. (A) The soil profile from Sentinel Peak, which extends 246 cm and overlies its unconsolidated colluvial basalt parent material. (B) The soil profile from Santa Rita Mountains, which extends 190 cm and overlies its unconsolidated limestone parent material. (C) The soil profile from Whetstone Mountains, which extends 200 cm and overlies its unconsolidated limestone parent material. (D) The soil profile from Tucson Mountains, which extends 304 cm and overlies its unconsolidated rhyolite/andesite parent material. (E) The soil profile from Saddlebrooke, which extends 400 cm and its unconsolidated mixed alluvium parent material. Scale: measuring tape, pickaxe, and shovel = 2 m; rock knife = 30 cm. See Tables 2-6 for GPS coordinate locations and soil profile descriptions.

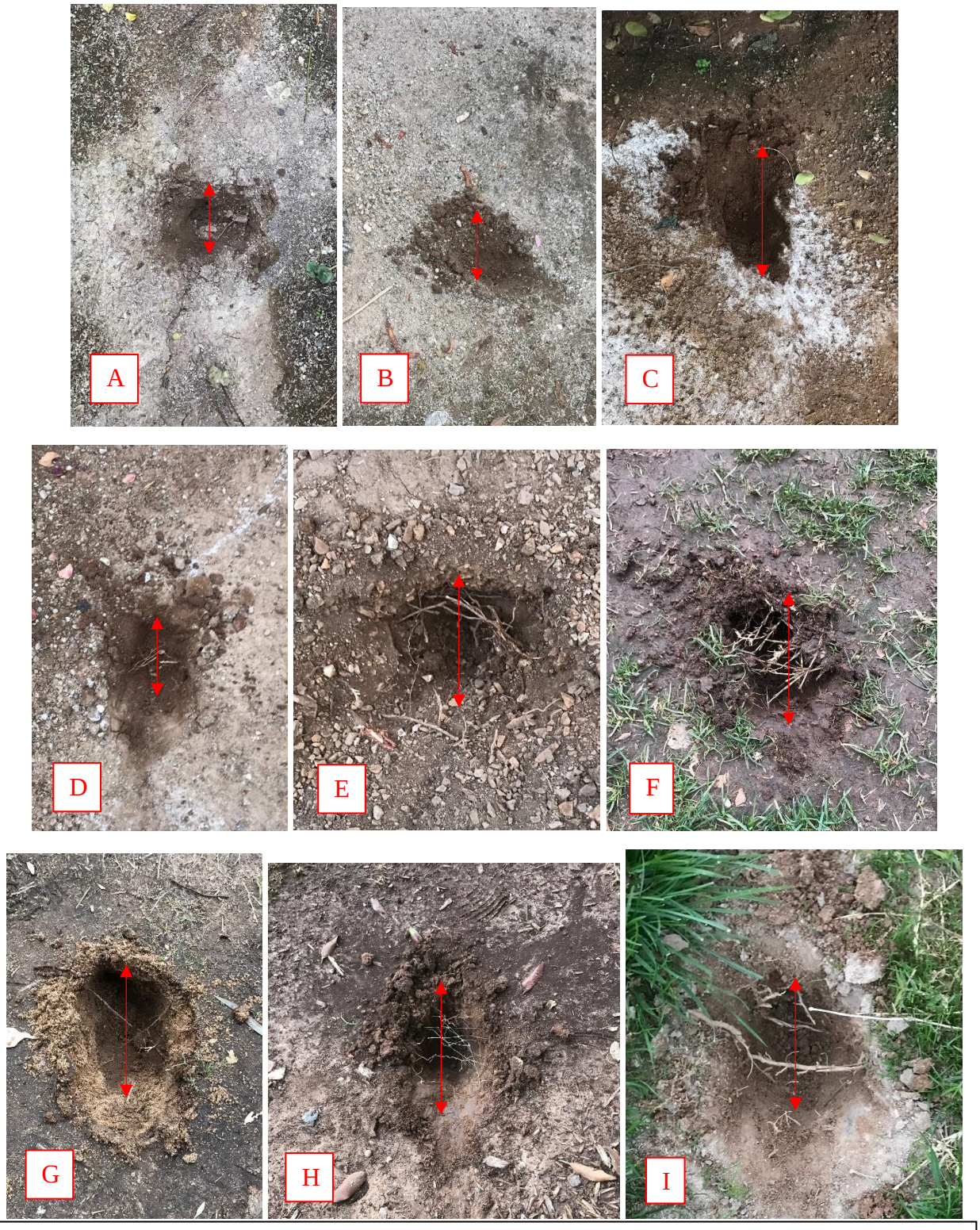

Figure 8. Pictures of the nine irrigated soils collected from the University of Arizona. (A-E) The five drip-irrigated soils. (F-I) The sprinkler-irrigated soils. The red double-arrowed line represents 15 cm. See Appendix C for Munsell soil color descriptions. GPS coordinates: 32°13’54” N 110°57’00” W.

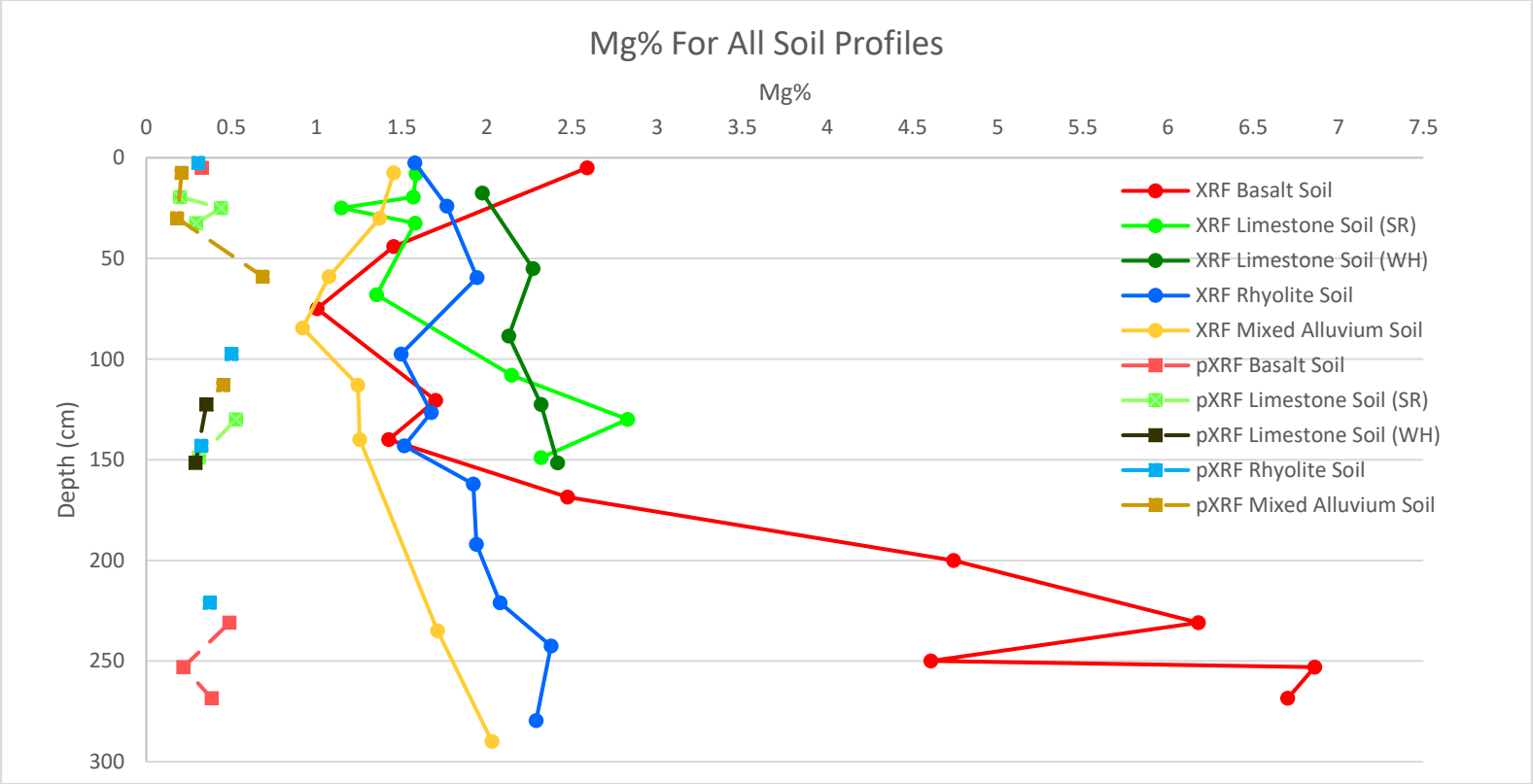

Figure 9. Scatterplots of the pXRF and XRF-measured Mg content in the five sampled profiles plotted against soil depth. The XRF data are solid circles and lines, while the pXRF data are dashed lines and squares. SR = Santa Rita Mountains; WH = Whetstone Mountains. pXRF Mg data for many horizons are too low to be

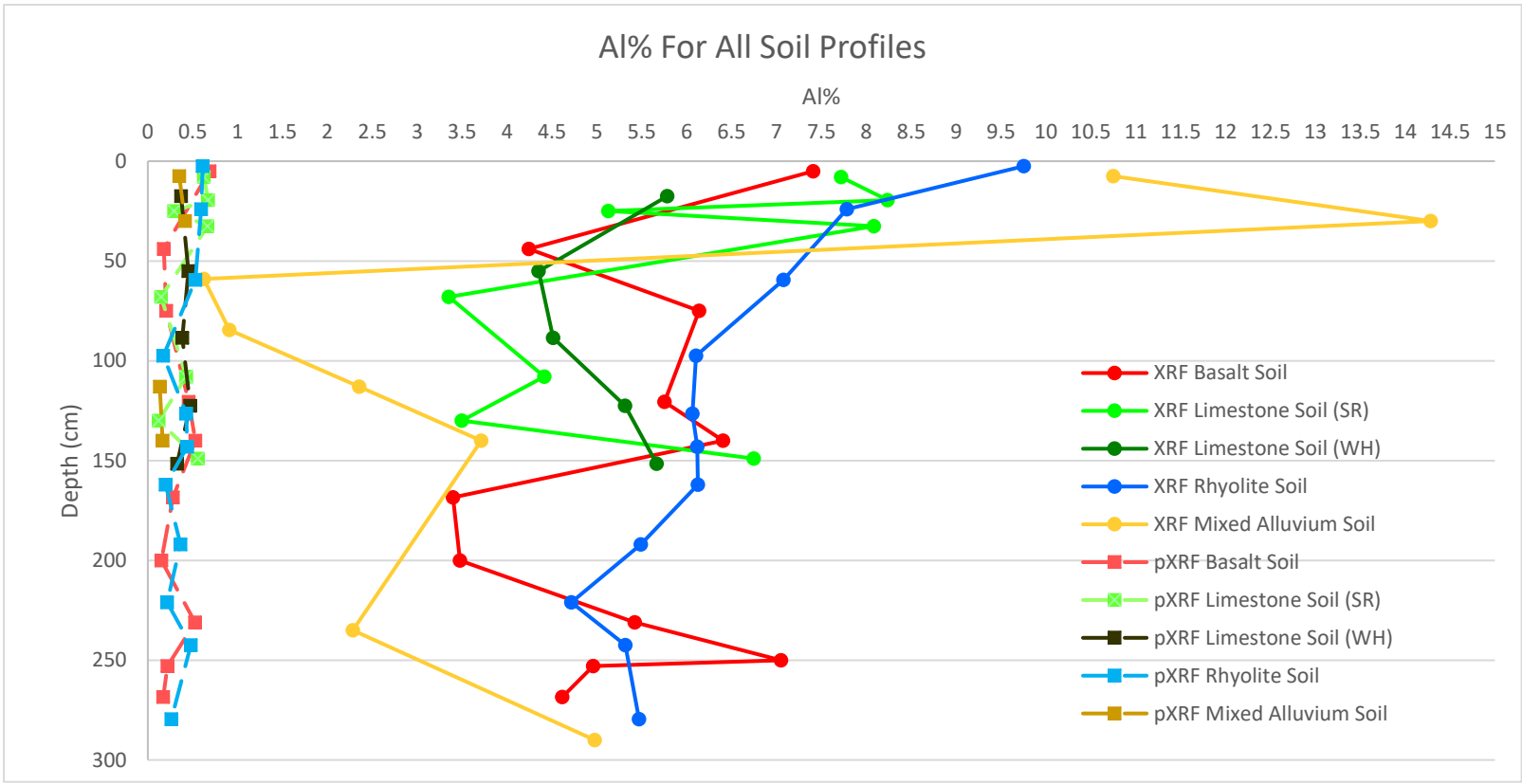

Figure 10. Scatterplots of the pXRF and XRF-measured Al content in the five sampled profiles plotted against soil depth. The XRF data are solid circles and lines, while the pXRF data are dashed lines and squares. SR = Santa Rita Mountains; WH = Whetstone Mountains.

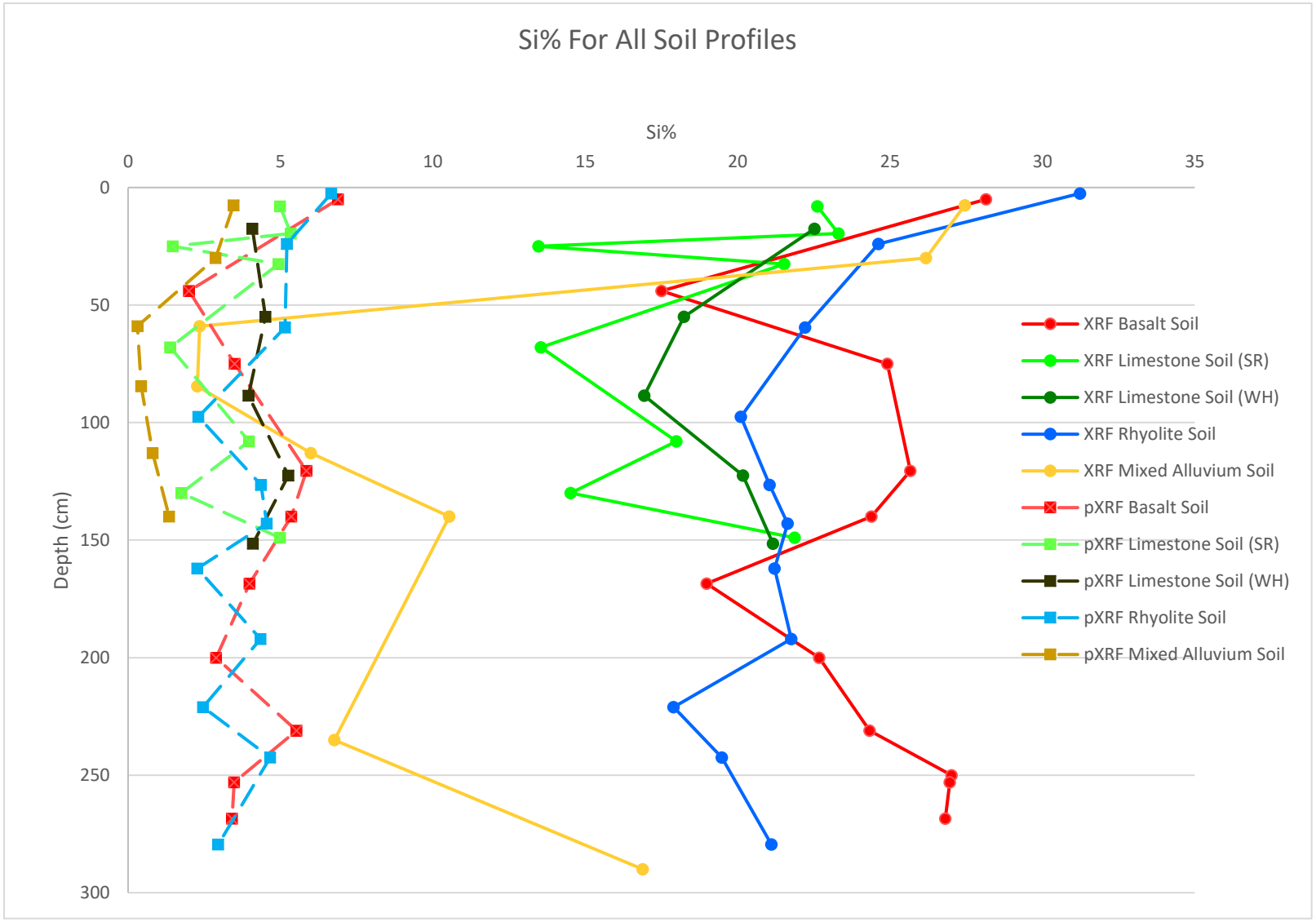

Figure 11. Scatterplots of the pXRF and XRF-measured Si content in the five sampled profiles plotted against soil depth. The XRF data are solid circles and lines, while the pXRF data are dashed lines and squares. SR = Santa Rita Mountains; WH = Whetstone Mountains.

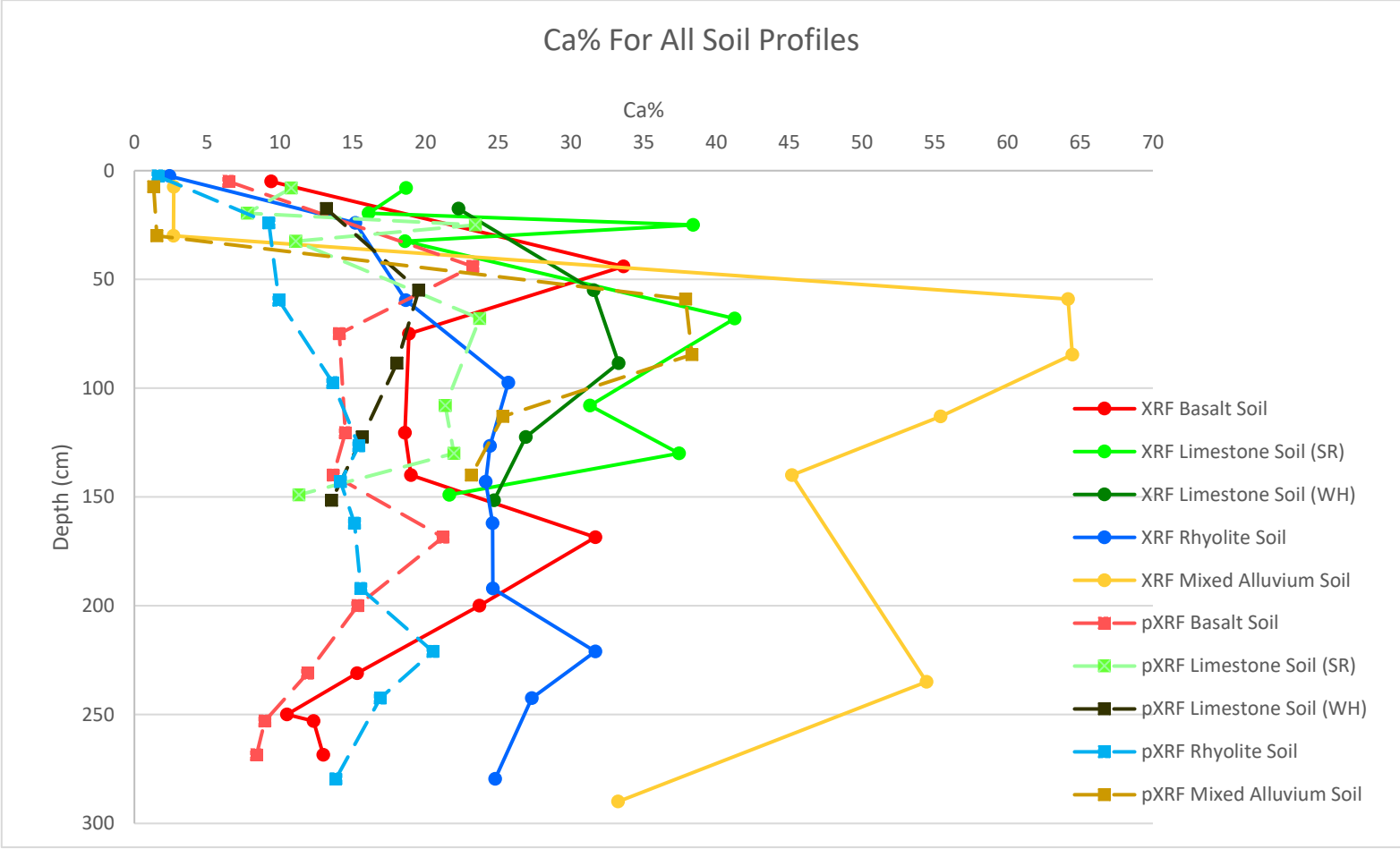

Figure 12. Scatterplots of the pXRF and XRF-measured Ca content in the five sampled profiles plotted against soil depth. The XRF data are solid circles and lines, while the pXRF data are dashed lines and squares. SR = Santa Rita Mountains; WH = Whetstone Mountains.

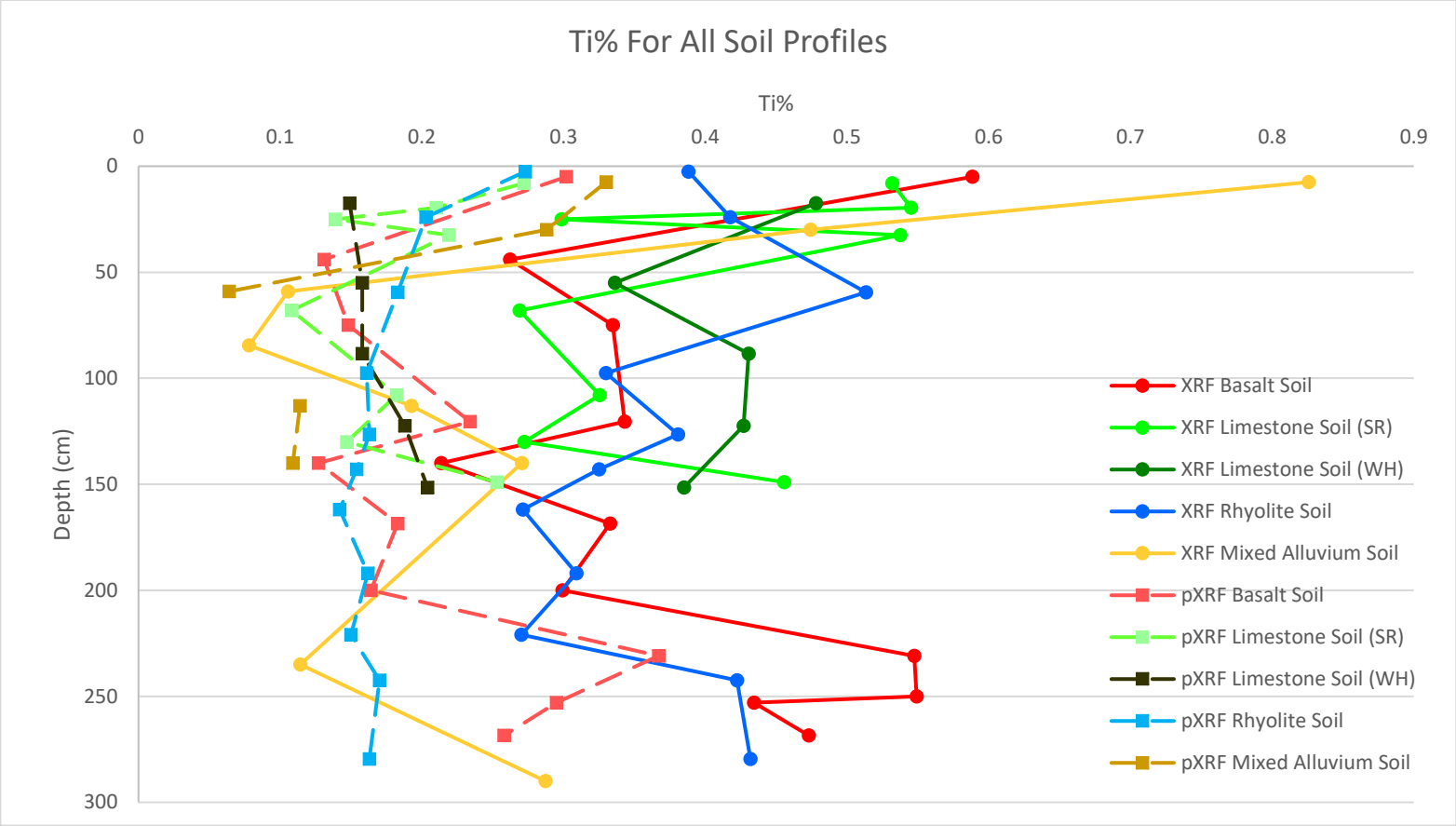

Figure 13. Scatterplots of the pXRF and XRF-measured Ti content in the five sampled profiles plotted against soil depth. The XRF data are solid circles and lines, while the pXRF data are dashed lines and squares. SR = Santa Rita Mountains; WH = Whetstone Mountains.

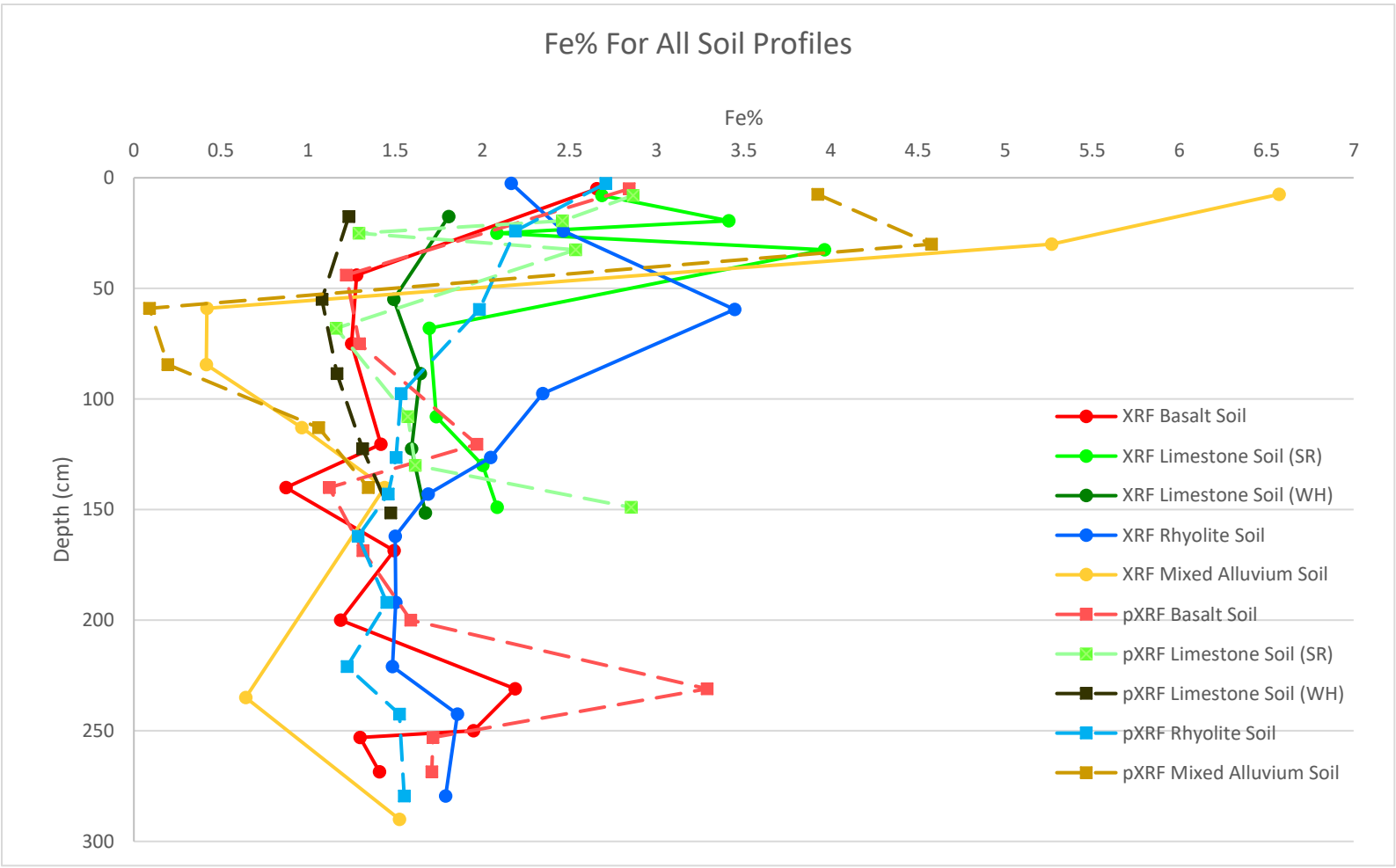

Figure 14. Scatterplots of the pXRF and XRF-measured Fe content in the five sampled profiles plotted against soil depth. The XRF data are solid circles and lines, while the pXRF data are dashed lines and squares. SR = Santa Rita Mountains; WH = Whetstone Mountains.

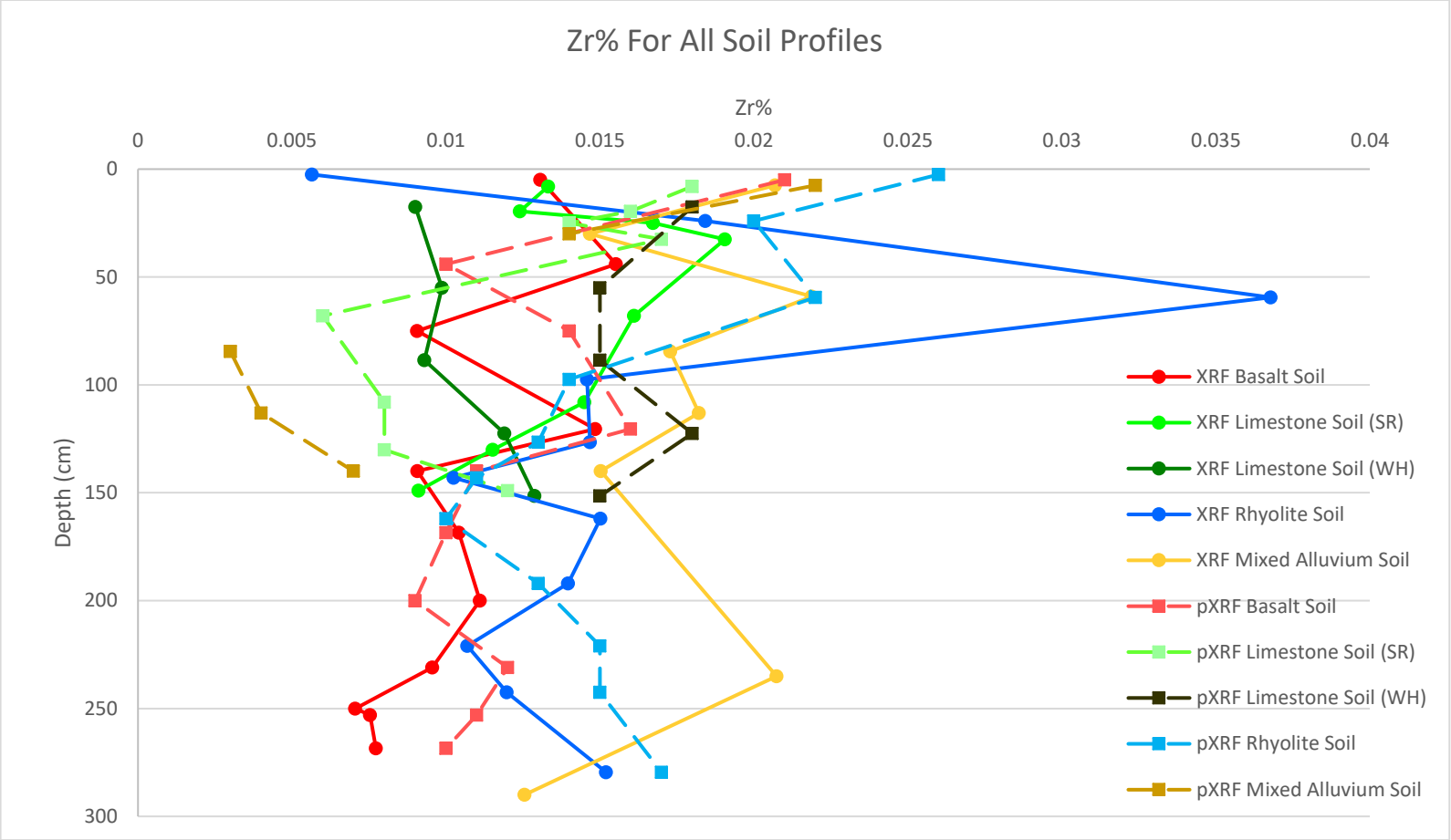

Figure 15. Scatterplots of the pXRF and XRF-measured Zr content in the five sampled profiles plotted against soil depth. The XRF data are solid circles and lines, while the pXRF data are dashed lines and squares. SR = Santa Rita Mountains; WH = Whetstone Mountains.

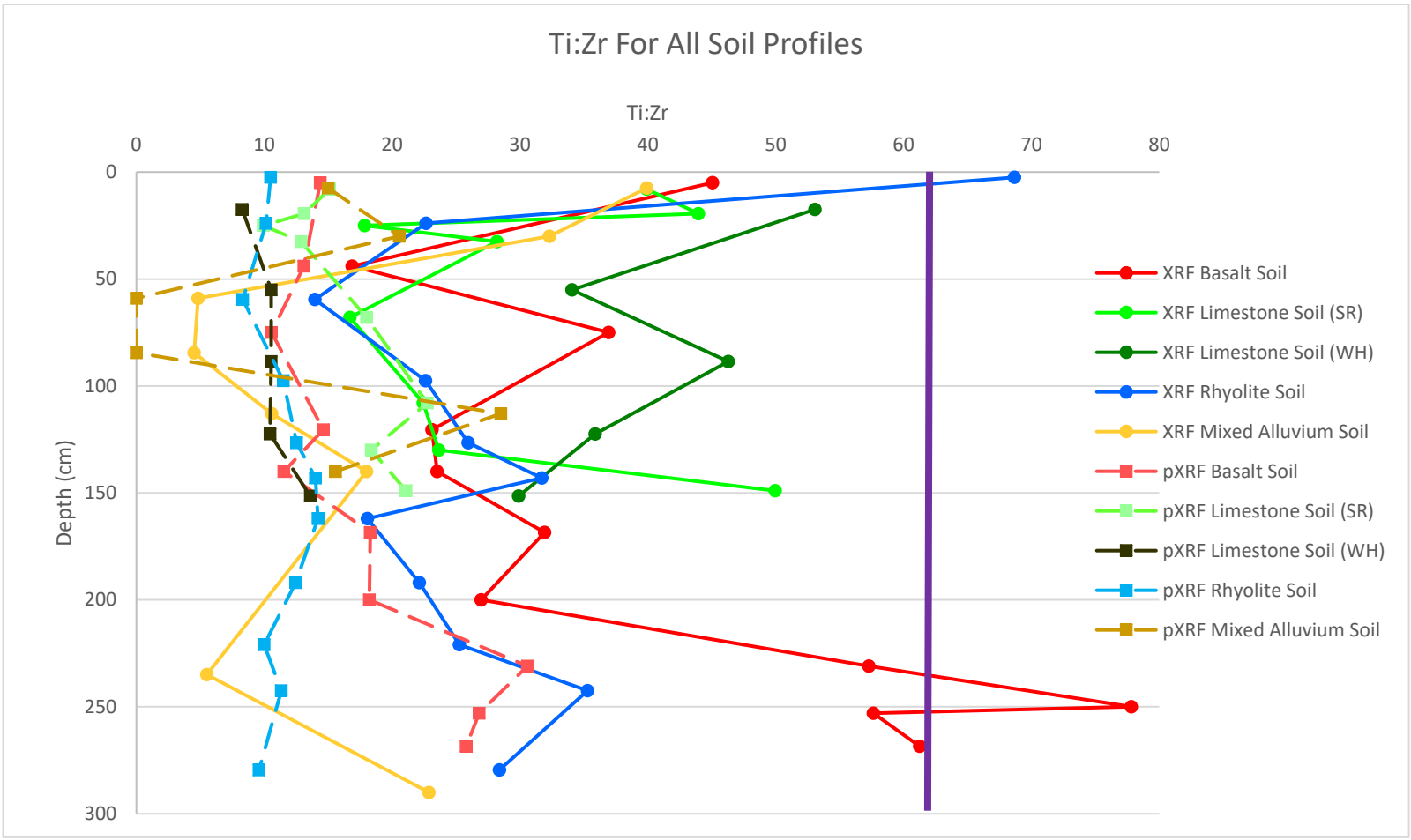

Figure 16. Scatterplots of the pXRF and XRF-measured Ti and Zr ratios in the five sampled soil profiles plotted against depth. The XRF data are represented by solid lines and circle data points, while the pXRF data are represented by dashed lines and square data points. SR and WH stand for the limestone-derived soils from the Santa Rita Mountains and the Whetstone Mountains, respectively. The proportion of these two elements that reflects input by dust has been calculated by Lybrand's unpublished data, which is used in the current study (Rasmussen, pers. comm. 2018). As such, the increases in Ti:Zr ratios are likely indicative of dust input. The solid purple line at 61.3 indicates the dust input, calculated using Lybrand's unpublished dust input calculation method using the Ti:Zr ratio (Rasmussen, pers. comm. 2018).

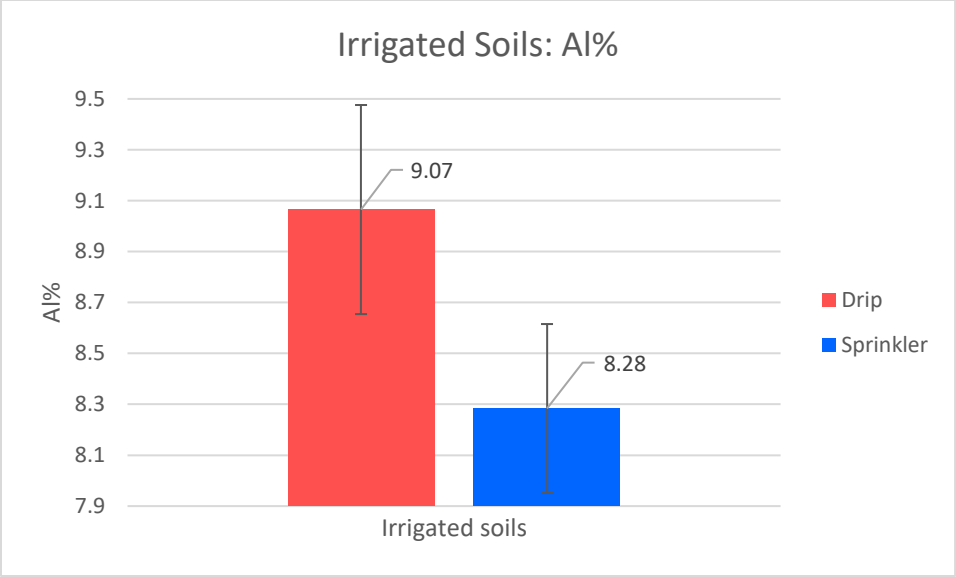

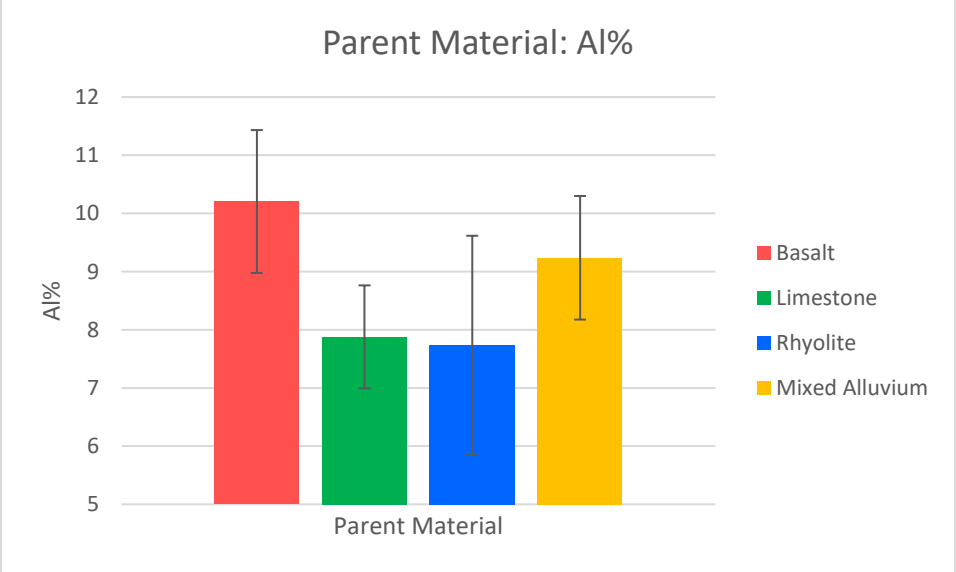

Figure 17. Bar charts of the XRF-measured Al content (top) of the drip- and sprinkler-irrigated soils and (bottom) of the parent material of the five sampled soil profiles. Standard deviation is calculated at 1σ. As there is no overlap between the drip- and sprinkler-irrigated soils' standard deviations, their Al concentrations are significantly different.

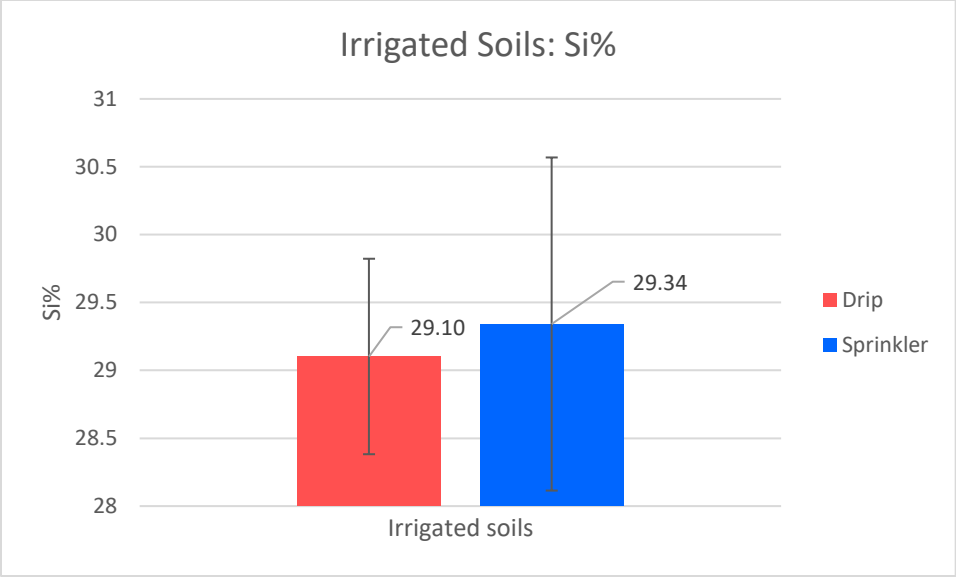

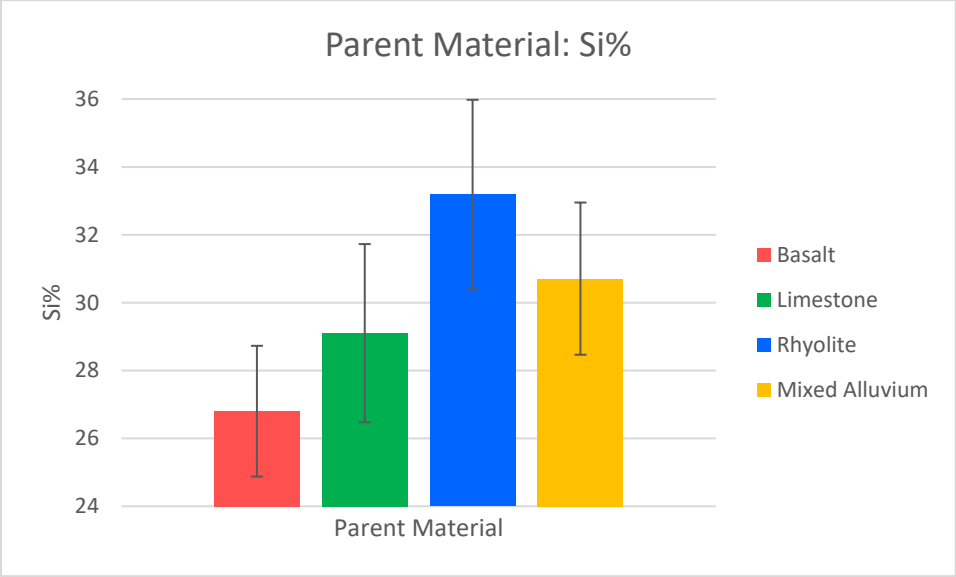

Figure 18. Bar charts of the XRF-measured Si content (top) of the drip- and sprinkler-irrigated soils and (bottom) of the parent material of the five sampled soil profiles. Standard deviation is calculated at 1σ.

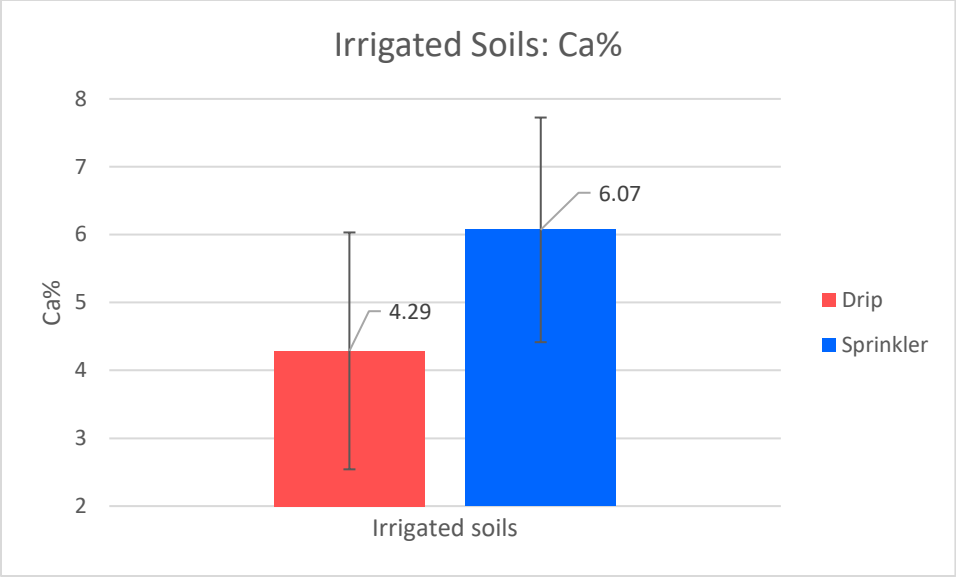

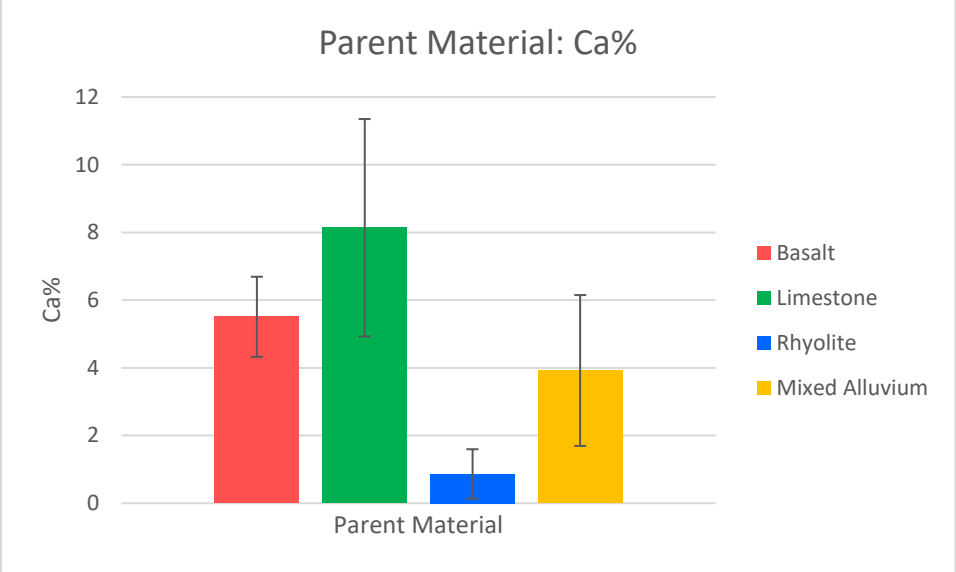

Figure 19. Bar charts of the XRF-measured Ca content (top) of the drip- and sprinkler-irrigated soils and (bottom) of the parent material of the five sampled soil profiles. Standard deviation is calculated at 1σ.

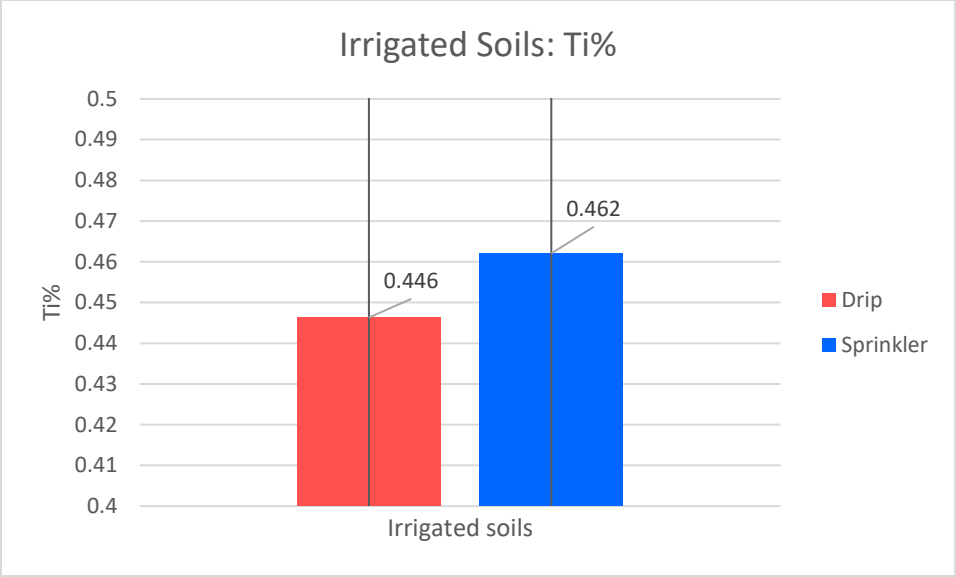

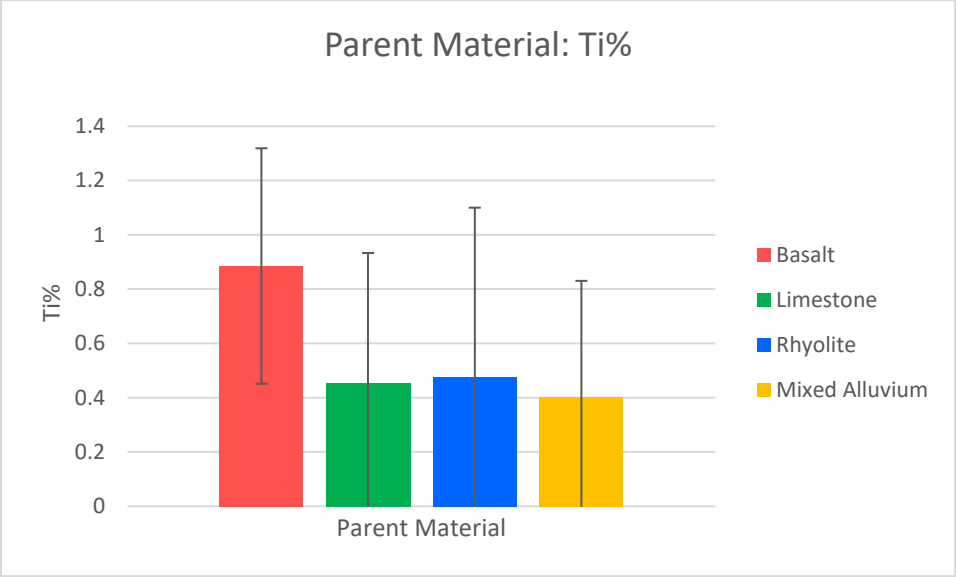

Figure 20. Bar charts of the XRF-measured Ti content (top) of the drip- and sprinkler-irrigated soils and (bottom) of the parent material of the five sampled soil profiles. Standard deviation is calculated at 1σ.

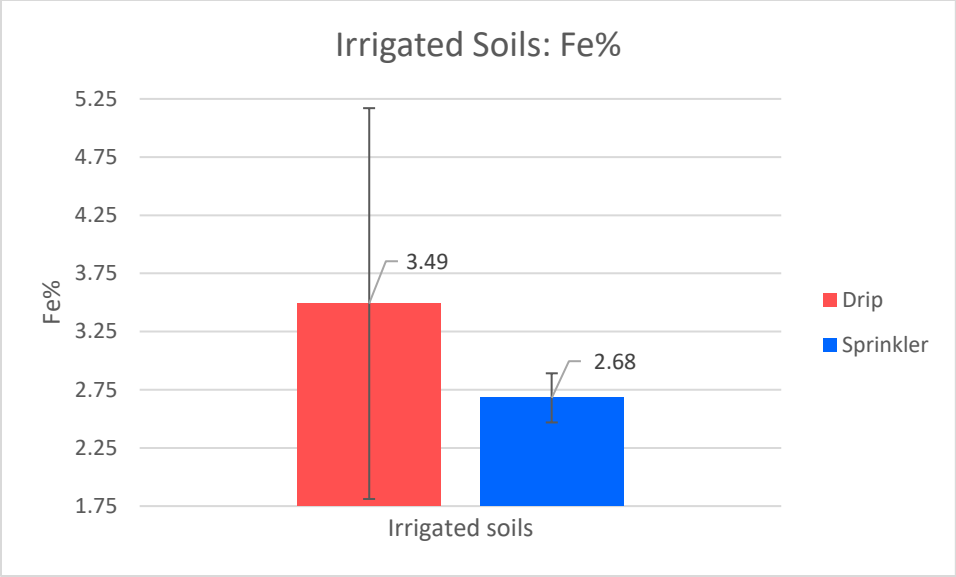

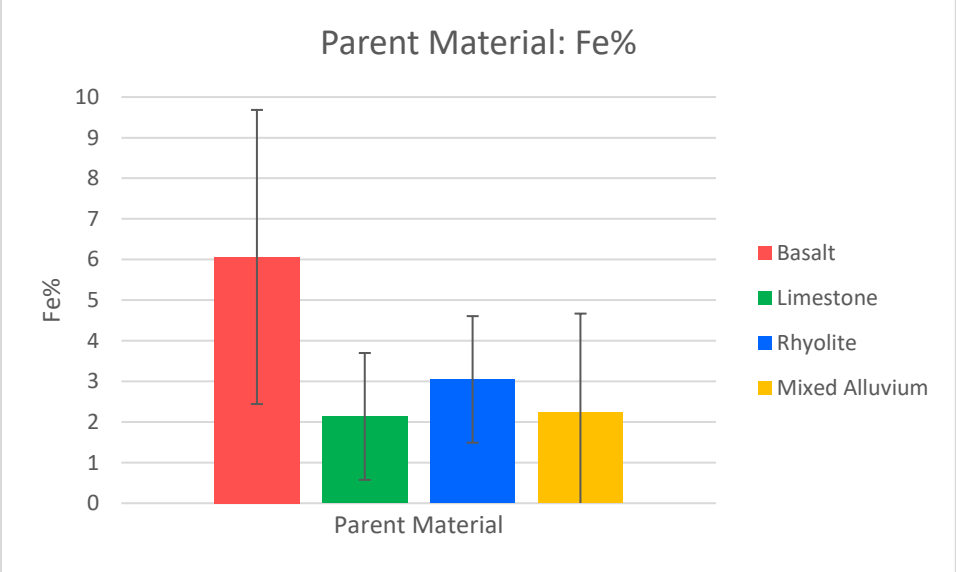

Figure 21. Bar charts of the XRF-measured Fe content (top) of the drip- and sprinkler-irrigated soils and (bottom) of the parent material of the five sampled soil profiles. Standard deviation is calculated at 1σ.

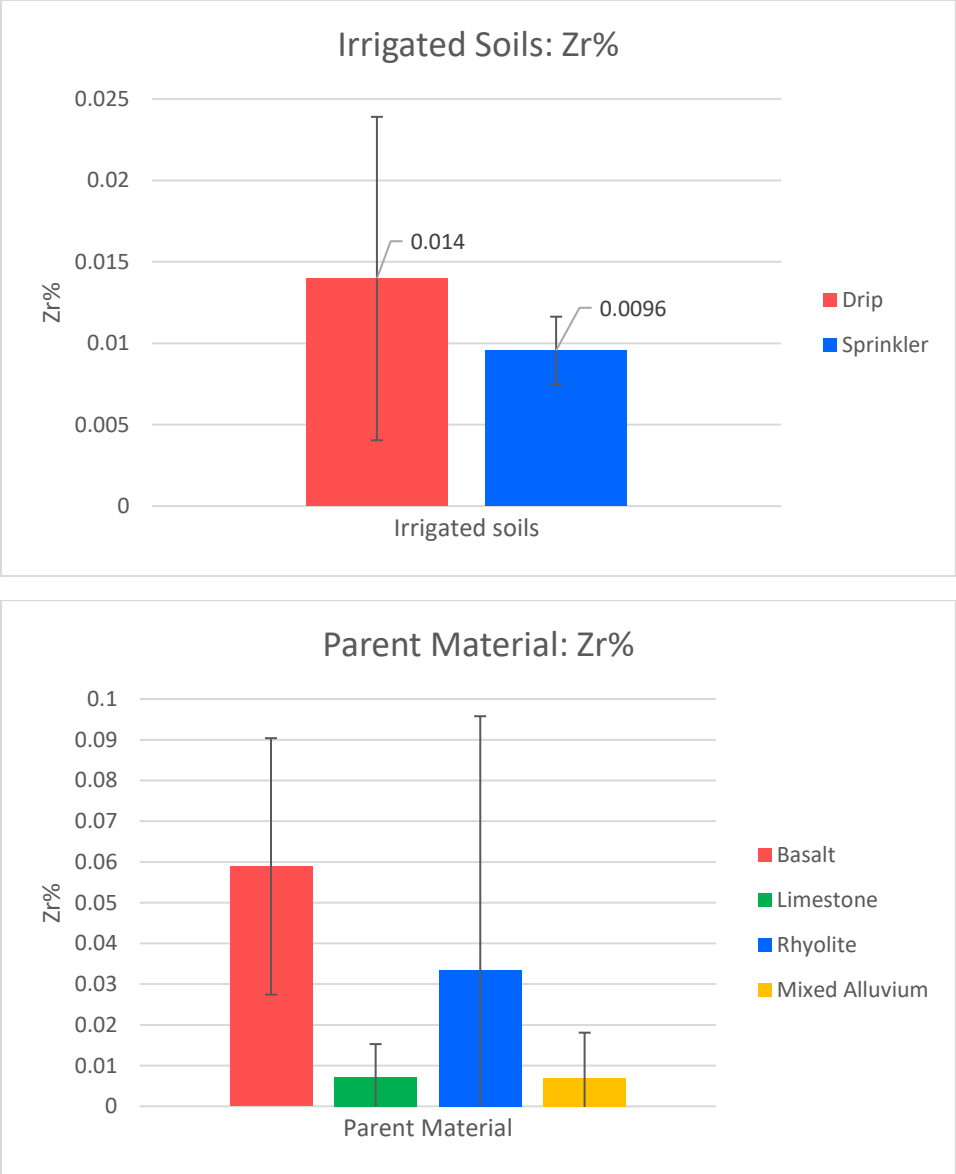

Figure 22. Bar charts of the XRF-measured Zr content (top) of the drip- and sprinkler-irrigated soils and (bottom) of the parent material of the five sampled soil profiles. Standard deviation is calculated at 1σ.

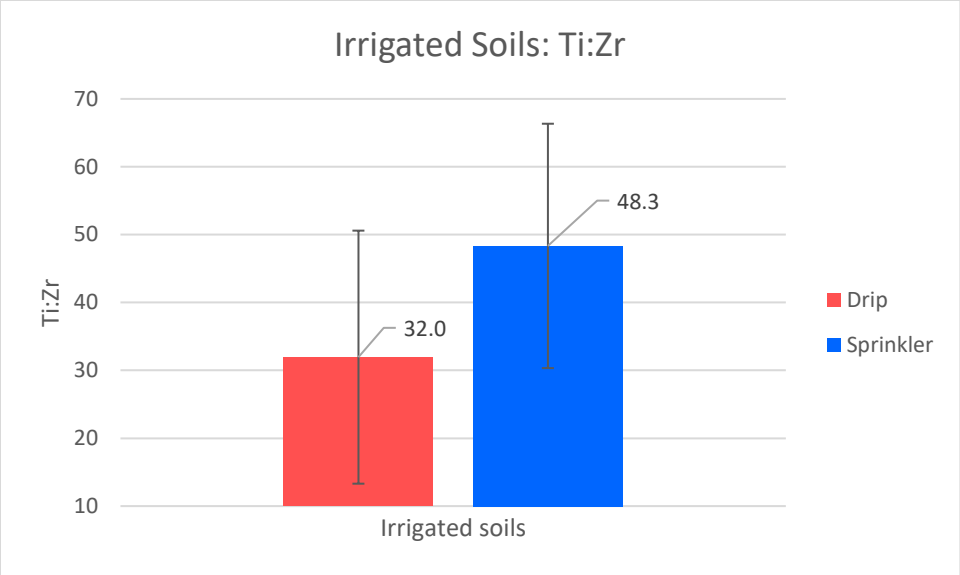

Figure 23. Bar charts of the XRF-measured Ti:Zr ratio of the drip- and sprinkler-irrigated soils. Standard deviation is calculated at 1σ.

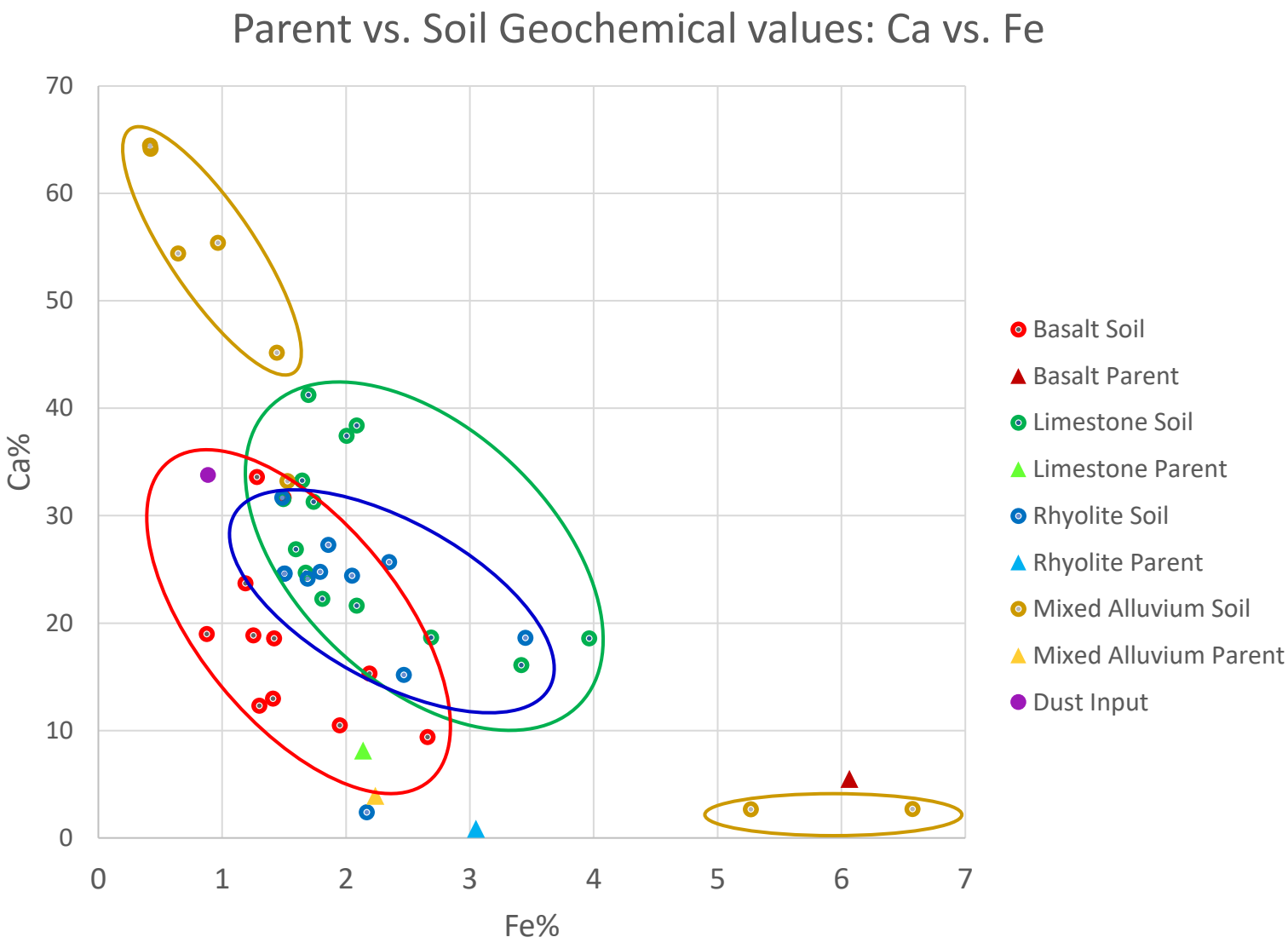

Figure 24. Bivariate plot of Ca vs. Fe of soil and parent material. Red data field plots basalt-derived soils; red triangle plots basalt parent datum. Green data field plots limestone-derived soils; green triangle plots limestone parent datum. Blue data field plots rhyolite-derived soils; blue triangle plots rhyolite parent datum. Two yellow data fields plot mixed-alluvium-derived soils; yellow triangle plots mixed alluvium parent datum. Elemental values derived from dust are denoted by the filled purple circle, and, hence, dust input was determined with Lybrand's data, which was adjusted to the Ti dust values (Rasmussen, pers. comm.).

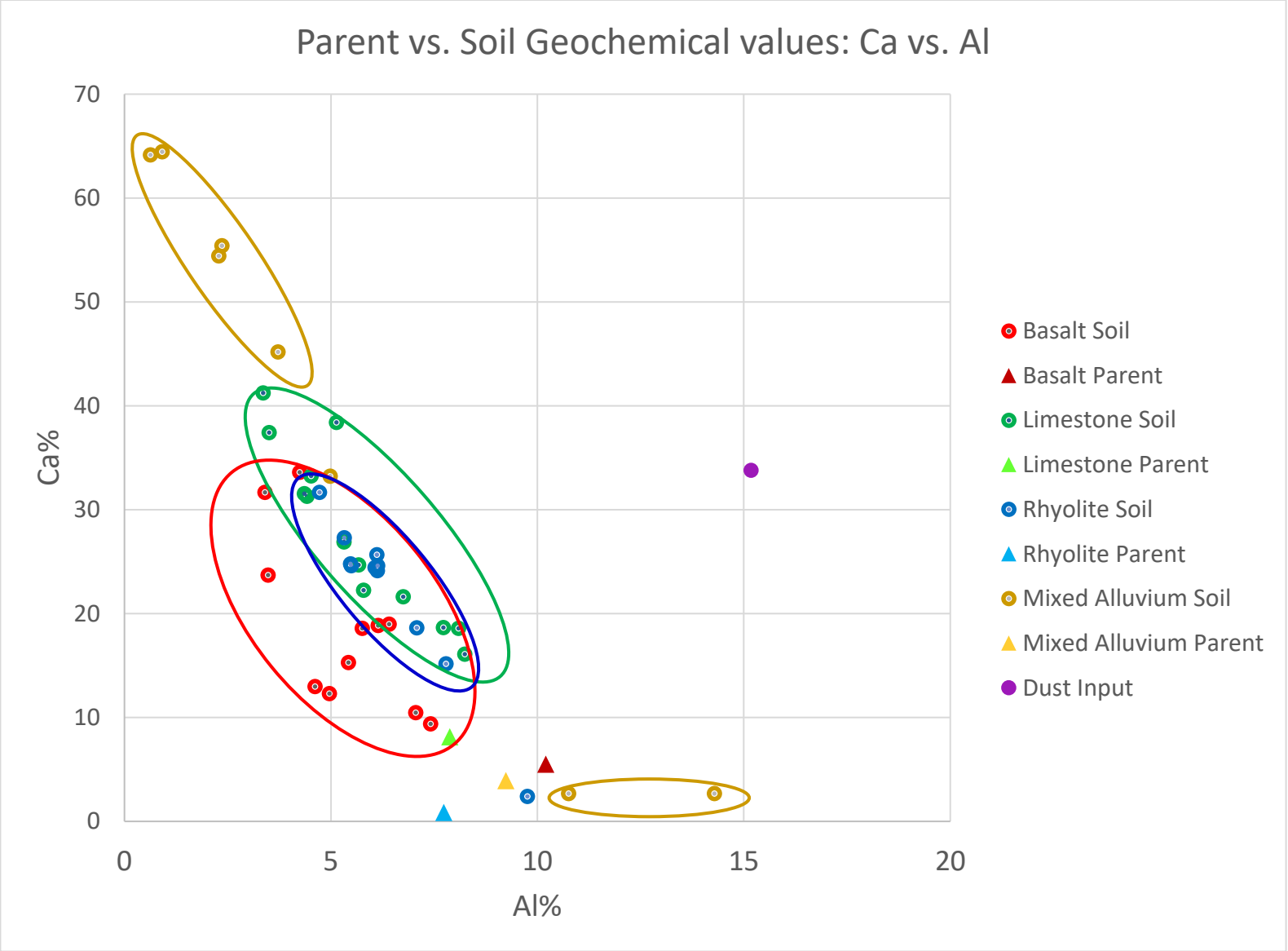

Figure 25. Bivariate plot of Ca vs. Al of soil and parent material. Red data field plots basalt-derived soils; red triangle plots basalt parent datum. Green data field plots limestone-derived soils; green triangle plots limestone parent datum. Blue data field plots rhyolite-derived soils; blue triangle plots rhyolite parent datum. Two yellow data fields plot mixed-alluvium-derived soils; yellow triangle plots mixed alluvium parent datum. Elemental values derived from dust are denoted by the filled purple circle, and, hence, dust input was determined with Lybrand's data, which was adjusted to the Ti dust values (Rasmussen, pers. comm.).

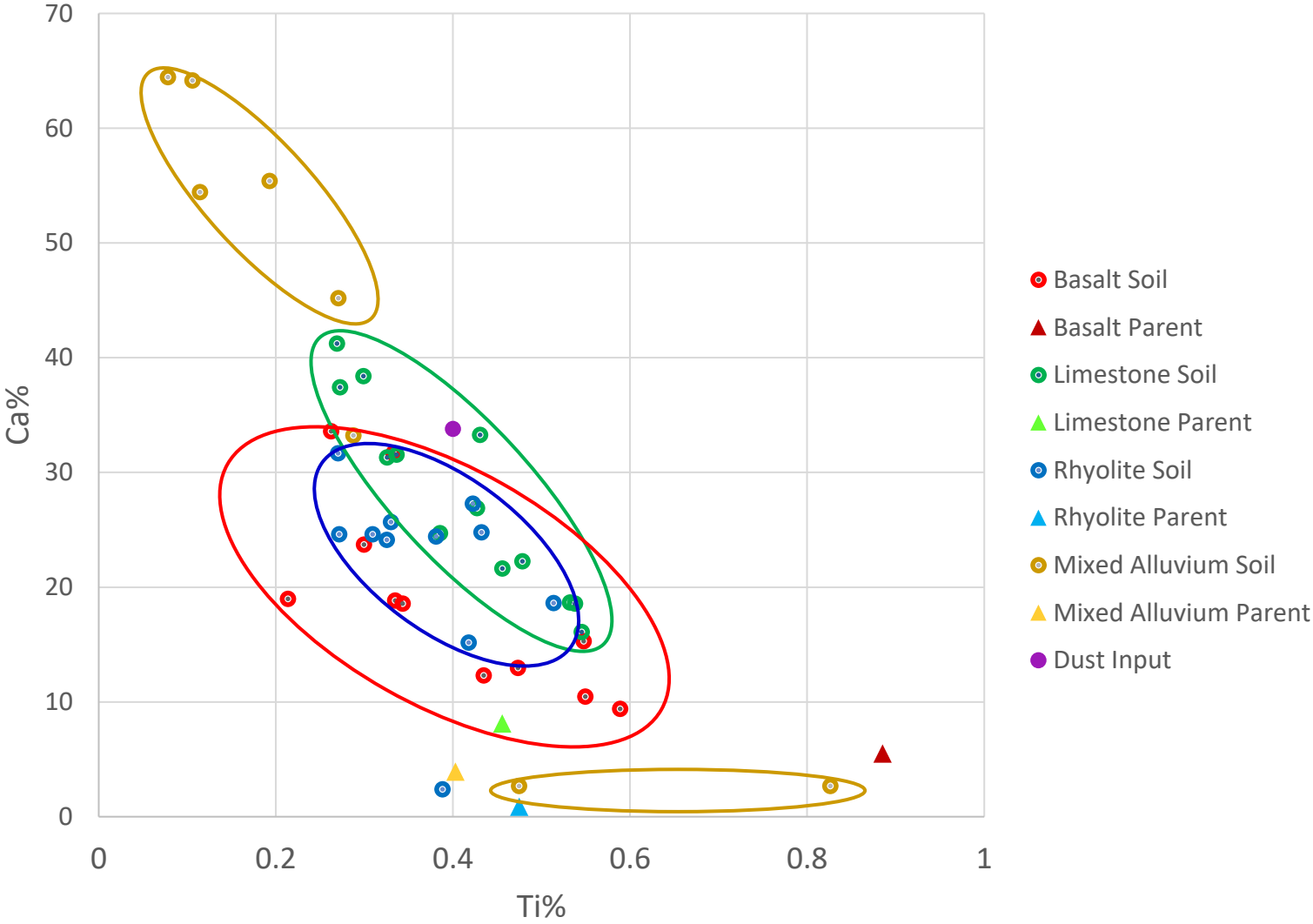

Figure 26. Bivariate plot of Ca vs. Ti of soil and parent material. Red data field plots basalt-derived soils; red triangle plots basalt parent datum. Green data field plots limestone-derived soils; green triangle plots limestone parent datum. Blue data field plots rhyolite-derived soils; blue triangle plots rhyolite parent datum. Two yellow data fields plot mixed-alluvium-derived soils; yellow triangle plots mixed alluvium parent datum. Elemental values derived from dust are denoted by the filled purple circle, and, hence, dust input was determined with Lybrand's data, which was adjusted to the Ti dust values (Rasmussen, pers. comm.).

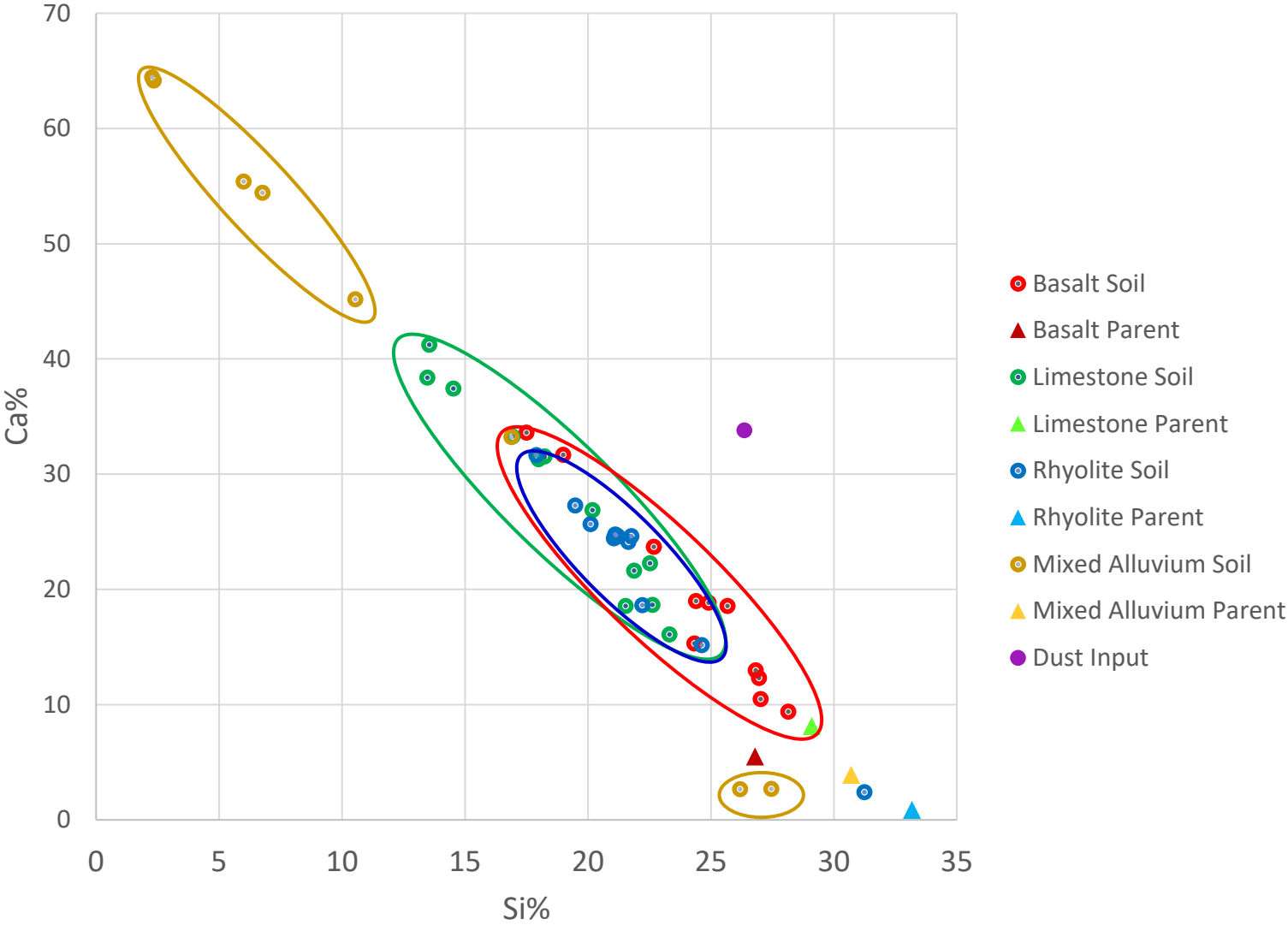

Figure 27. Bivariate plot of Ca vs. Si of soil and parent material. Red data field plots basalt-derived soils; red triangle plots basalt parent datum. Green data field plots limestone-derived soils; green triangle plots limestone parent datum. Blue data field plots rhyolite-derived soils; blue triangle plots rhyolite parent datum. Two yellow data fields plot mixed-alluvium-derived soils; yellow triangle plots mixed alluvium parent datum. Elemental values derived from dust are denoted by the filled purple circle, and, hence, dust input was determined with Lybrand's data, which was adjusted to the Ti dust values (Rasmussen, pers. comm.).

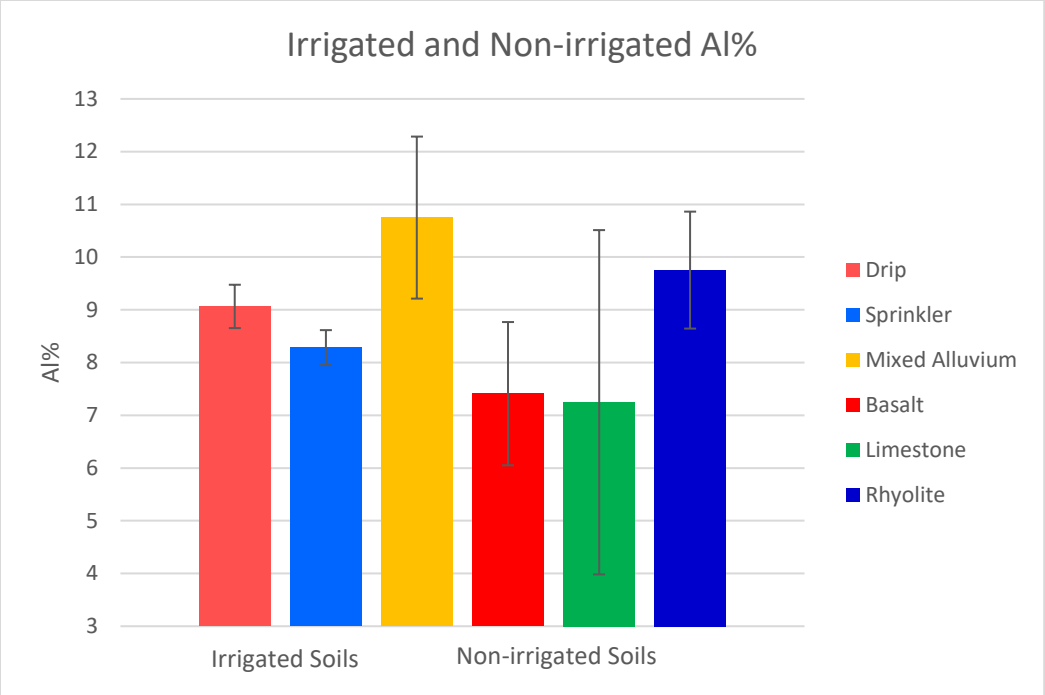

Figure 28. Bar charts of the soil mineral A-horizons' Al concentrations, which are grouped by irrigated soils and non-irrigated soil parent material. Standard deviation calculated at 1σ. Mixed alluvial soil differs from the sprinkler-irrigated mineral A-horizons with respect to the proportion of Al, as confirmed with an ANOVA test (Appendix B).

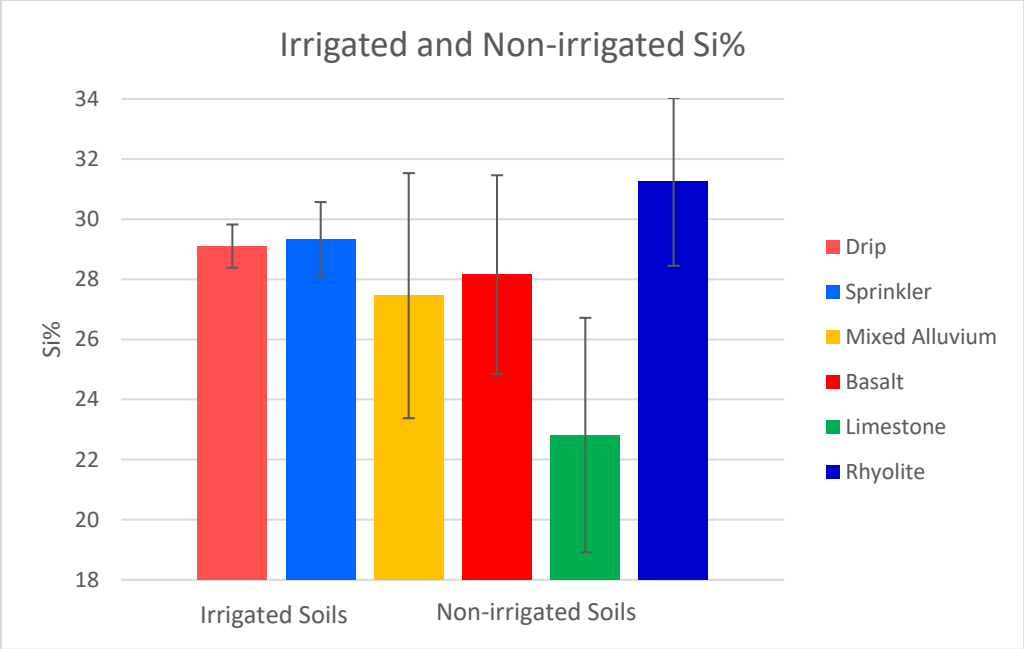

Figure 29. Bar charts of the soil mineral A-horizons' Si concentrations, which are grouped by irrigated soils and non-irrigated soil parent material. Standard deviation calculated at 1σ. There is no significant difference in the amount of silica between the irrigated soils and the non-irrigated mixed alluvium.

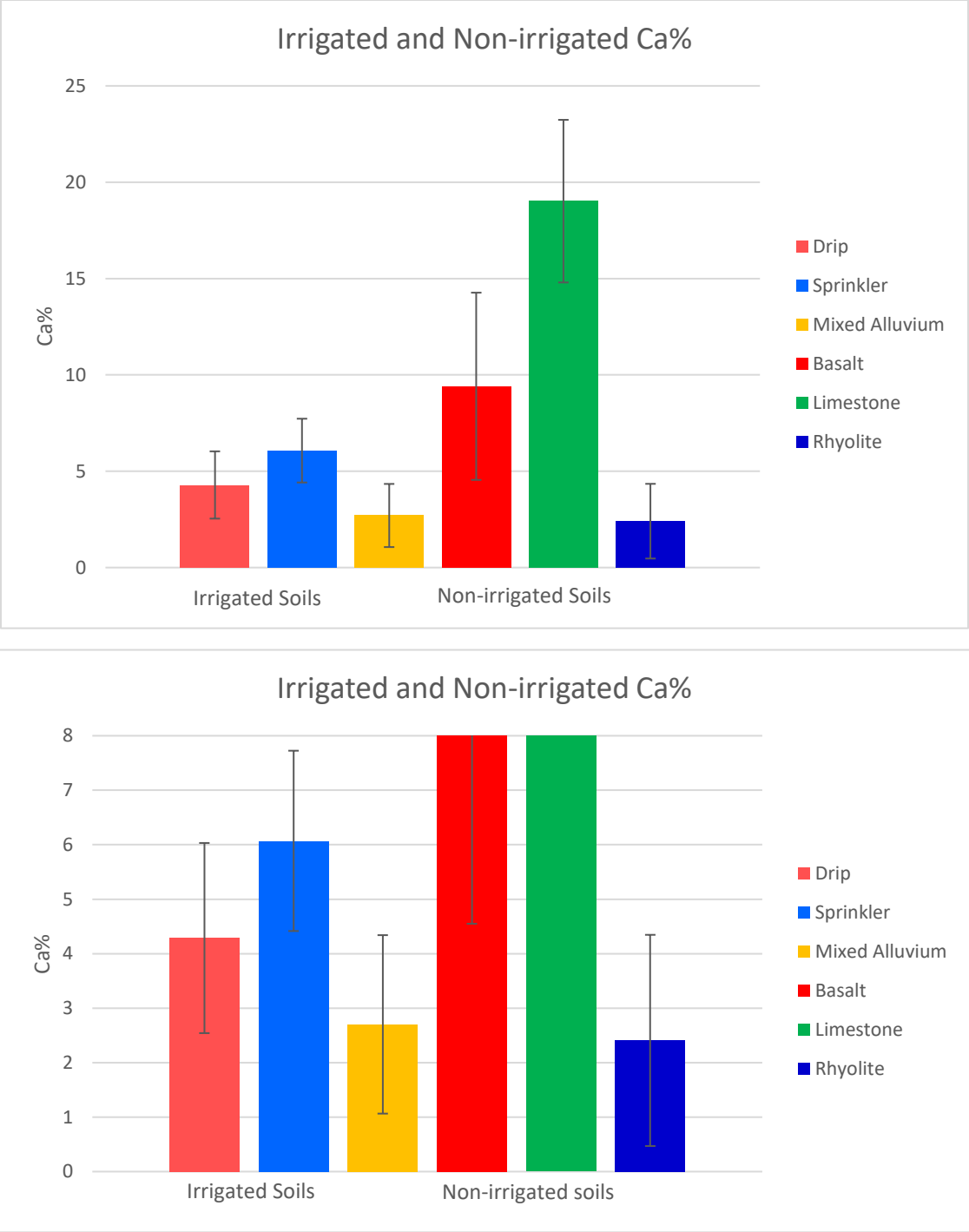

Figure 30. (Top) Bar charts of the soil mineral A-horizons' Ca concentrations, which are grouped by irrigated soils and non-irrigated soil parent material. (Bottom) The y-axis Ca% has been greatly reduced to see whether the mixed alluvium's standard deviation does overlap with the irrigated soils' standard deviation. Standard deviation calculated at 1σ. There is significantly less Ca in the mixed alluvial soil than the sprinkler-irrigated soils, as confirmed with an ANOVA test (Appendix B).

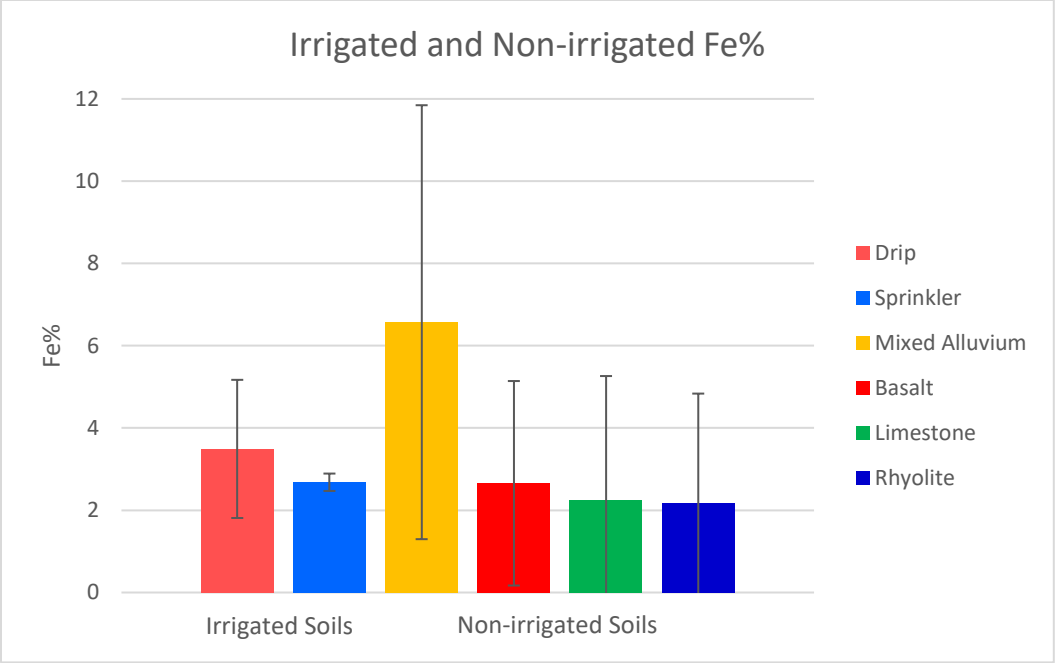

Figure 31. Bar charts of the soil mineral A-horizons' Fe concentrations, which are grouped by irrigated soils and non-irrigated soil parent material. Standard deviation calculated at 1σ. There is no significant difference in the amount of Fe between the irrigated soils and the non-irrigated mixed alluvium.

Site and Parent Material	Sample	Soil or Parent	Depth (cm)	H_2O pH	H_2O EC	KCl pH	$CaCl_2$ pH
Tucson Mtns. (Rhyolite/ Andesite)	2353	S	2.5	7.42	266.1	7.69	7.84
	2354	S	24	8.44	82.3	7.73	7.97
	2355	S	59.5	8.69	87.1	7.78	7.97
	2356	S	97.5	8.69	100.3	7.78	8.02
	2357	S	126.5	8.87	97.6	7.89	8.03
	2358	S	143	8.79	32.4	7.87	8.11
	2359	S	162	8.8	30.8	7.92	8.23
	2360	S	192	8.76	69.1	7.91	8.19
	2361	S	221	9.21	139.6	8.11	8.46
	2362	S	242.5	9.24	132.5	8.1	8.6
	2363	S	279.5	9.12	168.3	8.03	8.35
	2364	P	279.5	9	47.6	8.21	8.27
	Average			8.75	104.48	7.92	8.17
Sentinel Peak (Basalt)	2365	S	5	8.59	62	7.51	8.24
	2368	S	44	8.68	213.8	8.23	8.2
	2366	S	75	8.92	100	8.27	8.22
	2369	S	120.5	8.77	66.8	7.94	8.2
	2367	S	140	8.38	75.2	8.21	8.32
	2370	S	168.5	8.76	63.1	8.13	8.23
	2371	S	200	8.66	153.8	8.04	8.2
	2372	S	231	8.71	28.7	7.94	8.22
	2373	S	253	8.72	139.5	7.98	8.24
	2374	S	268.5	8.72	83.9	7.98	8.26
	Average			8.69	98.68	8.02	8.23
Santa Rita Mtns. (Limestone)	2375	S	8	8.35	123.9	7.6	8.15
	2376	S	19.5	8.48	44.6	7.97	8.14
	2377	S	25	8.83	133.1	8.21	8.22
	2378	S	32.5	8.72	138.8	8.01	8.27
	2379	S	68	8.94	115.3	8.36	8.37
	2380	S	108	8.45	1922.9	8.2	8.32
	2381	S	130	9.09	755	8.26	8.48
	2382	S	149	9.81	248	8.19	8.44
	2383	P	173	9.83	455.7	8.19	9.1
	Average			8.94	437.48	8.11	8.39
Saddlebrooke (Mixed Alluvium)	2384	S	7.5	7.82	172.5	6.96	7.33
	2385	S	30	8.43	145.6	7.76	7.6
	2386	S	59	8.7	256.7	8.87	7.98
	2387	S	84.5	9.03	141	8.82	8.03
	2388	S	113	8.91	118.3	8.67	8.16

	2389	S	140	9.05	110.3	7.81	8.18
	Average			8.66	157.40	8.15	7.88
	2390	S	17.5	8.57	145.9	7.91	8.07
Whetstone (Limestone)	2391	S	55	8.89	123.6	8.25	8.08
	2392	S	88.5	8.96	112.5	8.32	8.37
	2393	S	122.5	8.95	123.3	8.31	8.37
	2394	S	151.5	8.84	111.8	8.27	8.31
	Average			8.84	123.42	8.21	8.24

Table 1. Electrical conductivity (EC) and pH values for the soil horizons from the five soil profiles (see Fig. 7), using water, KCl, and $CaCl_2$ washes.

Sentinel Peak (Basalt)			
GPS Coordinates	*Soil Horizons*	*Horizon Description and Depth*	*Number of Samples Collected*
32°12’36” N 110°59’32” W	A (Horizon compared to irrigated soils)	Humus mineral mixture, little to no organics, gray, 0-10 cm	1
	A	Weak humus mineral mixture, rock mixture, light gray, 10-88 cm	2
	B (Bk)	Calcium Carbonate enriched layer, light gray, 88-153 and 246-277 cm	5
	Bkkm	Cemented layer, white, 153-246 cm	3
	C	Unconsolidated basalt parent material, 300+ cm	1

Table 2. Sentinel Peak’s GPS coordinate location using the WGS84 standard for the coordinate system, soil horizon descriptions and depths, and the number of samples collected and analyzed from each horizon.

The Santa Rita Mountains (Limestone)			
GPS Coordinates	*Soil Horizons*	*Horizon Description and Depth*	*Number of Samples Collected*
31°49’33” N 110°46’29” W	A (Horizons compared to irrigated soils)	Humus mineral mixture, little to no organics, dark brown, 0-23 cm	2
	A	Weak humus mineral mixture, light gray and brown, 23-98 cm	3
	B (Bk)	Calcium Carbonate enriched layer, white, 98-156 cm	3
	Bkkm	Cemented layer, white	N/A
	C	Unconsolidated limestone parent material, 156-190 cm	1

Table 3. Santa Rita Mountains’ GPS coordinate location using the WGS84 standard for the coordinate system, soil horizon descriptions and depths, and the number of samples collected and analyzed from each horizon.

Whetstone (Limestone)			
GPS Coordinates	*Soil Horizons*	*Horizon Description and Depth*	*Number of Samples Collected*
31°42’14” N 110°20’31” W	A (Horizon compared to irrigated soils)	Humus mineral mixture, little to no organics, light brown, 0-35 cm	1
	A	Weak humus mineral mixture, gray, 35-75 cm	1
	B (Bk)	Calcium Carbonate enriched layer, light brown/gray, 75-160 cm	3
	Bkkm	Cemented layer, white	N/A
	C	Unconsolidated limestone parent material, 200 cm	1

Table 4. Whetstone Mountains’ GPS coordinate location using the WGS84 standard for the coordinate system, soil horizon descriptions and depths, and the number of samples collected and analyzed from each horizon.

The Tucson Mountains (Rhyolite/Andesite)			
GPS Coordinates	*Soil Horizons*	*Horizon Description and Depth*	*Number of Samples Collected*
32°13’29” N 111°06’59” W	A (Horizon compared to irrigated soils)	Humus mineral mixture, little to no organics, dark brown, 0-5 cm	1
	A	Weak humus mineral mixture, light brown, 5-76 cm	2
	B (Bk)	Calcium Carbonate enriched layer, white and gray, 76-304 cm	8
	Bkkm	Cemented layer	N/A
	C	Unconsolidated rhyolite parent material, 255-304 cm	1

Table 5. Tucson Mountains’ GPS coordinate location using the WGS84 standard for the coordinate system, soil horizon descriptions and depths, and the number of samples collected and analyzed from each horizon.

Saddlebrooke (Mixed Alluvium)			
GPS Coordinates	*Soil Horizons*	*Horizon Description and Depth*	*Number of Samples Collected*
32°32’08” N 110°52’46” W	A (Horizon compared to irrigated soils)	Humus mineral mixture, little to no organics, dark brown/red, 0-15 cm	1
	A	Weak humus mineral mixture, dark brown to red, 15-73 cm	2
	B (Bk)	Calcium Carbonate enriched layer, white, 73-290 cm	5
	Bkkm	Cemented layer, white	N/A
	C	Unconsolidated mixed alluvium parent material, 400 cm	1

Table 6. Saddlebrooke’s GPS coordinate location using the WGS84 standard for the coordinate system, soil horizon descriptions and depths, and the number of samples collected and analyzed from each horizon.

Element	pXRF	XRF
Mg	0.357%	2.26%
Al	0.369%	5.74%
Si	3.70%	20.4%
K	0.903%	1.91%
Ca	15.0%	25.4%
Ti	0.196%	0.378%
Fe	1.83%	2.00%
Zr	0.0138%	0.0133%

Table 7. Mean elemental values of Mg, Al, Si, K, Ca, Ti, Fe, and Zr of non-irrigated soils obtained with pXRF and M4 TORNADO XRF analyses.